Editorial Manager(tm) for Neuroradiology
Manuscript Draft

Manuscript Number:

Title: IN VIVO PROTON MAGNETIC RESONANCE SPECTROSCOPY OF INTRAVENTRICULAR TUMOURS OF THE BRAIN

Article Type: Original

Section/Category: Diagnostic Neuroradiology

Keywords: Brain tumours; Brain tumours, diagnosis; Ventricular tumours, brain; Magnetic resonance spectroscopy

Corresponding Author: Dr Carles Majós, MD, PhD

Corresponding Author's Institution: IDI, Hospital Universitari de Bellvitge

First Author: Carles Majós, MD, PhD

Order of Authors: Carles Majós, MD, PhD; Carles Aguilera, MD; Mònica Cos, MD; Sara Castañer, MD; Ana P Candiota, PhD; Teresa Delgado-Goñi, MSc; Juan J Sánchez, MD; Angels Camins, MD; David Mato, MD; Juan J Acebes, MD, PhD; Carles Arús, PhD

Abstract: INTRODUCTION
Intraventricular tumours include an histologicaly diverse group of lesions, some of them infrequent, that are difficult to reach by surgery. Our aim was to evaluate the potential usefulness of proton MR spectroscopy in the characterisation of these tumours.

METHODS
We retrospectively evaluated the spectra of 52 intraventricular tumours that included 10 metastases, 7 PNETs, 6 glioblastomas, 5 meningiomas, 4 low grade astrocytomas, 4

ependymomas, 3 anaplastic astrocytomas, 2 lymphomas, 2 central neurocytomas, 2 colloid cysts, 2 pituitary adenomas, one subependymal giant cell astrocytoma, one choroid plexus carcinoma, one craniopharyngioma, one hemangioblastoma, and one germinoma. Single voxel proton MR spectroscopy was performed at TR, 2000 ms and TE both, 30 and 136 ms. A Kruskall-Wallis test was used to select the datapoints of the spectra in which there were differences between groups. Then, the Mann Whitney U test was used to search for the most discriminative datapoints of each group.

RESULTS

Characteristic trends were found for some tumour groups: High Glx and Ala in meningiomas ($p<0.001$ and $p<0.01$, respectively), high mobile lipids in metastasis ($p<0.001$), high Cho in PNET ($p<0.001$), high mI+Gly in ependymoma ($p<0.001$), high NAC in the absence of normal brain parenchyma pattern in colloid cysts, and high mI+Gly and Ala in central neurocytoma.

CONCLUSION

MR spectroscopy provides additional metabolic information that could be useful in the diagnosis of intraventricular brain tumours.

TITLE PAGE

ORIGINAL ARTICLE:
IN VIVO PROTON MAGNETIC RESONANCE SPECTROSCOPY OF INTRAVENTRICULAR TUMOURS OF THE BRAIN

Carles Majós[1,2], Carles Aguilera[1,2], Mònica Cos[1], Sara Castañer[1], Ana P Candiota[2,3], Teresa Delgado-Goñi[2,3], Juan J Sánchez[1], Àngels Camins[1], David Mato[4], Juan J Acebes[4,2], Carles Arús[3,2]

[1] Institut de Diagnòstic per la Imatge (IDI). Centre Bellvitge, Hospital Universitari de Bellvitge, Autovia de Castelldefels km 2.7, 08907, L'Hospitalet de Llobregat, Barcelona, Spain
[2] Centro de Investigación Biomédica en Red en Bioingeniería, Biomateriales y Nanomedicina (CIBER-BBN), 08193, Cerdanyola del Vallès, Spain.
[3] Department de Bioquímica i Biologia Molecular, Unitat de Bioquímica de Biociències, Edifici Cs, Universitat Autònoma de Barcelona, 08193, Cerdanyola del Vallés, Spain
[4] Department of Neurosurgery, Hospital Universitari de Bellvitge, C/ Feixa Llarga s/n, 08907, L'Hospitalet de Llobregat, Barcelona, Spain

Corresponding author: Carles Majós, Institut de Diagnòstic per la Imatge (IDI). Centre Bellvitge, Hospital Universitari de Bellvitge, Autovia de Castelldefels km 2.7, 08907 L'Hospitalet de Llobregat, Barcelona, SPAIN, Phone number: +34932630121, Fax number: +34932634273, e-mail: **cmajos@csub.scs.es**

Grants: Work funded in part by MEDIVO (MCYT SAF 2002-00440), MEDIVO2 (MEC SAF2005-03650), and Generalitat de Catalunya SGR2001-194, SGR2005-00863, XT2002-48 and XT2004-51. CIBER-BBN is an initiative of "Instituto de Salud Carlos III" (ISCiii) of Spain

INTRODUCTION

Proton MR spectroscopy (^{1}H MRS) is a non-invasive MR technique that provides biochemical information that could be useful in the diagnosis of brain lesions. In order to apply this information in daily clinical practice it is necessary to know the characteristics of every tumour group and the findings that could support a particular diagnosis. Prior work has established the usefulness of ^{1}H MRS in the diagnosis of the most common tumour groups (1-8) but other less prevalent tumours have not been evaluated in depth. The analysis of these tumours is relevant, in order to gain a wider knowledge of the spectroscopy of brain tumours that could be applied in daily clinical practice.

One of the groups for which there is a deficit of previous reported reference data is the one of intraventricular tumours. These tumours are located deep within the brain, and surgical approach may be of risk. On the other hand, some tumours of this group are of low grade and a conservative follow-up could be of choice. Accordingly, their radiological diagnosis should be as precise as possible. Sometimes, these tumours show a characteristic radiological appearance, but in other cases their radiological signature may be rather unspecific. Two types of tumours are found into the ventricles: tumours that can be found either inside or outside of the ventricles, and tumours that are characteristic of the ventricular system. The second group includes some tumour types that are highly infrequent. This is the reason why the references to these tumours in the literature are limited to a few case reports or to the analysis of a low number of cases of a particular tumour type (9-13). This wok analyses the spectroscopic findings of intraventricular tumours as a single group, including representatives of both subgroups and looking for the main differences between tumour types. Doing so, we aim to provide a global approach to the differential diagnosis of a ventricular mass by ^{1}H MRS.

METHODS

Patients

We retrospectively reviewed 539 consecutive cases from patients in which spectroscopy of a brain tumour was performed between August 1997 and March 2008. All tumours except some metastasis had a definitive diagnosis based on histology. In the case of metastasis, the diagnosis was accepted without need of histopathological assessment when three or more brain lesions and a primary extracranial tumour were present. In 52 cases (52/539; 9.65%), the main part of the tumour was located into the ventricular system, and were selected for the study (35 male and 17 female patients; age range, 17-77 years; mean age, 45 years). Distribution of cases by histology and ventricular location is shown in table 1. This retrospective study was included in a research project approved by our institutional review board, and informed consent was obtained from all patients.

MR Spectroscopy

Single voxel ^{1}H MRS was performed on a 1.5 T MR imaging unit (ACS-NT, Philips Medical Systems, Best, The Netherlands) after the conventional MR imaging examination. A standard receiver head coil was used in all cases. Volume of interest (VOI) ranged between $(1.5\ cm)^3$ and $(2\ cm)^3$ depending on tumour dimensions. The voxel was placed following criteria previously approved at our institution for performing ^{1}H MRS in brain tumours. Namely, the VOI size and location were determined with the aim of positioning the largest possible voxel within the tumoral area, with minimal contamination from the surrounding non tumoural tissue. At least two proton spectra were acquired from the same VOI for every case: 1) water-suppressed SE short TE (2000/30/92-184) (TR/TE/averages); and 2) water-suppressed SE long TE (2000/136/126-252). Spectrum analysis was performed off-line with the use of the MRUI software (www.mrui.uab.es/mrui) (14). The intensities of the individual data points included between 0 and 4.00 ppm were used as input for the normalisation method and statistical analysis. The data vector was normalised to unit length (1,15,16). According to this method, the intensity value of each data point was divided by the square root of the sum the squares of the values in the data vector. Only normalised intensity values for each data point were further used in the graphics and statistical analysis. Assignment of the resonances of interest,

including mobile lipids at 0.90 ppm (Lip 0.9) and at 1.30 ppm (Lip 1.3), lactate (Lact) doublet centred at 1.35 ppm, alanine (Ala) doublet centred at 1.45 ppm, N-acetyl-containing compounds (NAC) at 2.02 ppm, glutamate and glutamine (Glx) between 2.05 and 2.40 ppm, creatine plus phosphocreatine (Cr) at 3.03 ppm, choline and other trimethyl-amine-containing compounds (Cho) at 3.22 ppm, taurine and/or scylloinositol (Tau+sI) between 3.33 and 3.40 ppm, myoinositol and/or glycine (mI+Gly) at 3.55 ppm and alanine and/or glutamine and glutamate (Ala+Glx) at 3.70 ppm was based on previous studies (2,17-23). Mean spectra plots for each tumour group were produced by averaging the normalised spectra of the cases of the group.

Statistics

The aim of the study was to search for the data points of the spectrum that could characterise a tumour type. The reason being that we considered that these were the points that could support a particular diagnosis in a real clinical situation. In a first step, we analysed all data points of the spectrum between 0 and 4.00 ppm with a Kruskall-Wallis test in order to select the points that showed differences between groups. Only data points with significance level better than $p<0.05$ were retained for further analysis. Then, we searched for the most discriminative data points for every single group. This was done by dividing the data set in two groups: one with the tumour type being evaluated (i,e, meningioma) and another one containing all other cases (i,e, non-meningioma). The Mann Whitney U test for two independent samples was used to test the differences among these groups. The points showing the highest significance of differences were considered to be the most discriminative for the group being evaluated. The main limitation for the analysis was the low number of representatives of those groups. In that respect, the statistic test was considered of low confidence when only three or less representatives of the group were available, and only a qualitative assessment of semiquantitative data and mean spectra was performed on them. Because the number of representatives was also reduced in the other tumour types, the quantitative analysis was always supported with a qualitative assessment of average spectral pattern major features.

Discrimination between groups was further evaluated using linear discriminant analysis of preselected spectral features, and visualised by drawing 2D plots. Several 2D plots were constructed for each bilateral comparison with the normalised values of the parameters that could produce a better differentiation between groups. These parameters were selected both on the basis of average spectra and/or statistical analysis. Several comparisons were carried out. One approach considered tumour types regardless of their location into the ventricular system, while a second approach took also into account the location of the tumour into the lateral, third or fourth ventricles, respectively. All statistical computations were performed by using SPSS 14.0 software (SPSS Inc., Chicago, IL).

RESULTS

Global evaluation of intraventricular tumours

The mean spectra obtained for the tumour groups studied are shown in figure 1.

Table 2 shows the resonances with significant differences in the comparison between every particular group and the rest of cases. In this global evaluation, the most prominent findings were:

- High Glx levels at short and long TE ($p<0.001$) in meningiomas.
- High Ala levels in meningiomas at long TE ($p<0.01$). Non significant differences were found at short TE in the Ala resonance, but significance was achieved ($p<0.01$) for the Ala+Glx peak.
- Poor differences in the comparison between astrocytomas, divided in 3 groups (low grade astrocytoma, anaplastic astrocytoma and glioblastoma), and the other tumours, being Lip 0.9 the only resonance that showed significant differences between glioblastoma and the others, and only at long TE.
- High levels of lipids (Lip 0.9 and Lip 1.3) in metastasis at long and short TE ($p<0.001$ with the exception of Lip 0.9 at short TE in which $p<0.01$).

- When glioblastomas and metastases were combined into a single group, Lip 0.9 and Lip 1.3 at both, short and long TE, showed highly significant differences ($p<0.001$), slightly higher than metastases alone.
- High Cho levels in PNETs both at short and long TE ($p<0.001$).
- High mI+Gly in ependymomas, more significant at short TE (short TE $p<0.001$; long TE $p<0.05$).

According to these findings, Glx could be suggested as a possible marker for meningiomas, Lip for metastasis, Cho for PNET, and mI+Gly for ependymomas.

Tumours of the lateral ventricles

We found 25 tumours into the lateral ventricles, corresponding to 9 tumour types (table 1). In this location, meningioma could be differentially discriminated from other tumours using normalised Glx values. Figure 2A depicts the distribution of the cases found into the lateral ventricles according to their values for Glx at long and short TE. Using an LDA with these two parameters, a full discrimination (100%) between meningioma and non-meningioma was obtained in the lateral ventricle tumours.

Glioblastoma and metastasis were characterised by high mobile lipids. An 84 % correct discrimination between GBM+MET and non-GBM+MET was obtained with an LDA using the normalised intensity values of Lips at 1.3 ppm.

Only two central neurocytomas were included in the study and a statistical assessment was not performed. Qualitative analysis of the data pointed out that the most prominent findings of these tumours were high mI+Gly and high Ala, mainly at long TE. These two resonances differentiated central neurocytoma from the rest of tumours of the lateral ventricle when 2D plots were constructed (figure 2B). A 92% correct discrimination was obtained with mI+Gly at long TE.

The visual evaluation of the rest of groups pointed out that low grade astrocytoma was the tumour with the higher values of NAC both, at short and long TE, with a slight relative increase of Cho, and a prominent mI+Gly peak at

short TE. Anaplastic astrocytoma showed lower NAC and mI+Gly values, and higher Cho than low grade astrocytoma. Choroid plexus carcinoma showed very high levels of Cho at long TE, with increased mobile lipids. Lymphoma showed mobile lipids and high Cho values. Subependymal giant cell astrocytoma (SGCA) was noisy, being the most prominent finding high mI+Gly at short TE. Figure 3 depicts some selected examples of ^{1}H MRS in tumours of the lateral ventricles.

Tumours of the third ventricle

We found 11 tumours into the third ventricle, corresponding to 8 tumour types (table 1). This was the group with fewer representatives, and statistical analysis could not be performed for tumours of this location.

The qualitative assessment pointed out that colloid cysts were characterised by a loss of the pattern found in normal brain parenchyma, presence of lactate and a prominent NAC peak. NAC had some discriminative value in a 2D plot (figure 2C). High mobile lipids at both TE characterised metastases. Pituitary adenomas showed high Cho levels, with some NAC and Lact, and very low Cr. Craniopharyngioma showed a noisy pattern were no clear resonance could be detected. Low grade and anaplastic astrocytoma showed patterns similar to that found in other locations. In the single ependymoma case, high mI+Gly was the most prominent finding. Figure 4 depicts some examples of ^{1}H MRS in tumours of the third ventricle.

Tumours of the fourth ventricle

We found 17 tumours into the fourth ventricle, corresponding to 5 tumour types (table 1).

Ependymomas were well differentiated from all other tumours by the values of mI+Gly at short TE were a threshold of 0.23 for its normalised peak height fully discriminated (100%) ependymomas from non-ependymomas in the fourth ventricle (figure 2D).

PNET showed significant differences in Cho for both, short and long TE. Values at short TE allowed 94% of discrimination between PNET and non-PNET in the fourth ventricle.

Metastasis showed significant differences in mobile lipids (table 2). Lip 1.3 at short TE with a threshold of 0.33 for its normalised peak height fully discriminated (100%) between fourth ventricle metastasis and non-metastasis (figure 2E).

Both low grade astrocytomas in this location were very noisy. The main finding was a NAC peak better identified than in the rest of groups. Cho in this group was lower than in PNET and ependymoma on both, short and long TE.

Hemangioblastoma was represented by a single case. This tumour showed a pattern of high mobile lipids with increased Cho.

DISCUSSION

We have found that ^{1}H MRS can be a useful additional tool for the diagnosis of intraventricular tumours. Some of the tumour groups analysed in this study have shown some characteristic trends that may allow a confident discrimination. This is the case of ependymomas, in which high mI+Gly levels were found both at short and long TE. This trend allowed full discrimination (100% in our data set) between ependymoma and non-ependymoma tumours. Ependymoma is most commonly found in the fourth ventricle of young patients. In this age group and location, the main tumours to be included in the differential diagnosis are PNET and low grade astrocytoma. PNET showed a characteristic trend for displaying very high Cho levels both at short and long TE. High Cho has been previously reported as a characteristic finding of PNET (9,24,25) and supported 94 % discrimination between PNET and non-PNET tumours. In our series, the spectra of both fourth ventricle low grade astrocytomas were very noisy. This can be an intrinsic characteristic of this group due to its histological heterogeneity, commonly found to show cysts and calcifications. The visual

comparison between low grade astrocytoma, ependymoma and PNET pointed out higher NAC/Cr ratios and lower Cho normalised peaks in low grade astrocytoma. According to these findings, when a mass is found into the fourth ventricle, high mI+Gly would suggest ependymoma, while very high Cho would support PNET and a relatively preserved NAC peak would be in favour of low grade astrocytoma. In adulthood, metastasis has also to be considered in a tumour of the fourth ventricle. Metastases are characterised by high mobile lipids, indicating necrosis. This resonance was significantly higher in metastasis than in the other three groups reported above.

Most tumours found into the third ventricle are not primary of it, but originated outside the ventricular walls and grew into the ventricle. This is the case of pituitary adenoma, craniopharyngioma, germinoma, some astrocytic tumours and metastasis. In these tumours, an accurate analysis of the MR images may show signs that point to an extraventricular origin of the tumour, which would provide an important clue for the diagnosis. Nevertheless, in some cases it is difficult to find this kind of signs and the analysis of the MR spectra may bring useful additional information. Other tumours originate in the lateral ventricles and project into the third through the foramina of Monro. This may happen with central neurocytoma, SGCA and subependymoma. Maybe the most characteristic primary tumour of the third ventricle would be the colloid cyst. To find a small cystic tumour in the roof of the third ventricle between the columns of the fornix is quite pathognomonic. In these very characteristic cases, no additional information can be extracted from spectroscopy. Different happens in atypical large colloid cysts, in which their origin in the roof of the third ventricle may not be evident, and the differential diagnosis with craniopharyngioma and low grade astrocytoma should be considered (figure 4A). In these cases, a predominant NAC peak and presence of lactate, in the absence of a normal brain parenchymal pattern would support the diagnosis of colloid cyst. Increase of NAC in colloid cysts could seem paradoxical. Nevertheless, this has been previously reported in cystic tumours, and has been mostly attributed to N-acetyl groups of macromolecule-linked sialic acid (17). In our series, the colloid cysts pattern was different from craniopharyngioma, that showed highly noisy

spectra without a predominant resonance, and from low grade astrocytoma, that showed high Cho and persistent Cr.

Age and location into the ventricle largely influences the differential diagnosis of lateral ventricle tumours (3,26). For example, while meningioma is a common tumour in the atria of adulthood, central neurocytoma is most commonly found in the body of the lateral ventricle of young adults. Nevertheless, some overlap exists, and additional data from MR spectroscopy could be helpful in some cases. Brain meningiomas are known to show high levels of Ala, Glx and Cho (27,28). In the ventricular system, we have found that high Glx is the most differential ^{1}H MRS finding for meningioma (figure 2A). Metastasis may also appear at the same location than meningiomas and can also display similar MRI characteristics. The diagnosis will be quite certain when more than one lesion is found and a primary extracranial tumour is known. Nevertheless, even when a solitary mass appears in the atria, a metastasis should be considered. Mobile lipids detection by spectroscopy have been largely reported in metastasis and glioblastoma as a marker of necrosis, characteristic of these types of tumours. Our study confirms that this finding is also prevalent in intraventricular metastasis, and that it can be confidently used to identify metastasis in the lateral ventricle.

Central neurocytoma is a tumour almost exclusively located in the body of the lateral ventricle that appears in middle-aged adults. Previous work has reported these tumours to show high mI+Gly and Cho levels, jointly with Ala (10,11). Our study confirms these findings, and demonstrates that high Ala and mI+Gly at long TE strongly suggest central neurocytoma (92% discrimination in our present set of tumours). Choroid plexus papillomas are more commonly found in young patients, and have been reported to show high mI+Gly and relatively low Cho (9,12,13). Choroid plexus carcinomas show higher Cho levels (12,13), but lower mI. In the case included in our series there was a lipid resonance both at short and long TE that could be explained by the fact that this was a malignant choroid plexus carcinoma. Glial tumours of low grade of malignancy, including the WHO grade I subgroup SGCA, are the most common tumours found into the lateral ventricle in young patients. This diagnosis could be

supported by a relatively preserved NAC resonance, slightly increased Cho/Cr ratio, high mI+Gly at short TE, and absence of mobile lipids and Ala.

Several limitations have to be considered in this study. First, it should be taken into account the low number of representatives for some groups. This is an inherent limitation of this kind of uncommon tumours that could impair the reproducibility of the results of the present work. The limitation was present in this study in spite of the relatively large number of cases accrued. Larger multicenter series could partially solve this limitation, but then the possible limitations of including cases acquired with different MR scanners and, possibly, with different MRS protocols, may arise. A second limitation was the absence of representatives of some groups, such as subependymoma or choroid plexus papilloma. Again, this limitation arises from the low prevalence of intraventricular tumours. Nevertheless, we consider that this study is of value in order to advance in the differential diagnosis of brain tumours by accruing spectra from uncommon tumour types. Finally, patients under 16 years of age were not included in the study because our hospital does not admit paediatric patients. This could determine the relative incidence of certain tumours and has to be taken into account when putting our results in perspective.

REFERENCES

1. Tate AR, Underwood J, Acosta DM, et al. Development of a decision support system for diagnosis and grading of brain tumours using in vivo magnetic resonance single voxel spectra. NMR Biomed 2006;19:411-34.
2. Burtscher IM, Skagerberg G, Geijer B, et al. Proton MR spectroscopy and preoperative diagnostic accuracy: an evaluation of intracranial mass lesions characterized by stereotactic biopsy findings. *AJNR Am J Neuroradiol* 2000;21:84-93.
3. Majós C, Alonso J, Aguilera C, et al. Proton magnetic resonance spectroscopy (1H MRS) of human brain tumours: assessment of differences between tumour types and its applicability in brain tumour categorization. Eur Radiol 2003;13:582-591.
4. Law M, Yang S, Wang H, et al. Glioma grading: sensitivity, specificity, and predictive values of perfusion MR imaging and proton MR spectroscopic imaging compared with conventional MR imaging. *AJNR Am J Neuroradiol* 2003;24:1989-98.
5. Al-Okaili RN, Krejza J, Woo JH, et al. Intraaxial brain masses: MR Imaging-based diagnostic strategy-–Initial experience. Radiology 2007;243:539-50.
6. Preul MC, Caramanos Z, Collins DL, et al. Accurate, noninvasive diagnosis of human brain tumors by using proton magnetic resonance spectroscopy. Nat Med 1996;2:323-325.
7. Dowling C, Bollen AW, Noworolski SM, et al. Preoperative proton MR spectroscopy imaging of brain tumors: correlation with histopathologic analysis of resection specimens. AJNR Am J Neuroradiol 2001;22:604-612.

8. Howe FA, Barton SJ, Cudlip SA, et al. Metabolic profiles of human brain tumors using quantitative in vivo 1H Magnetic resonance spectroscopy. Magn Reson Med 2003;49:223–232.
9. Panigrahy A, Krieger MD, Gonzalez-Gomez I, et al. Quantitative short echo time 1H-MR spectroscopy of untreated pediatric brain tumors: preoperative diagnosis and characterization. *AJNR Am J Neuroradiol* 2006;27:560-72.
10. Chuang MT, Lin WC, Tsai HY, et al. 3-T proton magnetic resonance spectroscopy of central neurocytoma: 3 case reports and review of the literature. J Comput Assist Tomogr 2005;29:683-8.
11. Kim DG, Choe WJ, Chang KH, et al. In vivo proton magnetic resonance spectroscopy of central neurocytomas. Neurosurgery 2000;46:329-34.
12. Horská A, Ulug AM, Melhem ER, et al. Proton magnetic resonance spectroscopy of choroid plexus tumors in children. J Magn Reson Imaging 2001;14:78-82.
13. Krieger MD, Panigrahy A, McComb JG, et al. Differentiation of choroid plexus tumors by advanced magnetic resonance spectroscopy. Neurosurg Focus 2005;18:E4.
14. Van den Boogaart A. Quantitative data analysis of *in vivo* MRS data sets. Magn Reson Chem 1997;35:S146-52.
15. Tate AR, Griffiths JR, Martínez-Pérez I, et al. Towards a method for automated classification of 1H MHRS spectra from brain tumours. NMR Biomed 1998;11:177-91.
16. Ladroue C, Howe FA, Griffiths JR, Tate AR. Independent component analysis for automated decomposition of in vivo magnetic resonance spectra. Magn Reson Med 2003;50:697-703.

17. Candiota AP, Majós C, Bassols A, et al. Assignment of the 2.03 ppm resonance in in vivo 1H MRS of human brain tumour cystic fluid: contribution of macromolecules. MAGMA 2004;17:36-46.
18. Barba I, Moreno A, Martinez-Perez I, et al. Magnetic resonance spectroscopy of brain hemangiopericytomas: high myoinositol concentrations and discrimination from meningiomas. J Neurosurg 2001;94:55-60.
19. Wang Z, Sutton LN, Cnaan A, et al. Proton MR spectroscopy of pediatric cerebellar tumors. *AJNR Am J Neuroradiol* 1995;16:1821-33.
20. Ernst T, Hennig J. Coupling effects in volume selective 1 H spectroscopy of major brain metabolites. Magn Reson Med 1991;21:82-96.
21. Poptani H, Gupta RK, Roy R, et al. Characterization of intracranial mass lesions with in vivo proton MR spectroscopy. *AJNR Am J Neuroradiol* 1995;16:1593-603.
22. Meyerand ME, Pipas JM, Mamourian A, et al. Classification of biopsy-confirmed brain tumors using single-voxel MR spectroscopy. *AJNR Am J Neuroradiol* 1999;20:117-23.
23. Negendank WG, Sauter R, Brown TR, et al. Proton magnetic resonance spectroscopy in patients with glial tumors: a multicenter study. J Neurosurg 1996;84:449-58.
24. Majós C, Alonso J, Aguilera C, et al. Adult primitive neuroectodermal tumor: Proton MR Spectroscopic findings with possible application for differential diagnosis. Radiology 2002;225:556-66.

25. Kovanlikaya A, Panigrahy A, Krieger MD, et al. Untreated pediatric primitive neuroectodermal tumor in vivo: quantitation of taurine with MR spectroscopy. Radiology 2005;236:1020-5.
26. Jelinek J, Smirniotopoulos JG, Parisi JE, et al. Lateral ventricular neoplasms of the brain: differential diagnosis based on clinical, CT, and MR findings. *AJNR Am J Neuroradiol* 1990;11:567-74.
27. Majós C, Alonso J, Aguilera C, et al. Utility of proton MR spectroscopy in the diagnosis of radiologically atypical intracranial meningiomas. Neuroradiology 2003;45:129-36.
28. Kinoshita Y, Yokota A. Absolute concentrations of metabolites in human brain tumors using in vitro proton magnetic resonance spectroscopy. NMR Biomed 1997;10:2-12.

FIGURE CAPTIONS

Figure 1. Mean spectra for the different intraventricular tumour groups at short and long TE. For groups with only one representative (from 1W to 1AD) their single spectra are shown except for craniopharyngioma which is shown at figures 4H and 4I. Tentative resonance assignments according to literature and previous work are shown overlaid in the spectra.
A and B, metastasis.
C and D, primitive neuroectodermal tumour.
E and F, glioblastoma.
G and H, meningioma.
I and J, low grade astrocytoma.
K and L, ependymoma.
M and N, anaplastic astrocytoma.
O and P, lymphoma.
Q and R, central neurocytoma.
S and T, colloid cyst.
U and V, pituitary adenoma.
W and X, subependymal giant cell astrocytoma.
Y and Z, choroid plexus carcinoma.
AA and AB, hemangioblastoma.
AC and AD, germinoma

Figure 2. 2D plots illustrating the performance of some normalised peak intensities for discriminating between one tumor type and the rest of cases found in the same ventricular location (LV, lateral ventricle; 3^{rd}V, third ventricle; 4^{th}V, fourth ventricle). Values shown on each axis correspond to the exact ppm value given on the axis legend. Each point depicted in the graphics corresponds to a single case.
A, Glx at long ("x" axis) and short ("y" axis) TE for the discrimination between meningioma and non-meningioma in the lateral ventricle.
B, mI+Gly ("x" axis) and Ala ("y" axis) at long TE for the discrimination between central neurocytoma and non-central neurocytoma in the lateral ventricle.

C, NAC at short (“x” axis) and long (“y” axis) TE for the discrimination between colloid cyst and non-colloid cyst in the third ventricle.
D, mI+Gly at short (“x” axis) and long (“y” axis) TE for the discrimination between ependymoma and non-ependymoma in the fourth ventricle.
E, Lip 1.3 at short (“x” axis) and long (“y” axis) TE for the discrimination between metastsis and non-metastasis in the fourth ventricle.

Figure 3. ^{1}H MRS in characteristic examples of tumours of the lateral ventricles. A, Meningioma. Axial T1-weighted images after contrast show a mass into the left atrium. The tumour has well defined margins and slightly heterogeneous contrast enhancement. ^{1}H MRS at short (B) and long (C) TE shows increase of Glx, partially inverted at long TE due to J-coupling. There is also some Ala that can be better seen at long TE, as well as the increase in the Ala+Glx peak. These findings are characteristic of meningioma
D, Metastasis. Coronal T1-weighted image after contrast shows a tumour into the left lateral ventricle that grows into the third ventricle through the foramen of Monro (arrows). ^{1}H MRS at short (E) and long (F) TE show lipids at both TE, that are a marker of metastasis and glioblastoma.
G, Central neurocytoma. Axial T1-weighted image after contrast shows a tumour into the right lateral ventricle with a large anterior cyst (asterisk), a solid enhancing component in the posterior part (white arrows) and a central area with microcysts and calcifications (black arrow). ^{1}H MRS at short (H) and long (I) TE shows high Cho without lipids at long TE. There is also some mI+Gly and Ala visible, that is a characteristic finding of central neurocytoma.
J, Low grade astrocytoma. Axial T1-weighted image after contrast shows a non-enhancing tumour into the right ventricular atrium (arrows). ^{1}H MRS at short (K) and long (L) TE shows a relatively preserved Cho/NAC ratio, that may suggest a low grade astrocytoma. There is also high mI+Gly at short TE that decreases at long TE and has been related to high myoinositol content in low grade astrocytomas. Note differences with central neurocytoma in figure 3I, in which mI+Gly remains high at long TE and can be mainly related to glycine.

Figure 4. ^{1}H MRS in characteristic examples tumours of the third ventricle.

A, Colloid cyst. Coronal T1-weighted image without contrast administration shows an hyperintense cyst in the third ventricle. The image is compatible with colloid cyst, but the location and large size are not typical. ^{1}H MRS at short (B) and long (C) TE shows absence of Cho and Cr, with large NAC and presence of Lact. This pattern is similar to the one found in the other colloid cysts.
D, Anaplastic astrocytoma. Coronal T1-weitghted image after contrast administration shows a slightly enhancing tumour in the third ventricle (arrows). ^{1}H MRS at short (E) and long (F) TE show increased Cho/Cr and Cho/NAC ratios. There can also be a somewhat higher mI+Gly at short TE.
G, Craniopharyngioma. Coronal FLAIR image shows an hyperintense cystic lesion in the third ventricle (arrows) MRS at short (H) and long (I) TE show a noisy spectrum were no peak could be confidently identified.

Figure 5. ^{1}H MRS in diverse tumours of the fourth ventricle.
A, Ependymoma. Axial T1-weitghted image after contrast shows a nodular tumour in the fourth ventricle with a cystic intratumoural area. ^{1}H MRS at short (B) and long (C) TE show largely increased mI+Gly, mainly at short TE, that is characteristic of ependymoma. There is also a prominent Tau+sI peak.
D, Primitive neuroectodermal tumour. Axial T1-weitghted image after contrast shows a mass in the fourth ventricle with mild enhancement. There are some small cystic areas into the tumour. ^{1}H MRS at short (E) and long (F) TE show a very prominent Cho peak, characteristic of this kind of tumours. There is also some Ala and mI+Gly.
G, Metastasis. Axial T1-weitghted image after contrast shows a nodular mass in the fourth ventricle. ^{1}H MRS at short (H) and long (I) TE show lipids at both TE, characteristic of necrosis from metastasis and glioblastoma.
J, Low grade astrocytoma. Axial T1-weitghted image after contrast shows a very heterogeneous cystic tumour with irregular walls. ^{1}H MRS at short (K) and long (L) TE is noisy. Some NAC can be probably seen at short TE.

Table 1

Click here to download Table: Table 1.doc

Table 1. Distribution of the cases by diagnosis and location

Diagnosis	Lateral ventricle	Third ventricle	Fourth ventricle	Total
Metastasis	5*	2*	4	10*
Primitive neuroectodermal tumour			7	7
Glioblastoma	6			6
Meningioma	5			5
Low grade astrocytoma	1	1	2	4
Ependymoma		1	3	4
Anaplastic astrocytoma	2	1		3
Lymphoma	2			2
Central Neurocytoma	2			2
Colloid cyst		2		2
Pituitary adenoma		2		2
Subependymal giant cell astrocytoma	1			1
Choroid plexus carcinoma	1			1
Craniopharyngioma		1		1
Hemangioblastoma			1	1
Germinoma		1		1
Total	25*	11*	17	52

* One metastasis affected both the lateral and third ventricles (see figure 3D)

Table 2
Click here to download Table: Table 2.doc

Table 2. Significance level of differences between the tumour group being considered and the rest of tumours *

Tumour group	P<0.001**	P<0.01**	P<0.05**
Meningioma TE, 30 ms	Glx	Ala+Glx	
Meningioma TE, 136 ms	Glx	Ala; Tau+sI	Lip 1.3; Cho
Glioblastoma TE, 30 ms			
Glioblastoma TE, 136 ms			Lip 0.9
Metastasis TE, 30 ms	Lip 1.3; NAC; Glx; mI+Gly	Lip 0.9; Cho; Ala+Glx	Glx; Ala
Metastasis TE, 136 ms	Lip 0.9; Lip 1.3	Ala; Glx	
Glioblastoma+Metastasis TE, 30 ms	Lip 0.9; Lip 1.3; NAC	Glx; Cho; mI+Gly; Ala+Glx	Glx
Glioblastoma+Metastasis TE, 136 ms	Lip 0.9; Lip 1.3		Ala
Primitive Neuroectodermal Tumour TE, 30 ms	Cho		
Primitive Neuroectodermal Tumour TE, 136 ms	Cho		Lip 0.9; NAC
Ependymoma TE, 30 ms	Lip 1.3; Lact; mI+Gly		Tau+sI
Ependymoma TE, 136 ms	Tau+sI		Lact; Glx; mI+Gly

* Tumour groups with 3 or less representatives each were not evaluated with the statistic test. No significant differences were found for low grade astrocytoma.
** Glx, glutamate and glutamine (2.05 to 2.40 ppm); Ala+Glx, alanine and/or glutamate and glutamine (3.7 ppm); Ala, alanine (1.45 ppm); Tau+sI, taurine and/or scylloinositol (3.33 to 3.40 ppm); Lip 1.3, mobile lipids (1.3 ppm); Cho, choline and other trimethyl-amine-containing compounds (3.22 ppm); NAC, N-Acetyl-containing compounds (2.02 ppm); mI+Gly, myoinositol and/or glycine (3.55 ppm); Lip 0.9, mobile lipids (0.9 ppm); Lact, lactate (1.35 ppm)

figure 1A

Click here to download high resolution image

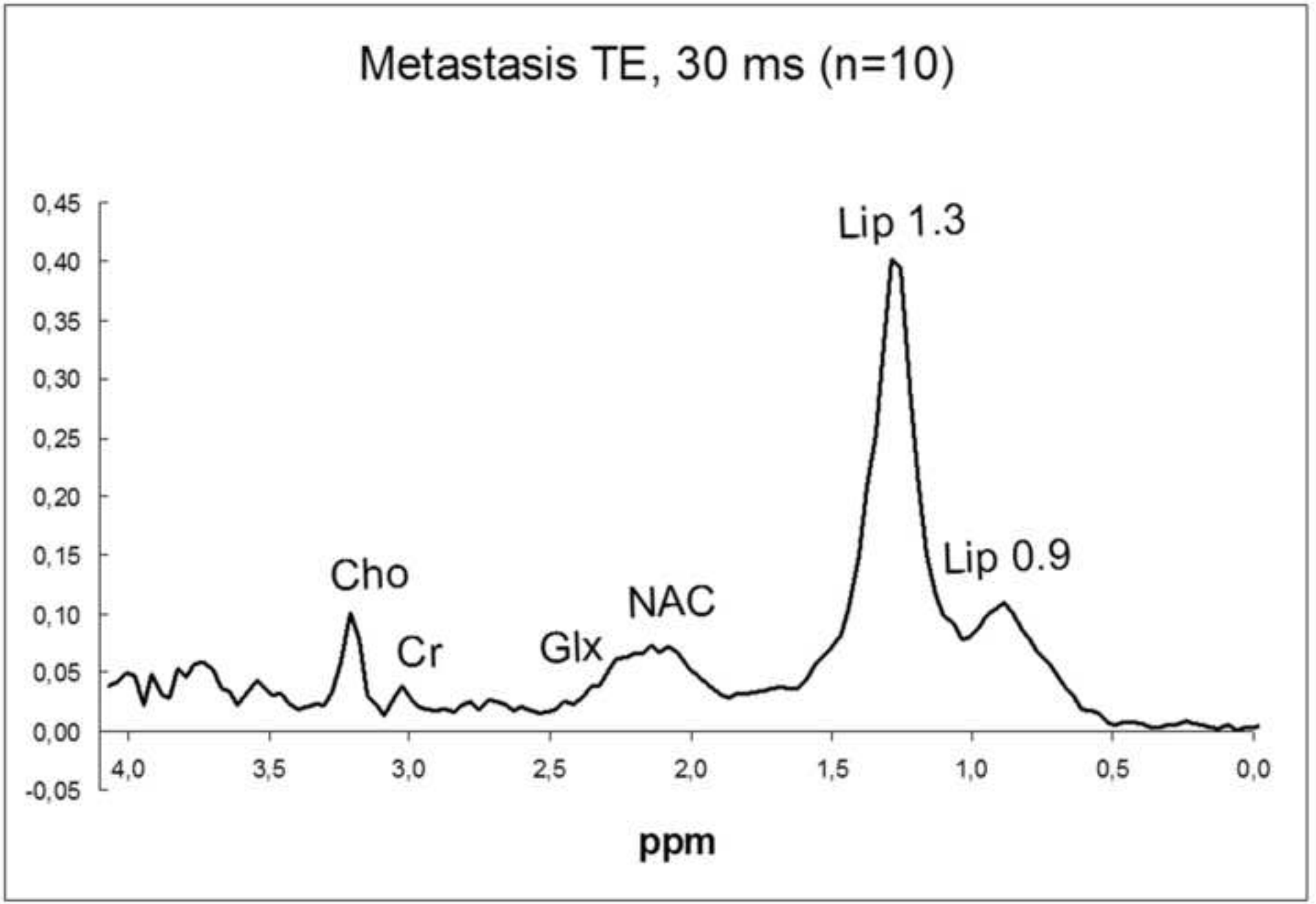

Figure 1B

Click here to download high resolution image

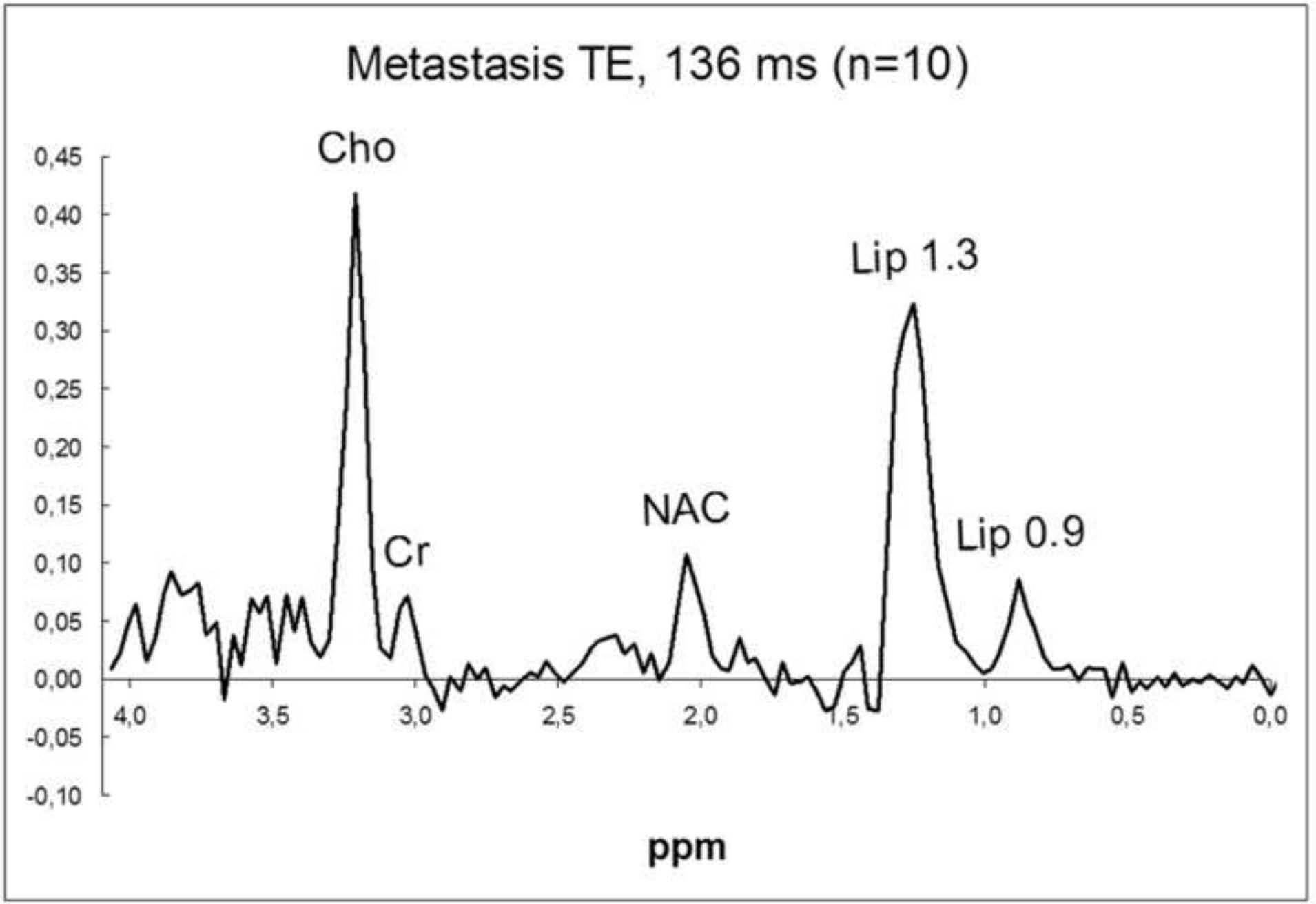

Figure 1C

Click here to download high resolution image

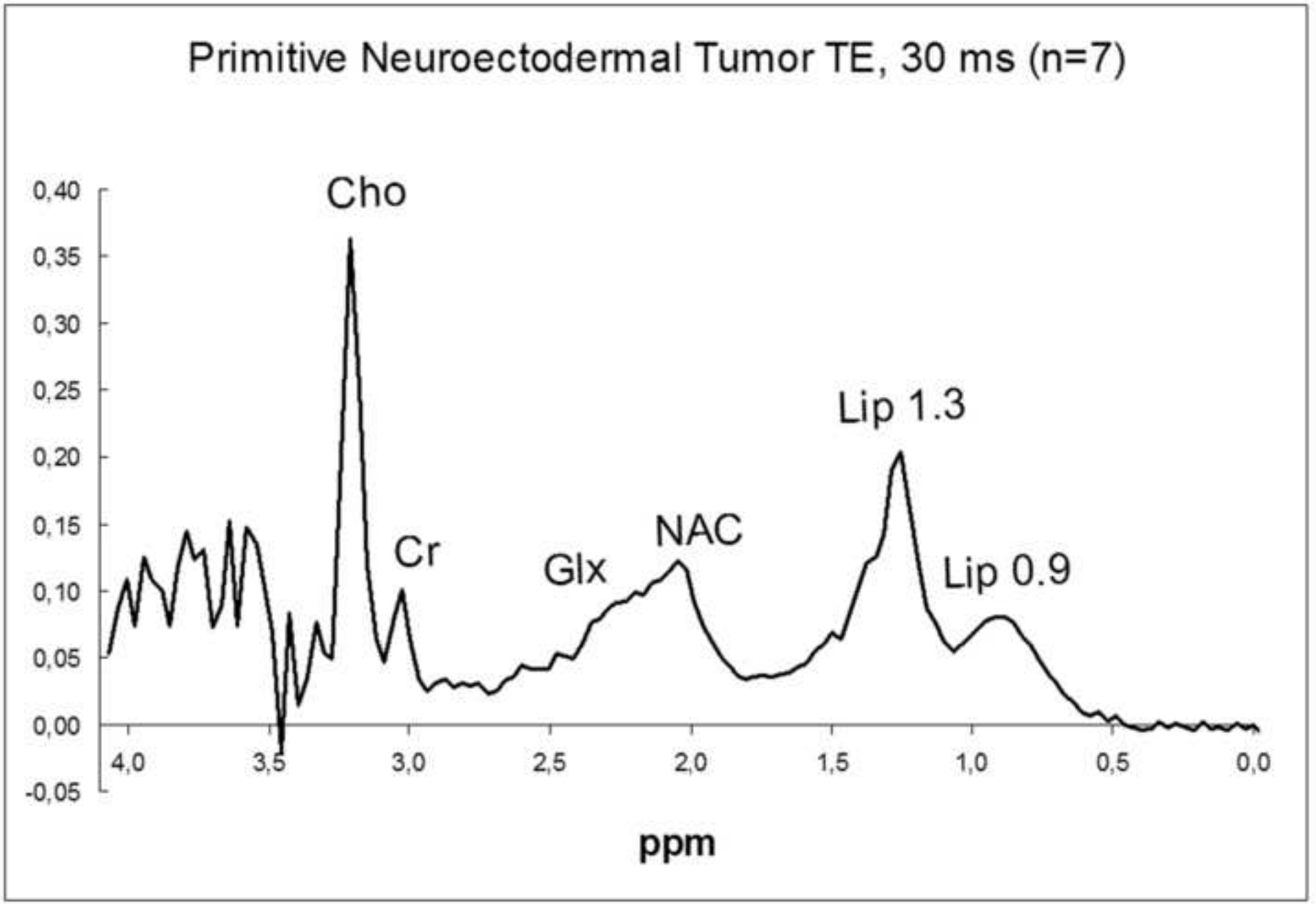

Figure 1D

Click here to download high resolution image

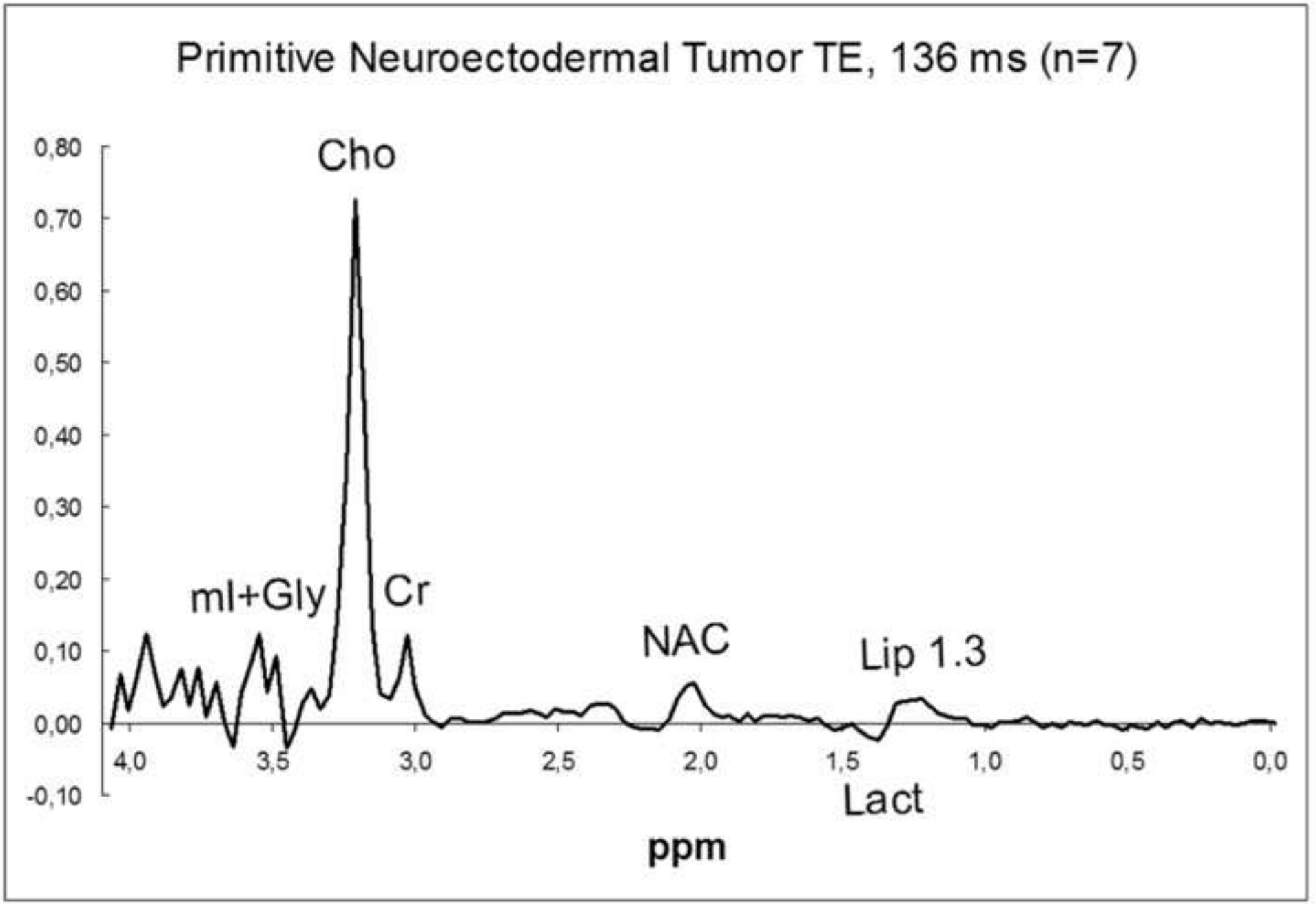

Figure 1E

Click here to download high resolution image

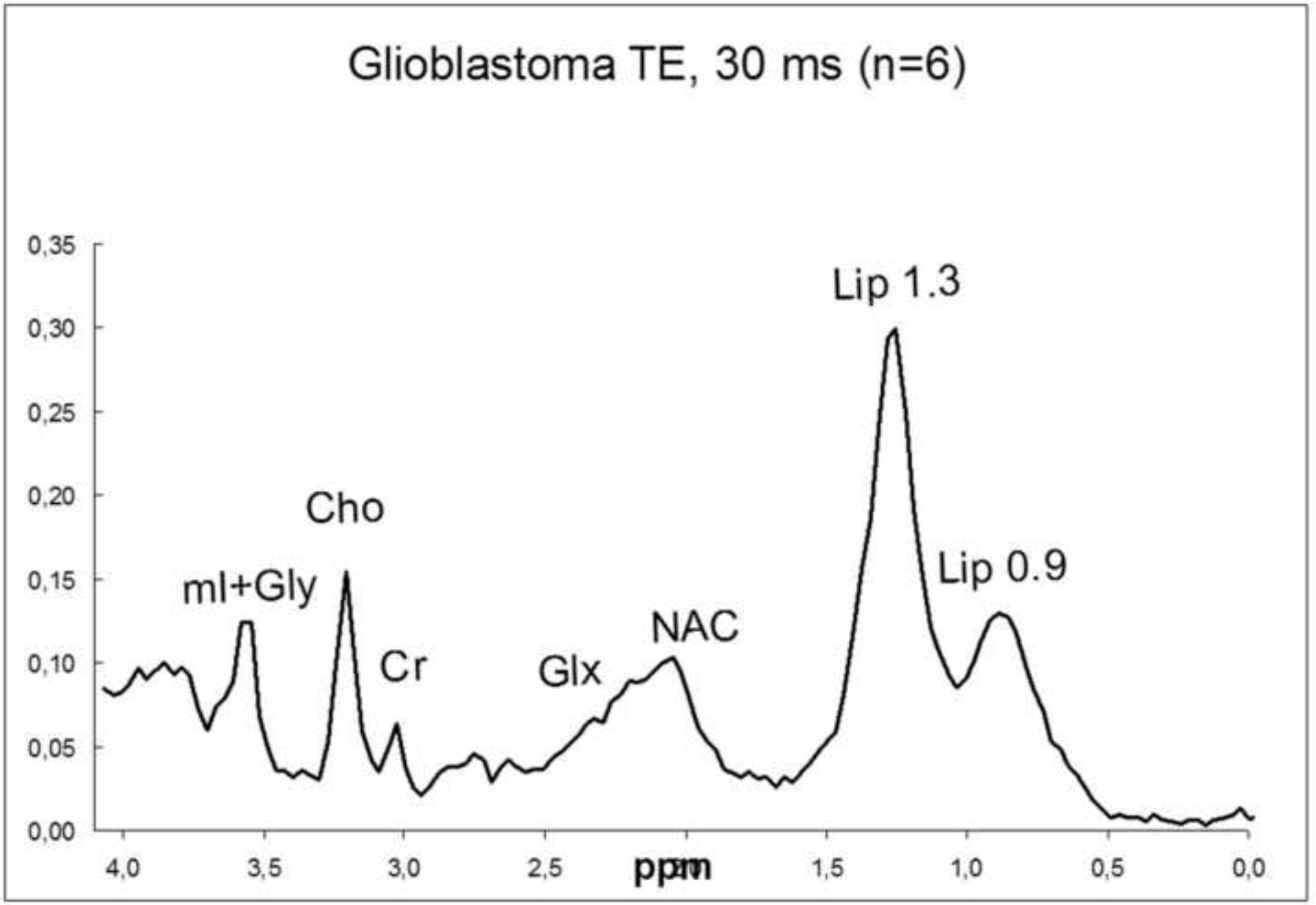

Figure 1F

Click here to download high resolution image

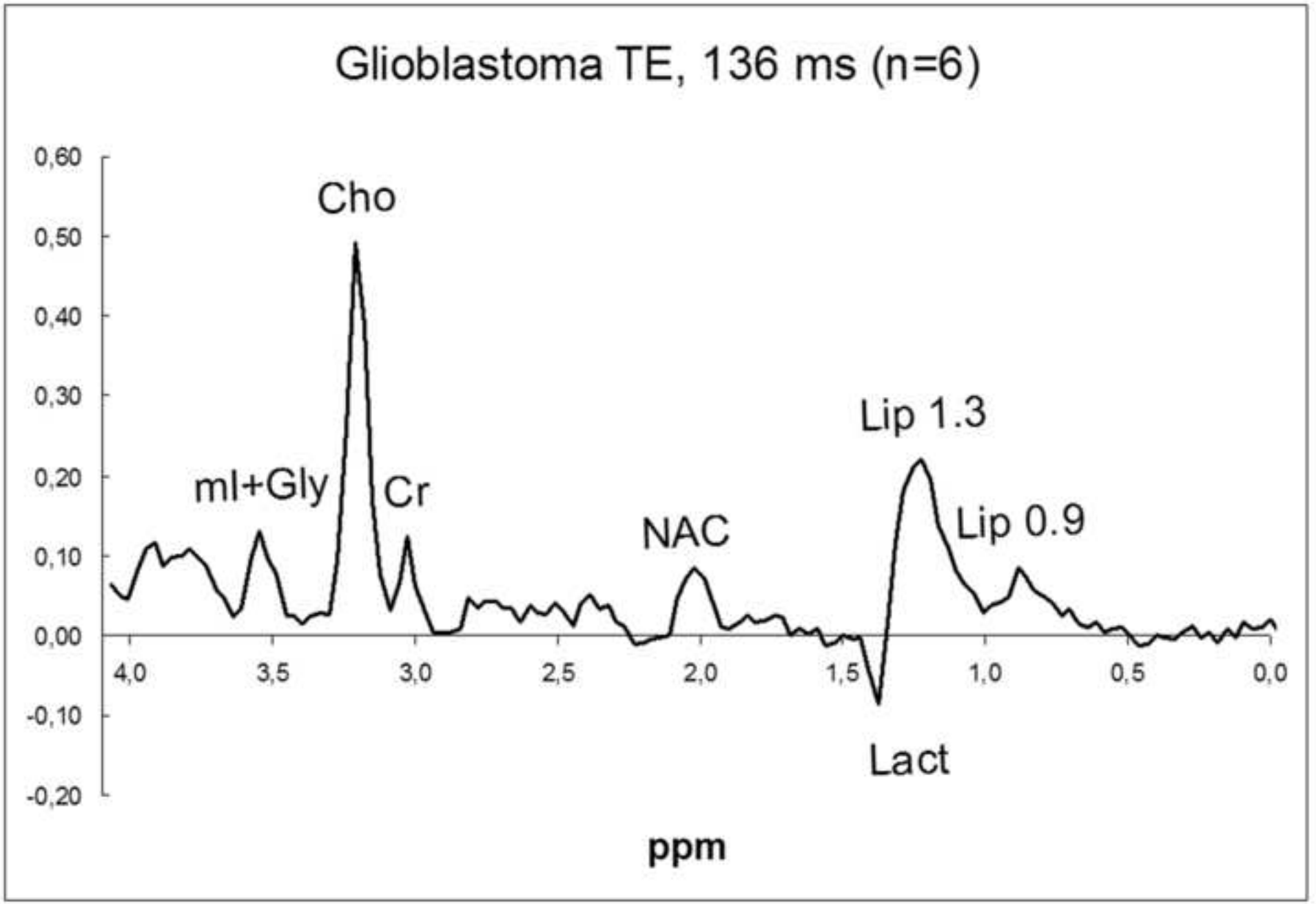

Figure 1G

Click here to download high resolution image

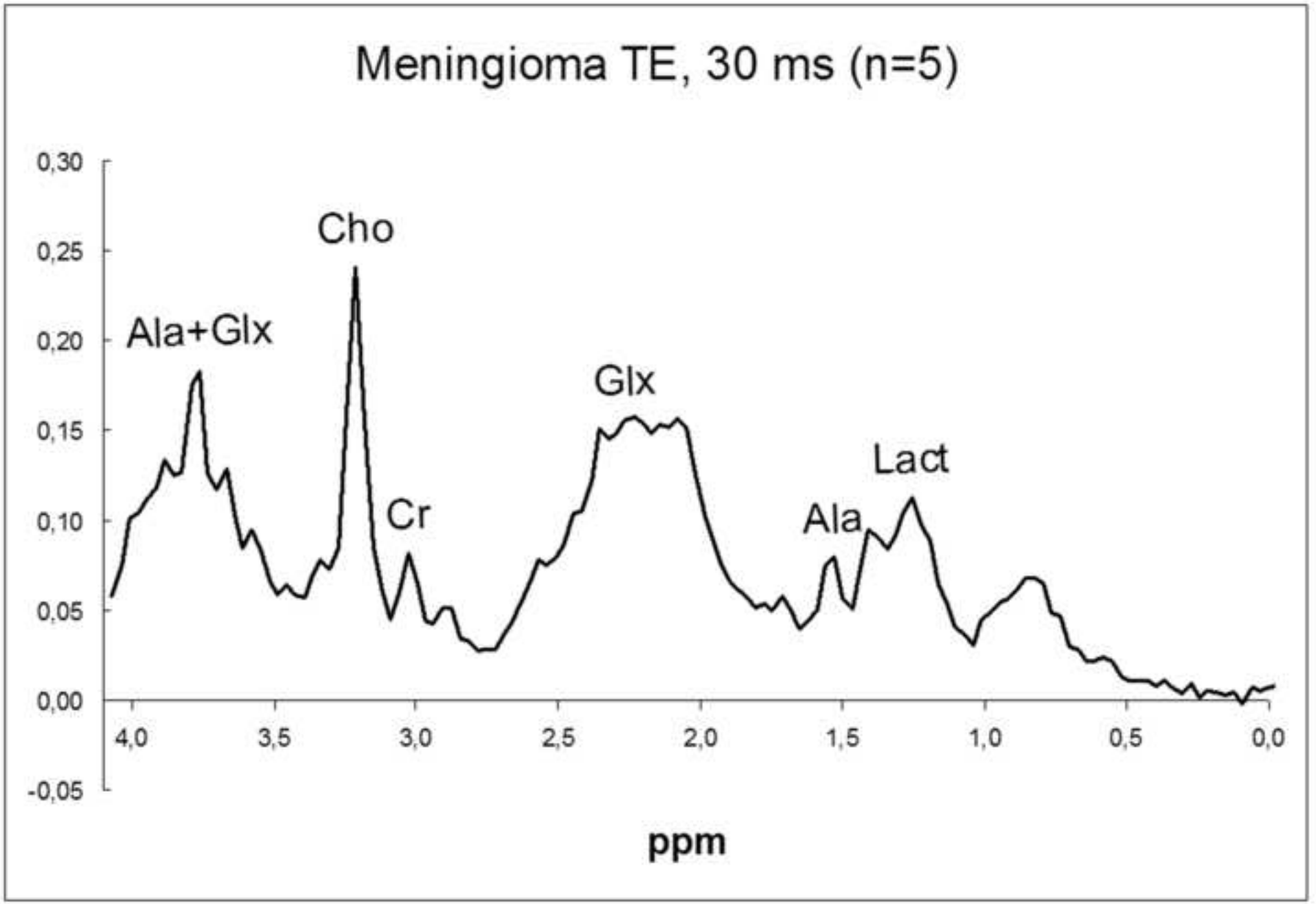

Figure 1H

Click here to download high resolution image

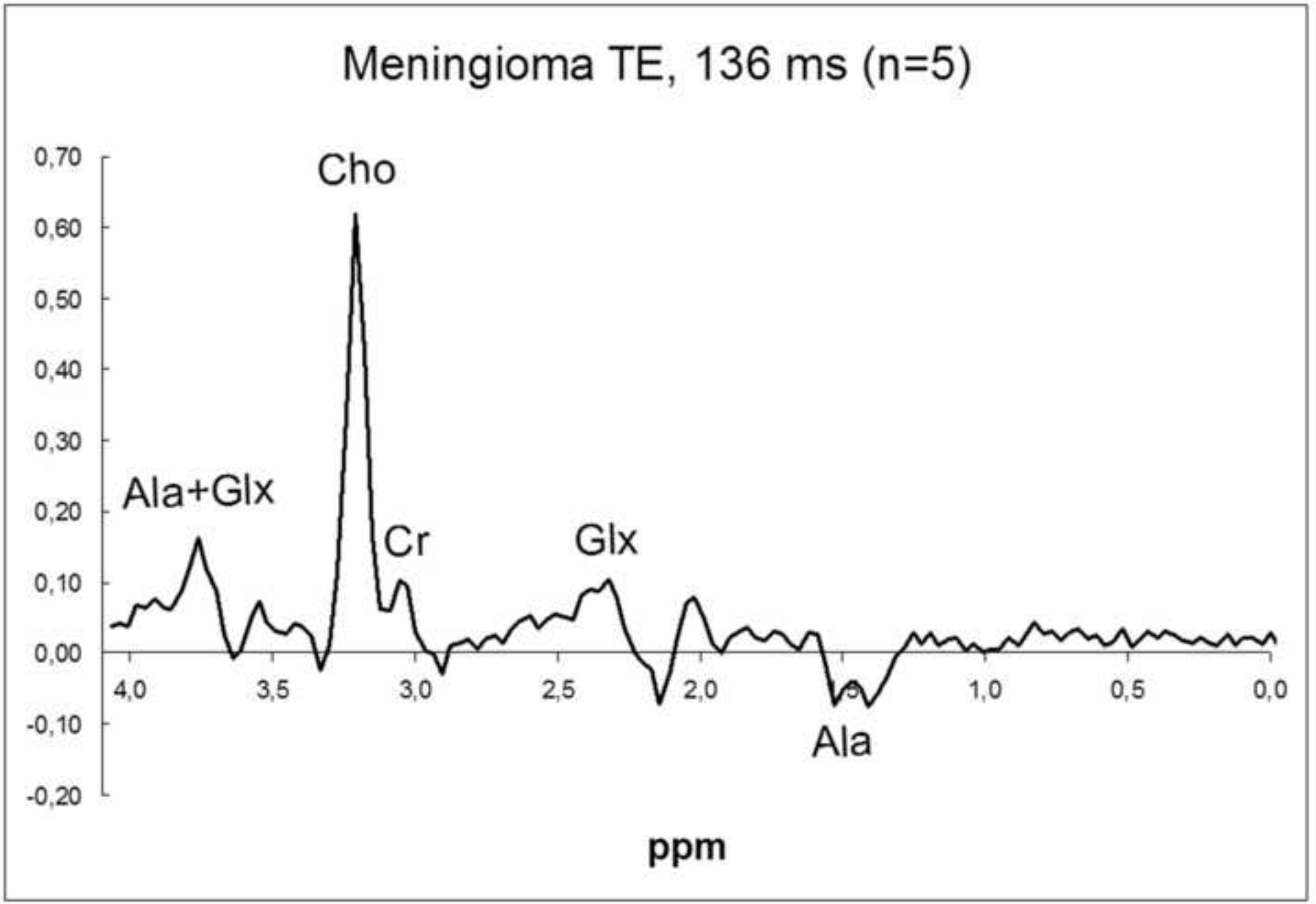

Figure 1I

Click here to download high resolution image

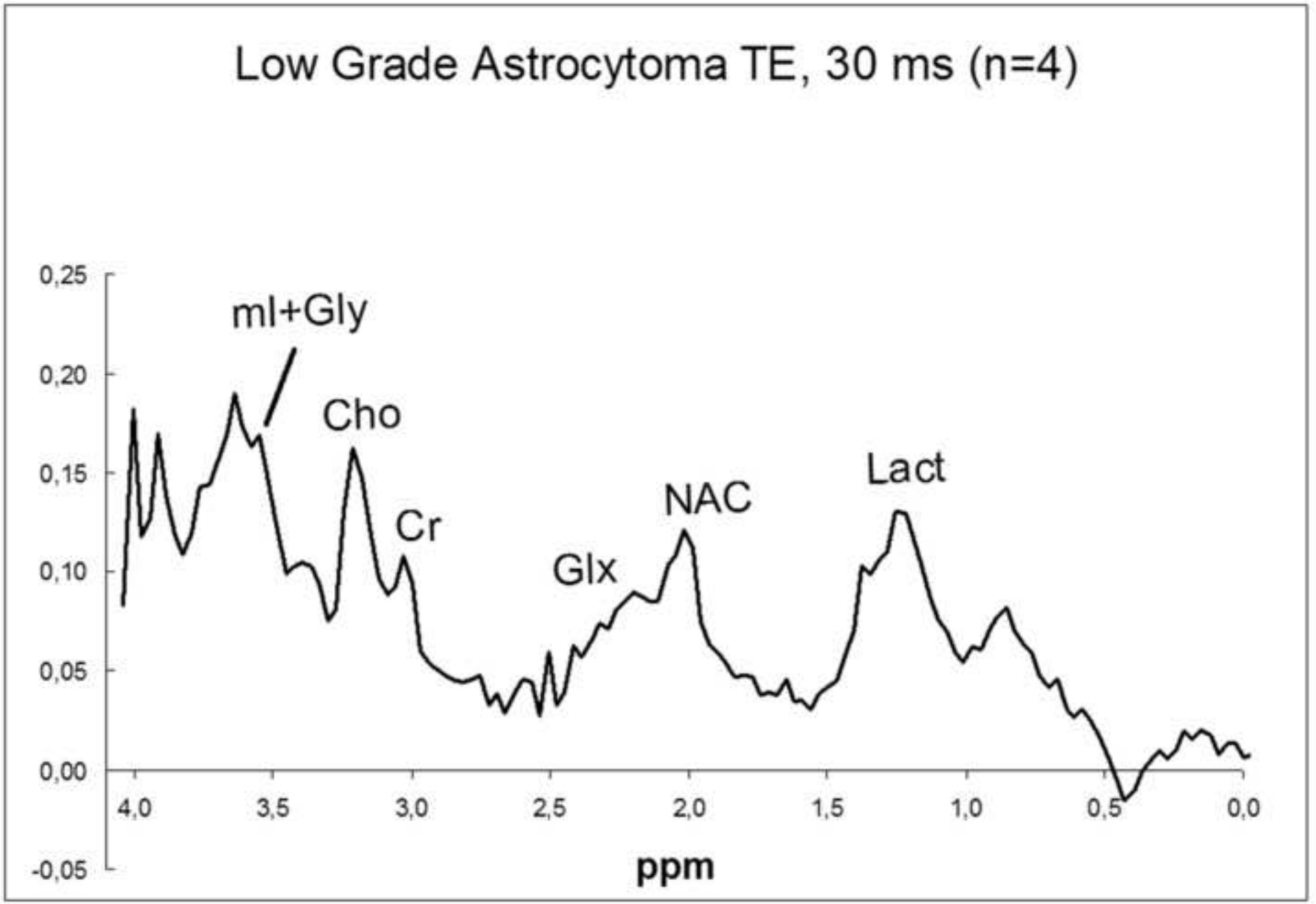

Figure 1J

Click here to download high resolution image

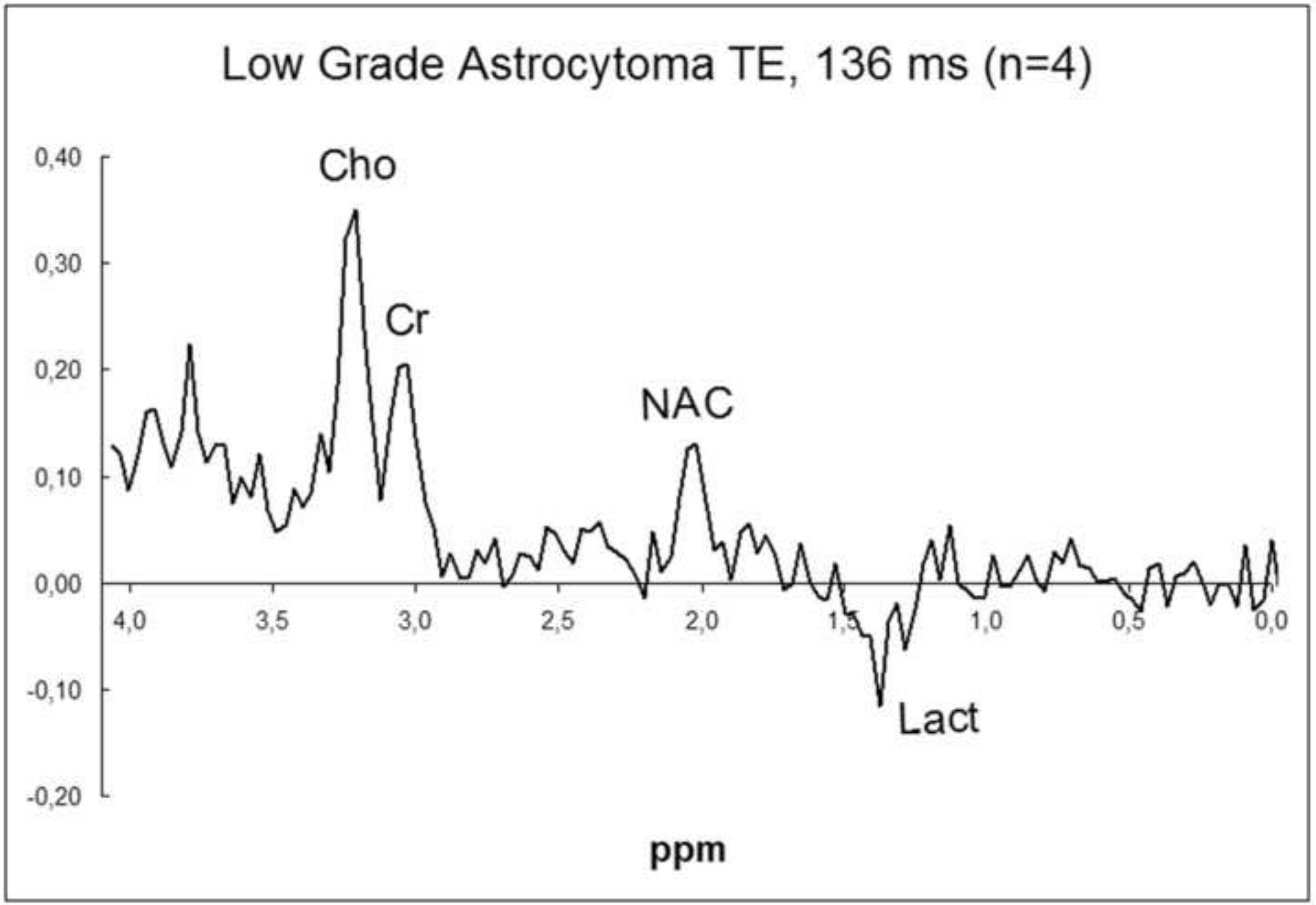

Figure 1K

Click here to download high resolution image

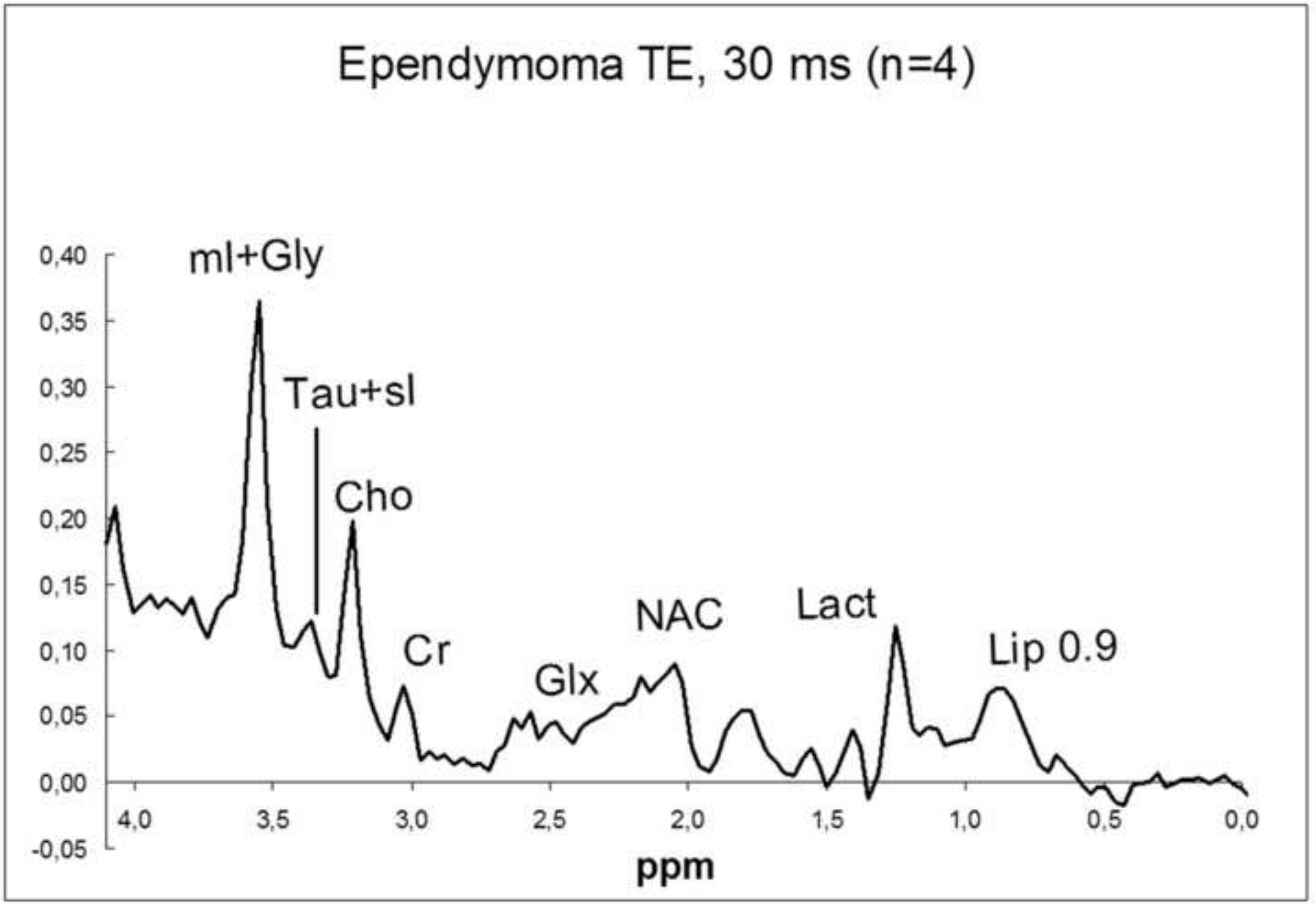

Figure 1L

Click here to download high resolution image

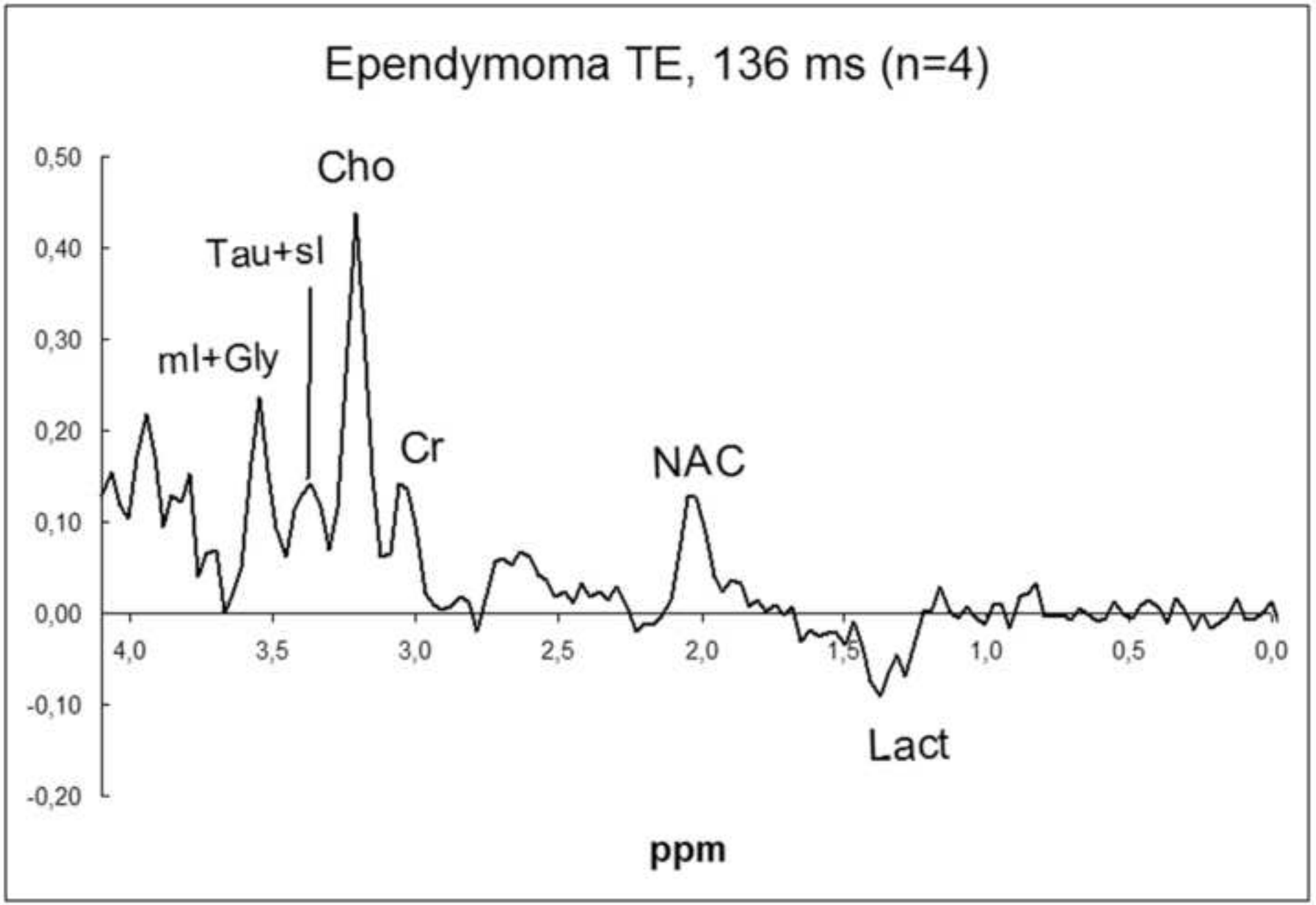

Figure 1M

Click here to download high resolution image

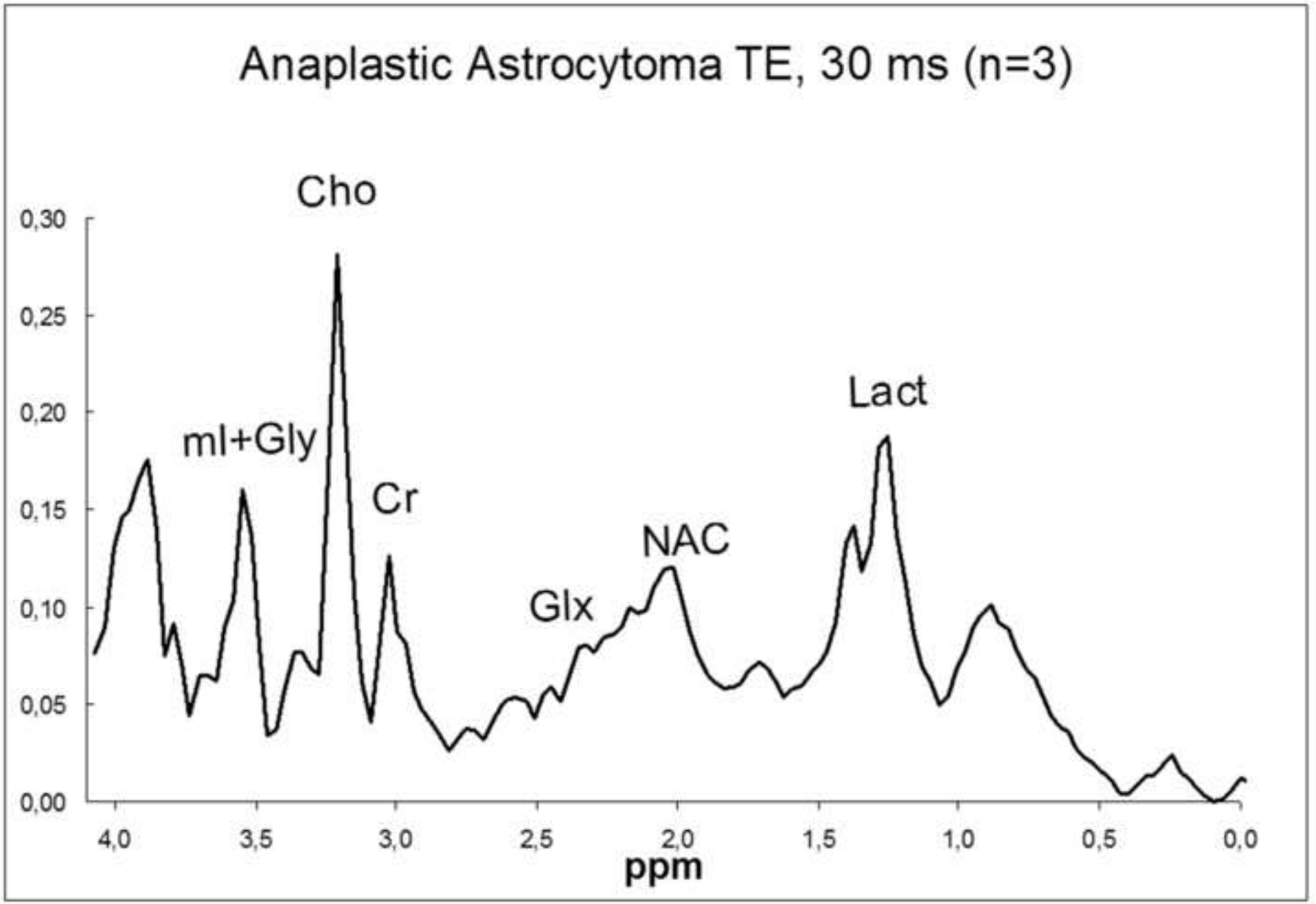

Figure 1N

Click here to download high resolution image

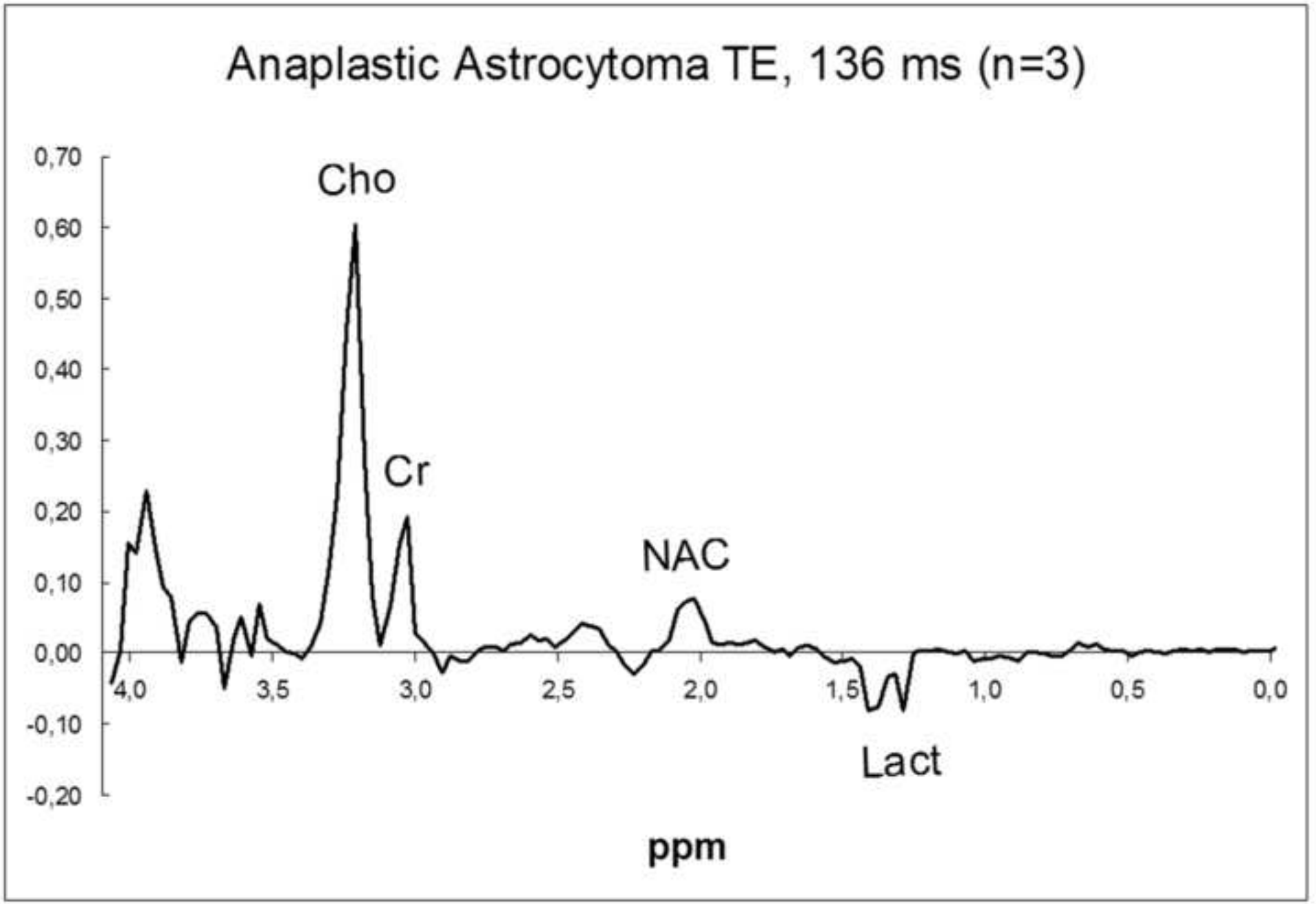

Figure 1O

Click here to download high resolution image

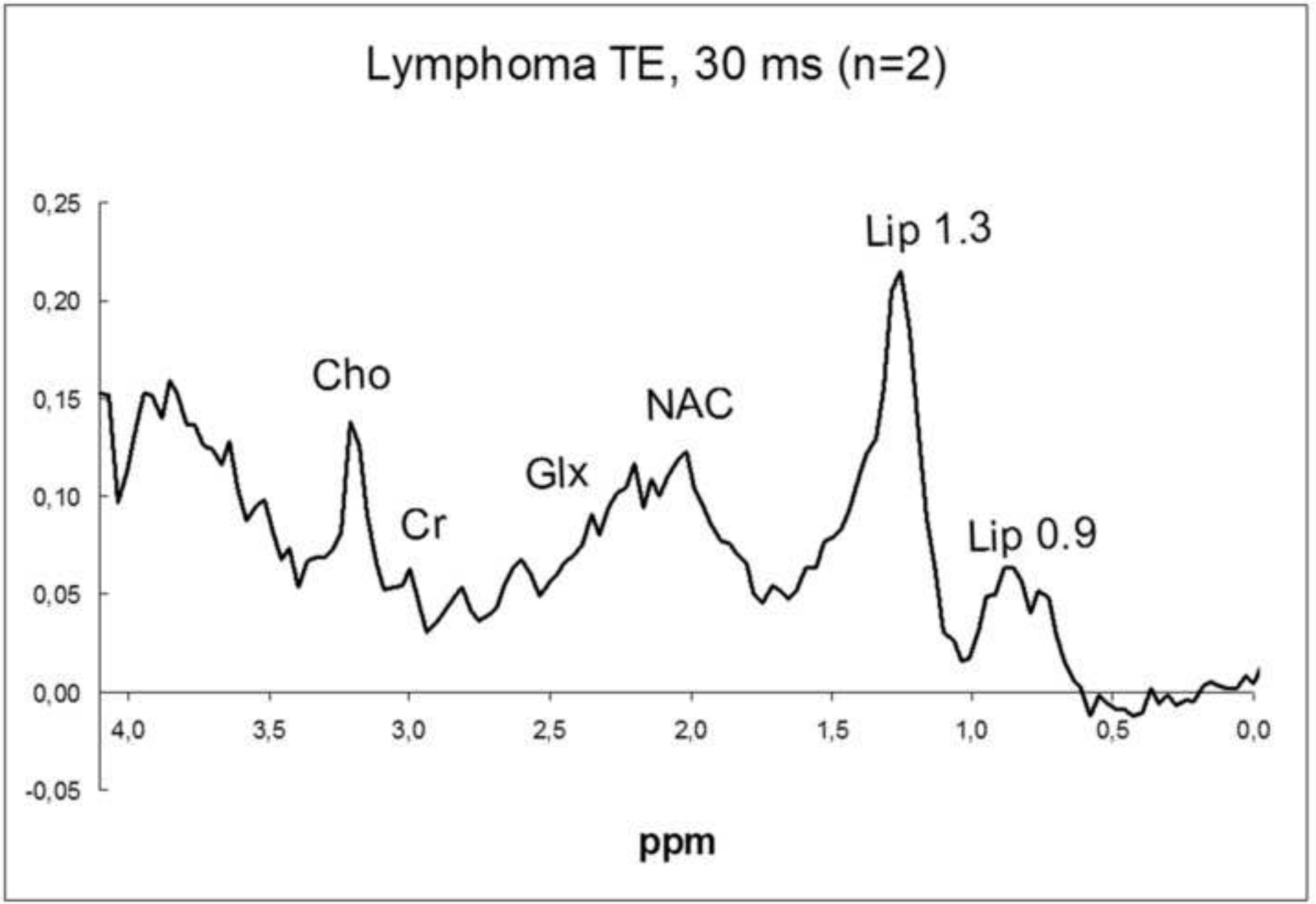

Figure 1P

Click here to download high resolution image

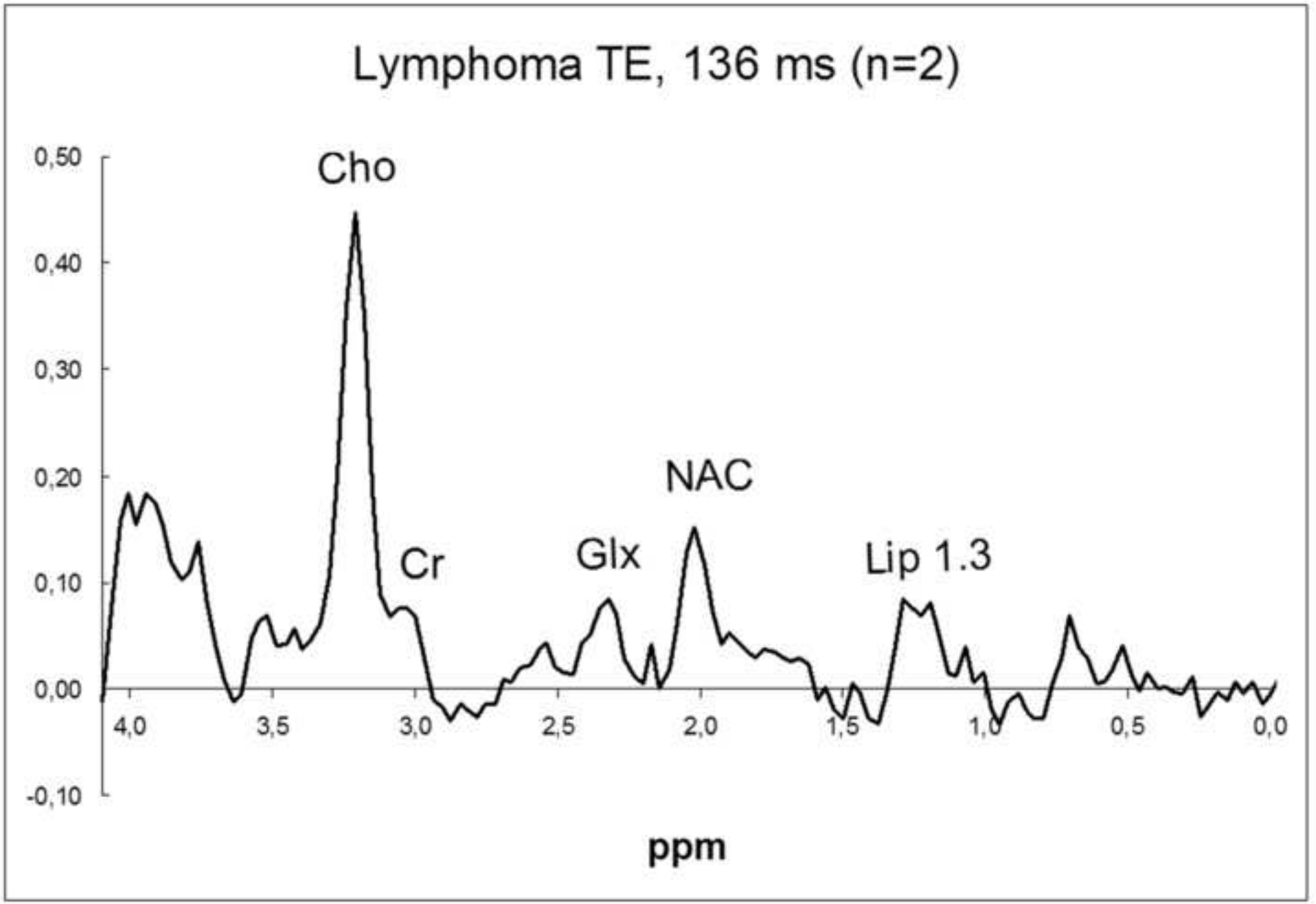

Figure 1Q

Click here to download high resolution image

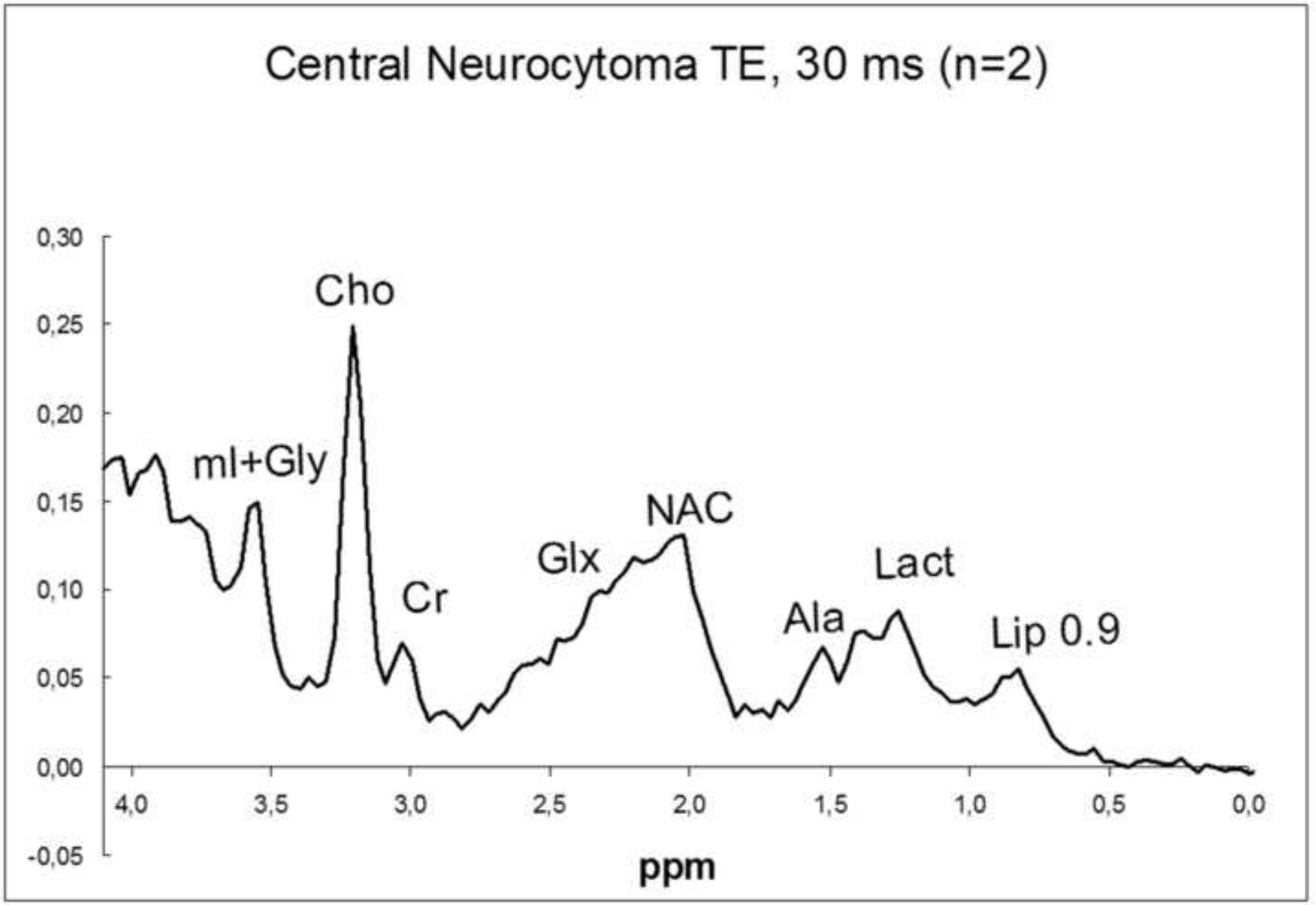

Figure 1R

Click here to download high resolution image

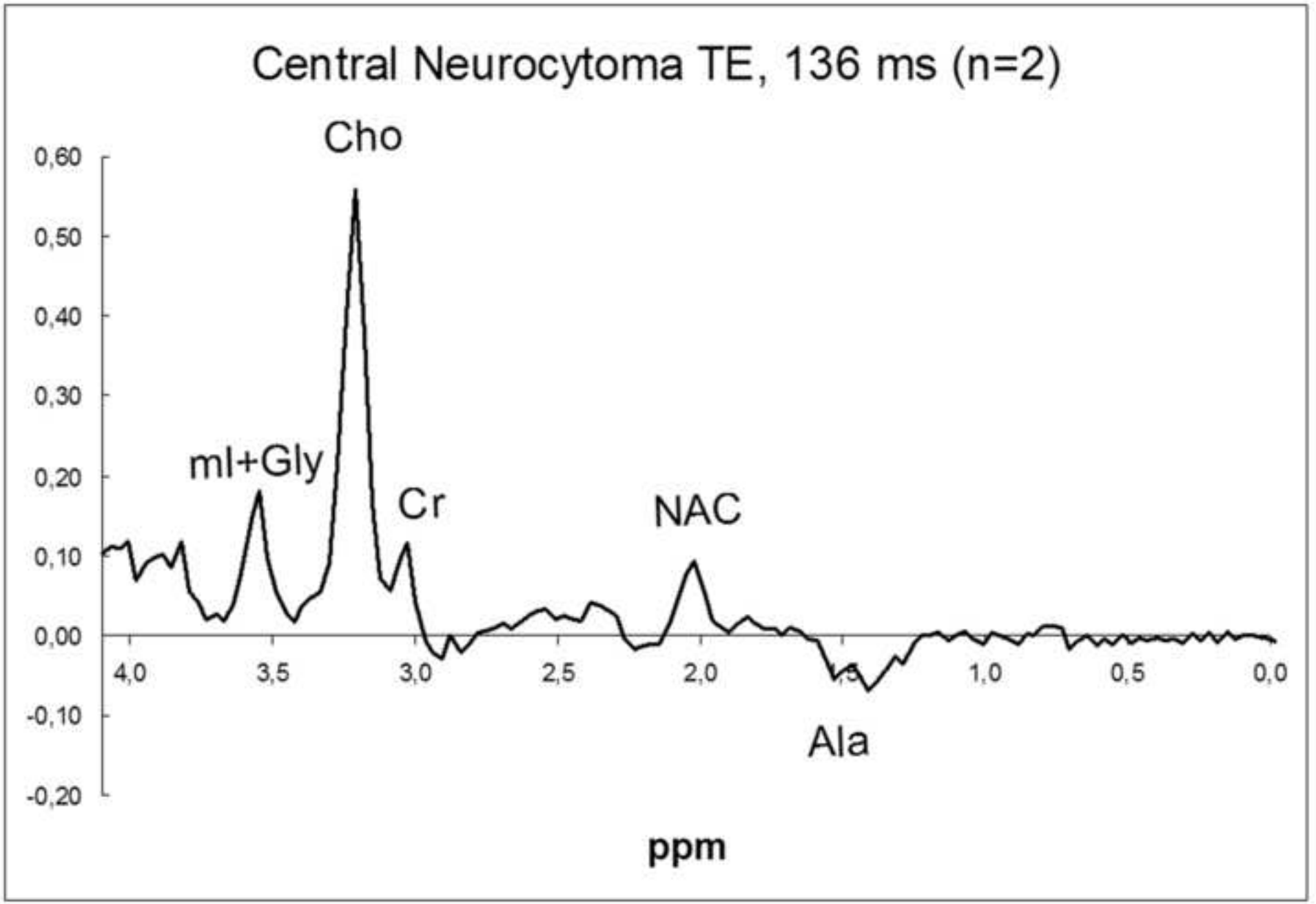

Figure 1S

Click here to download high resolution image

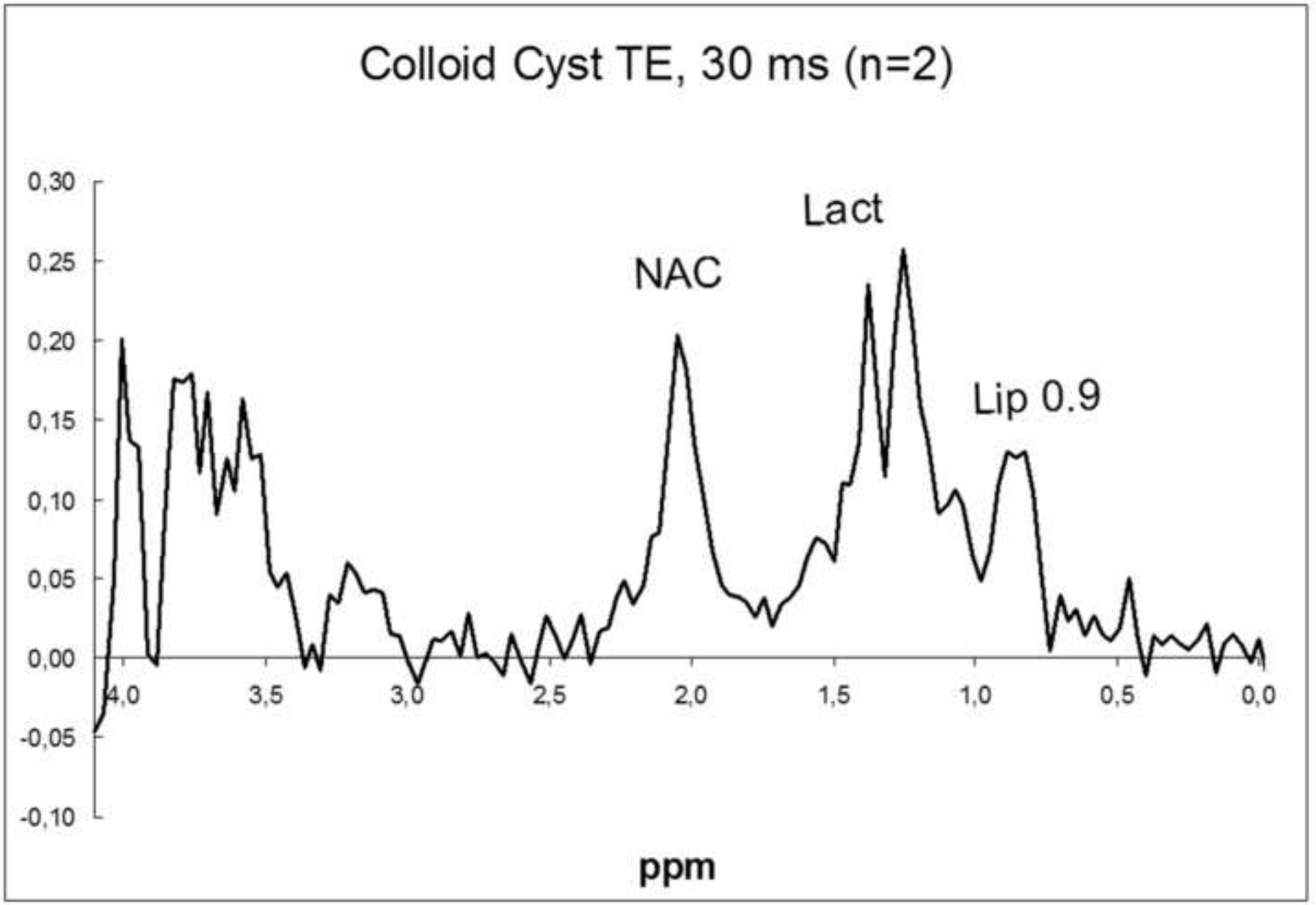

Figure 1T

Click here to download high resolution image

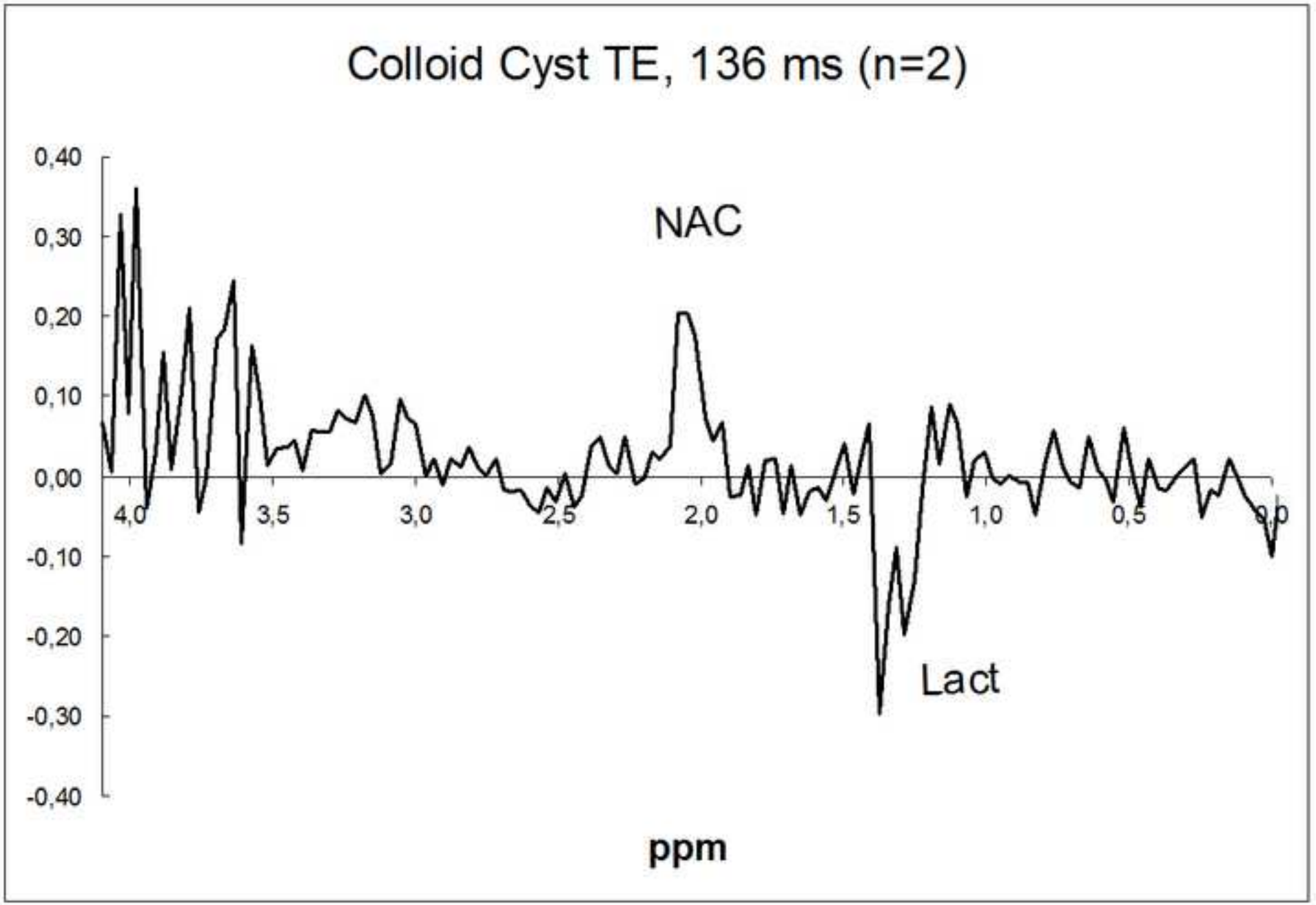

Figure 1U

Click here to download high resolution image

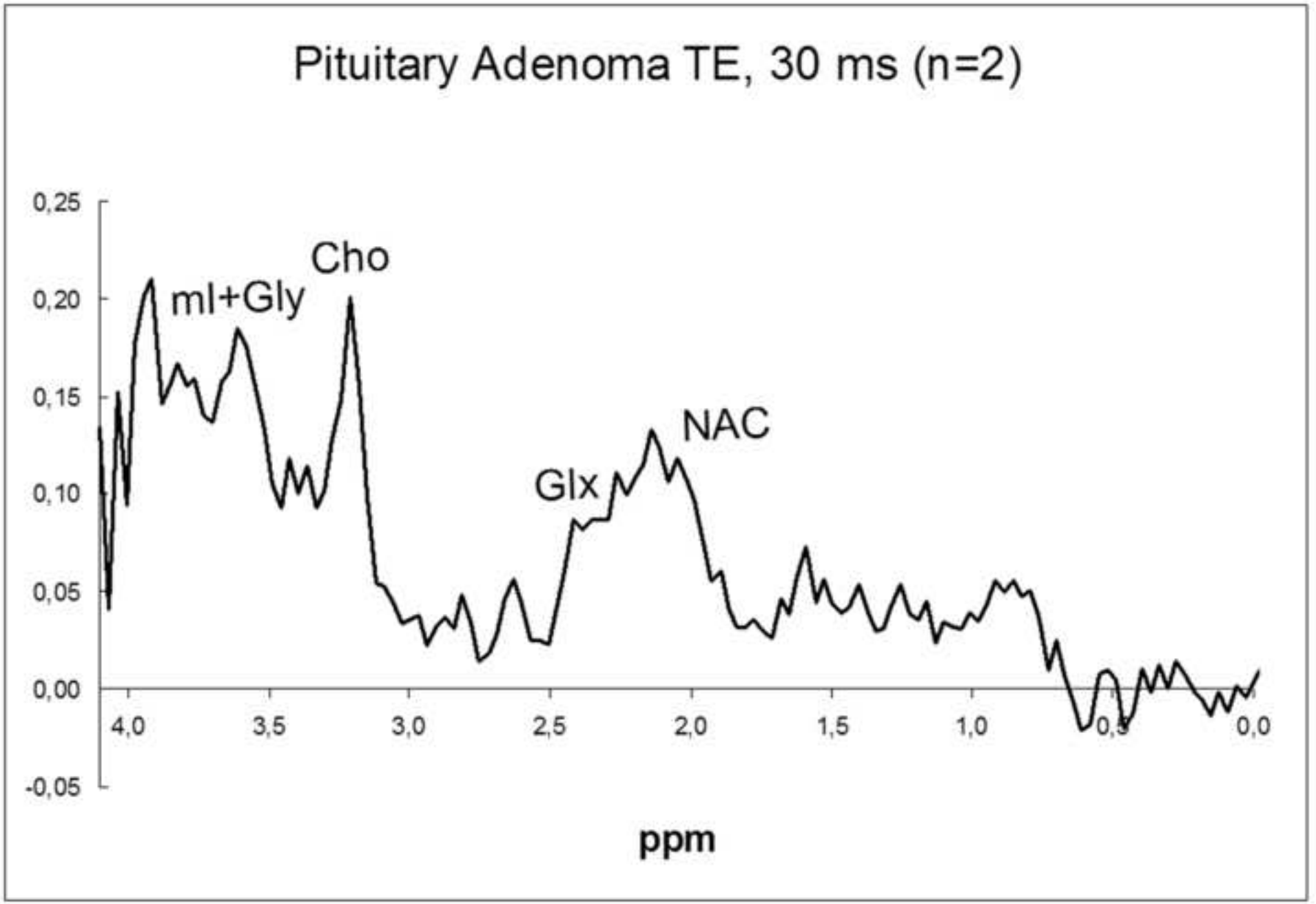

Figure 1V

Click here to download high resolution image

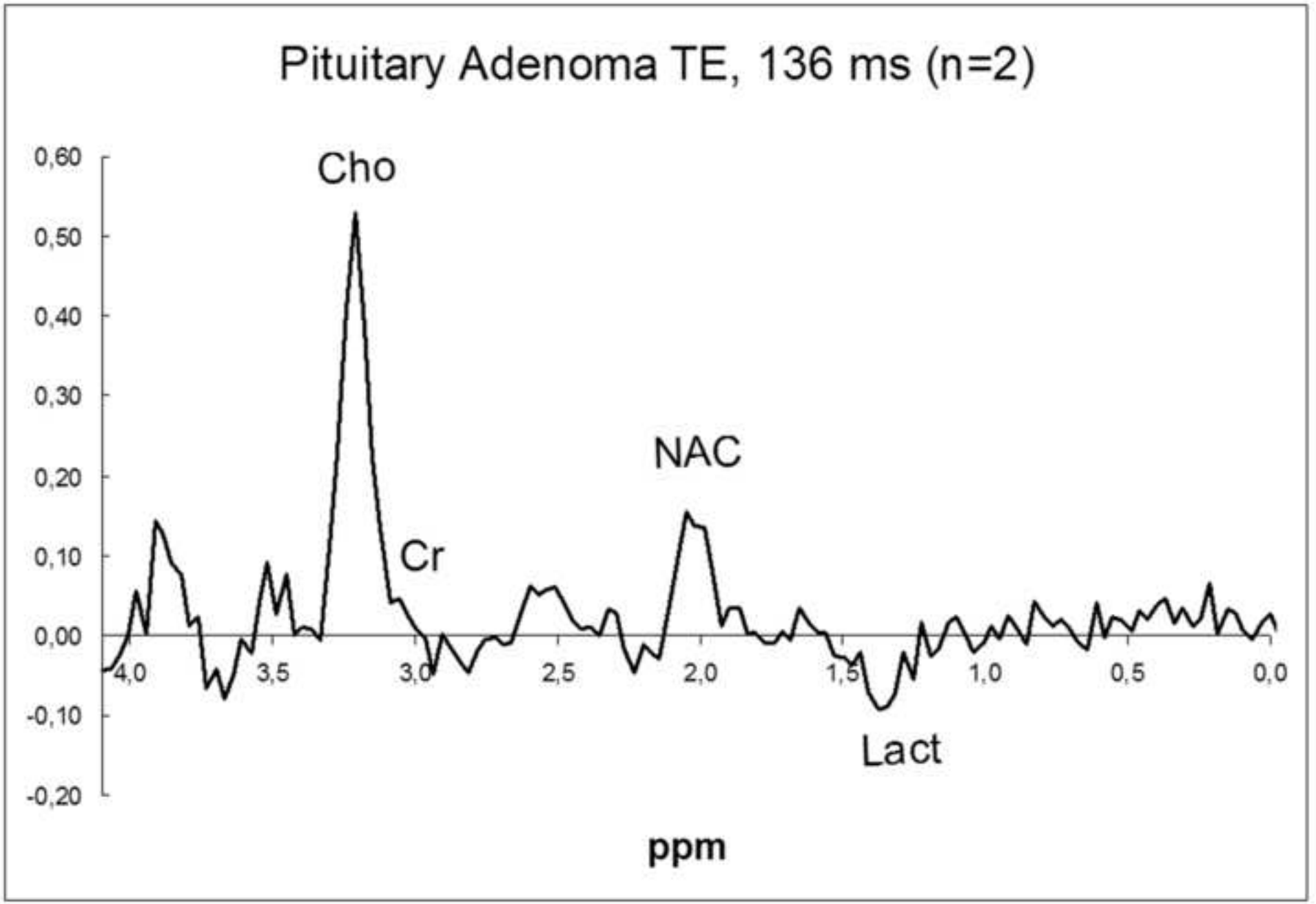

Figure 1W

Click here to download high resolution image

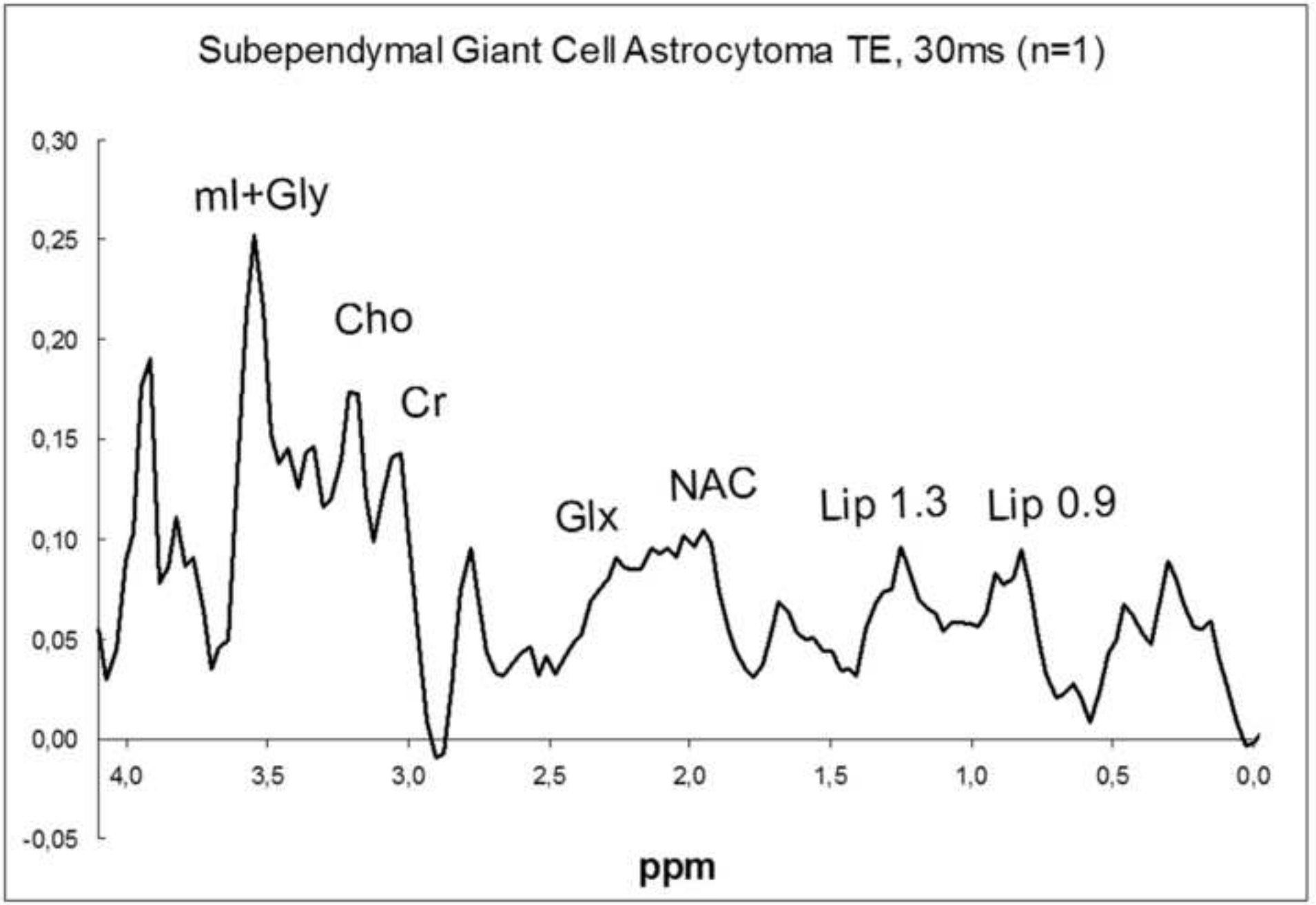

Figure 1X

Click here to download high resolution image

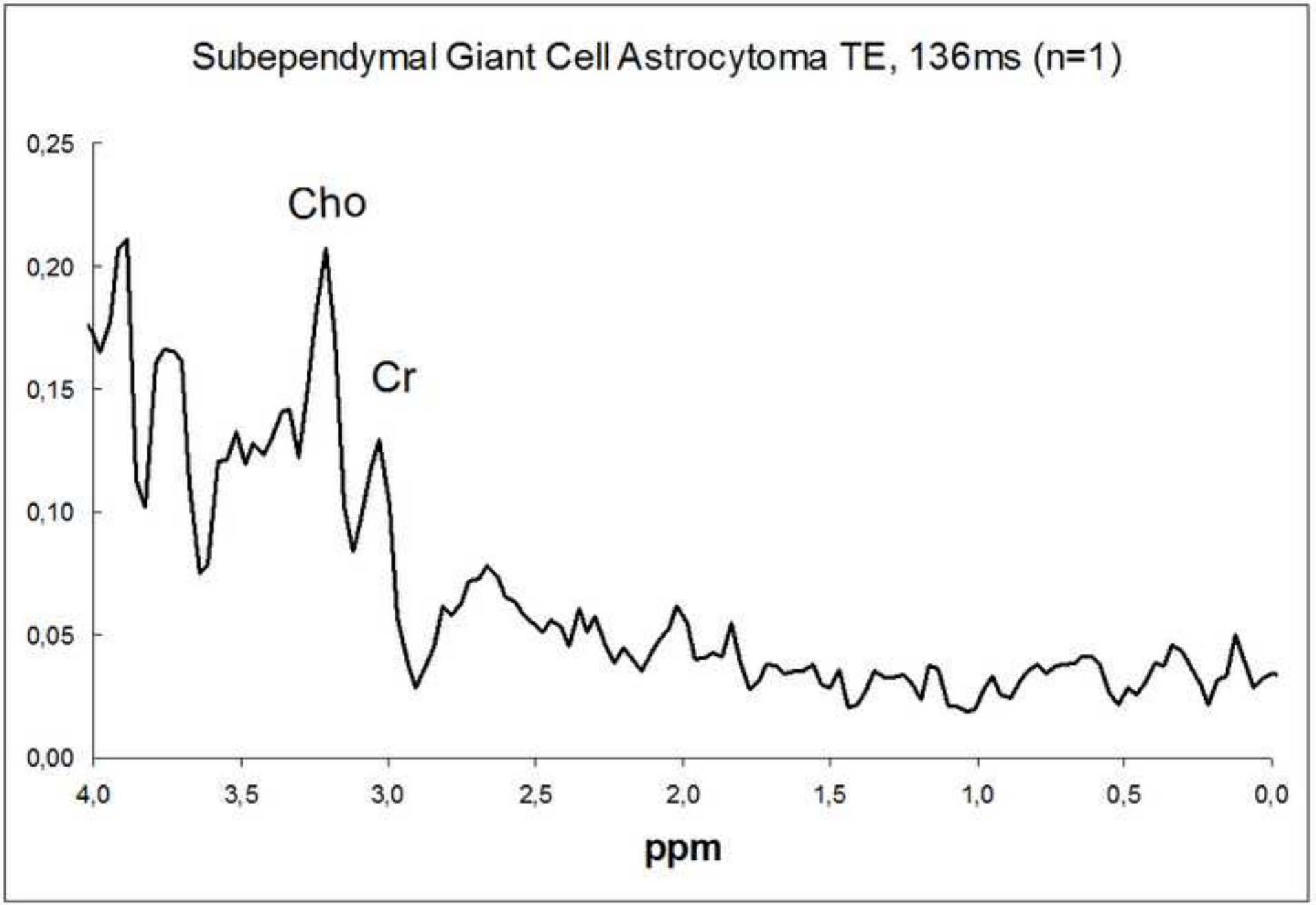

Figure 1Y

Click here to download high resolution image

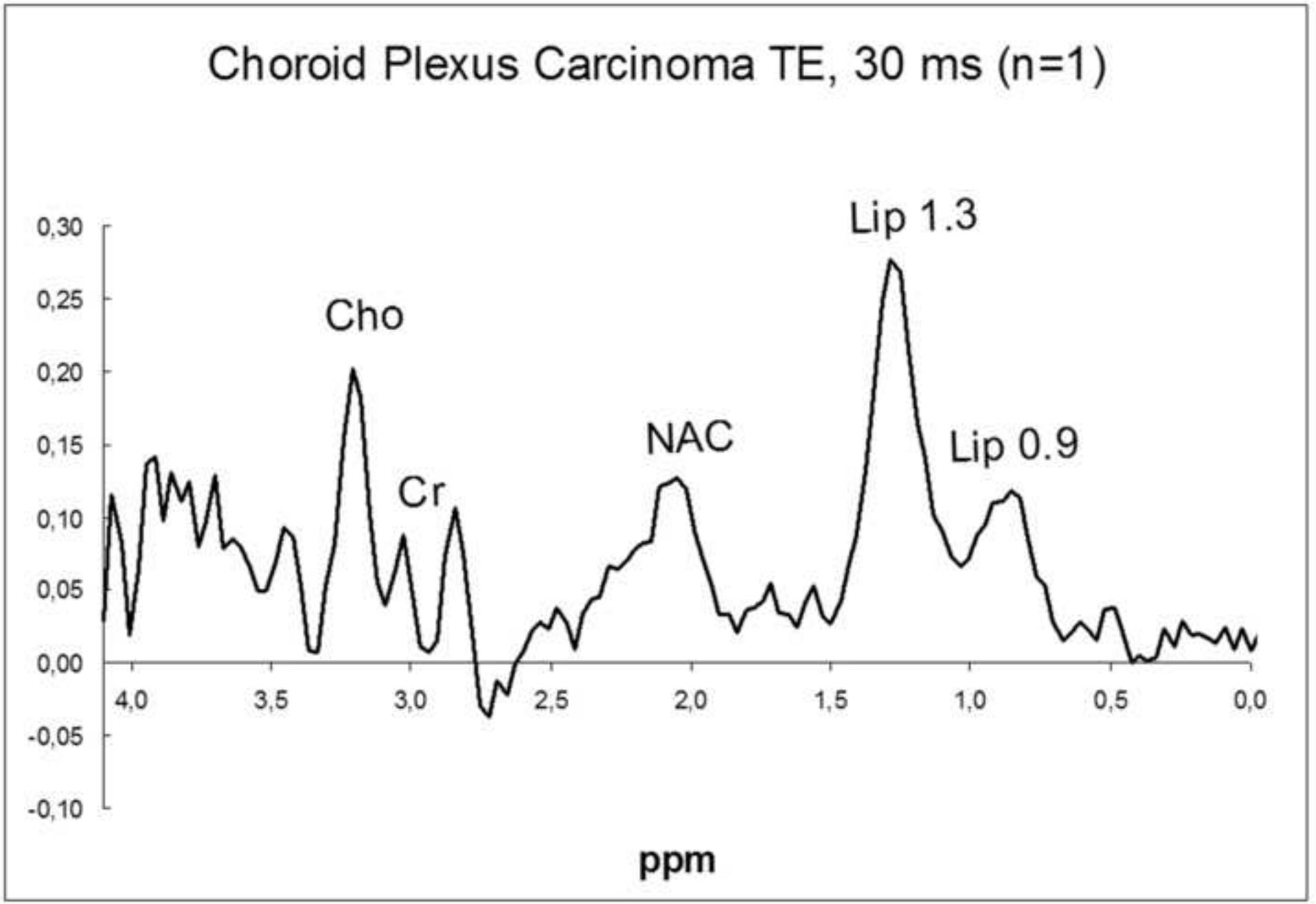

Figure 1Z

Click here to download high resolution image

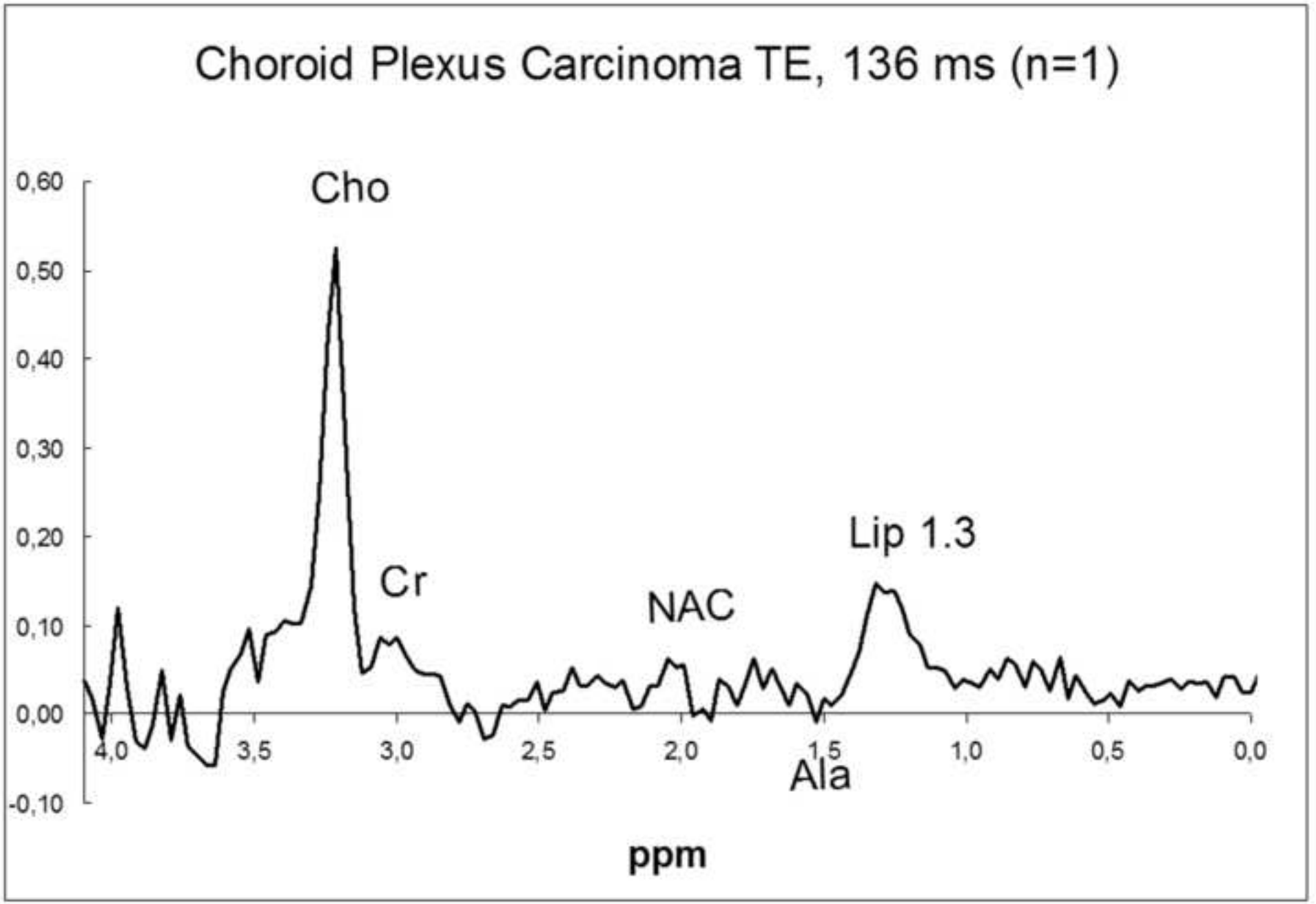

Figure 1AA

Click here to download high resolution image

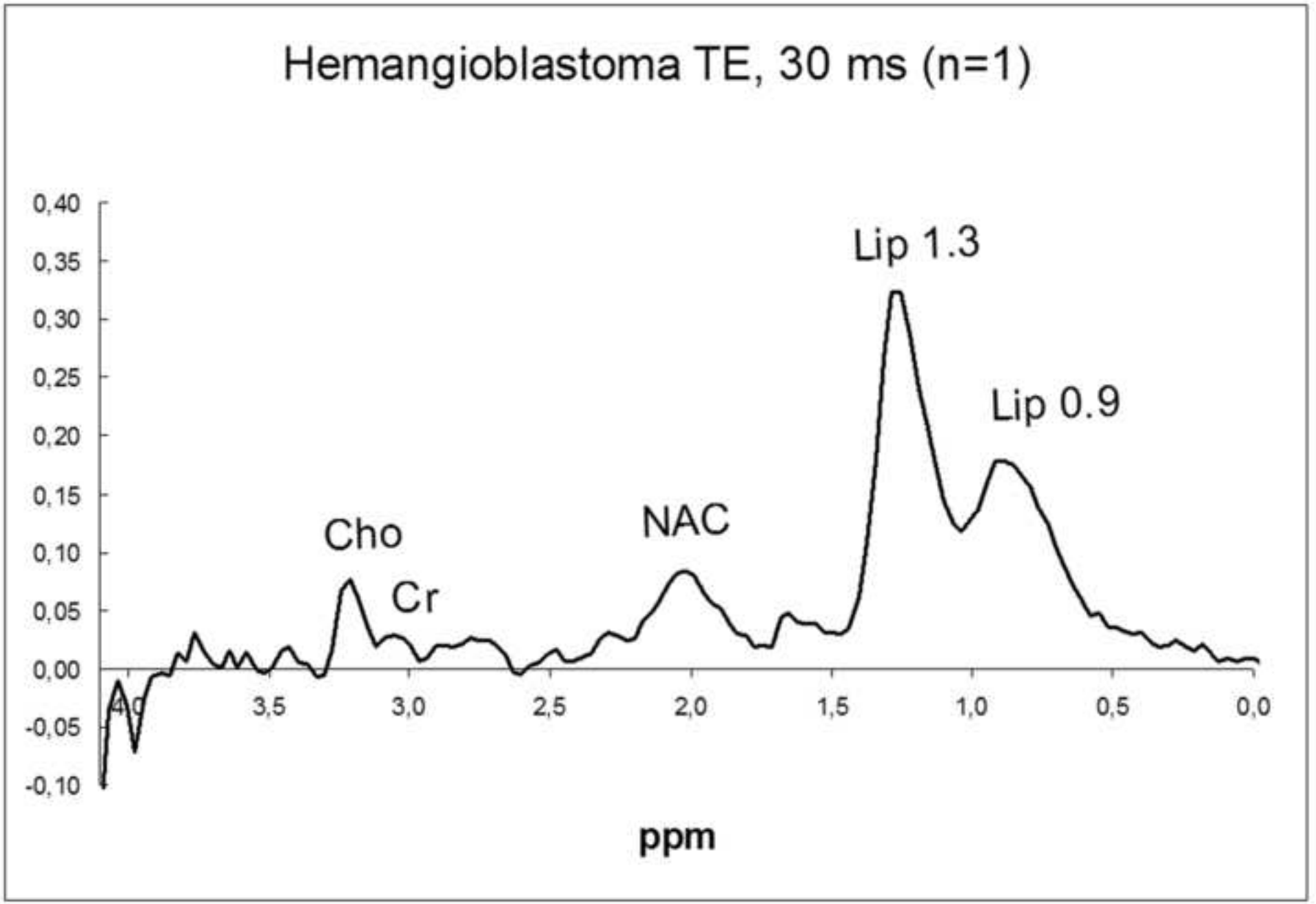

Figure 1AB

Click here to download high resolution image

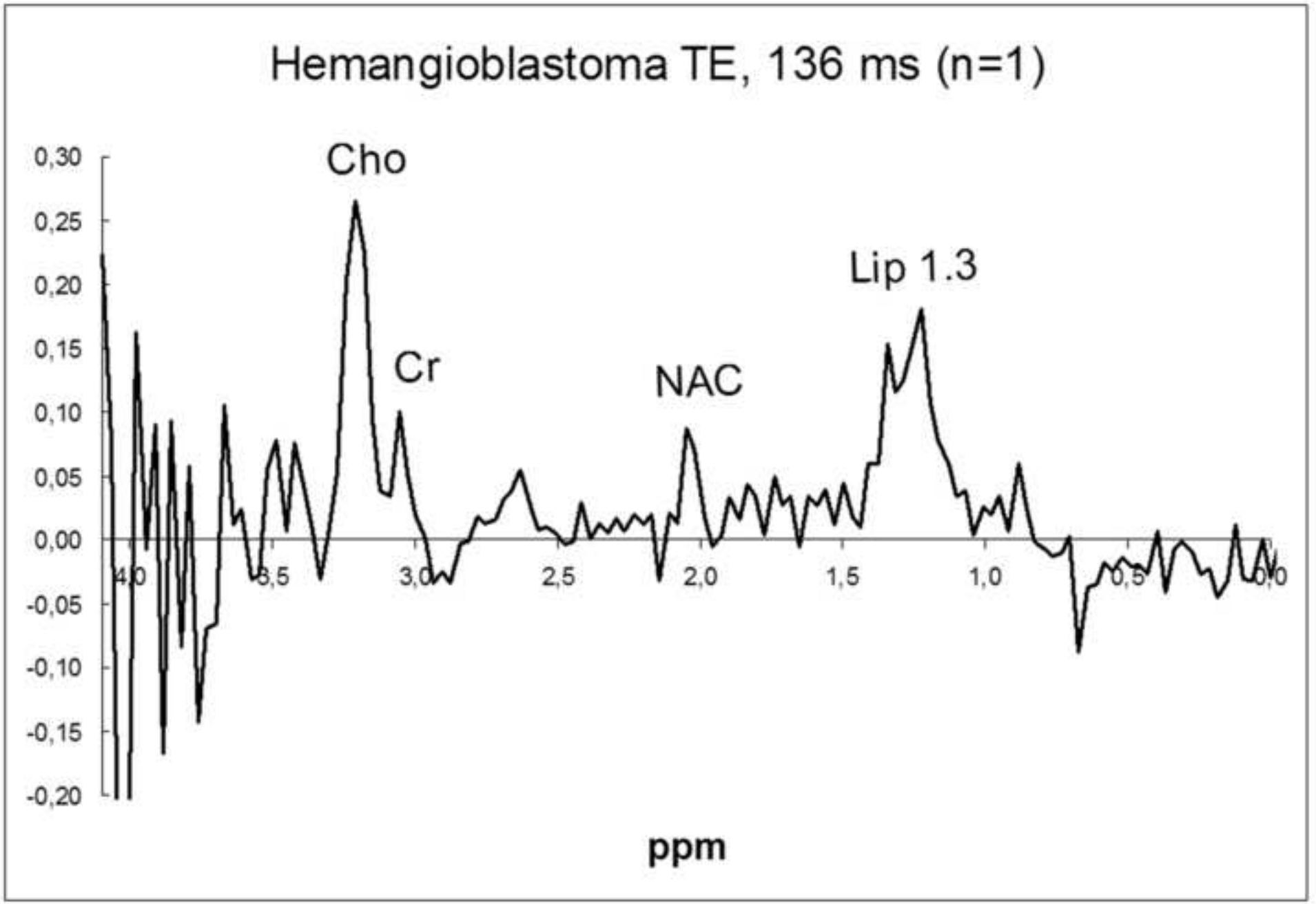

Figure 1AC

Click here to download high resolution image

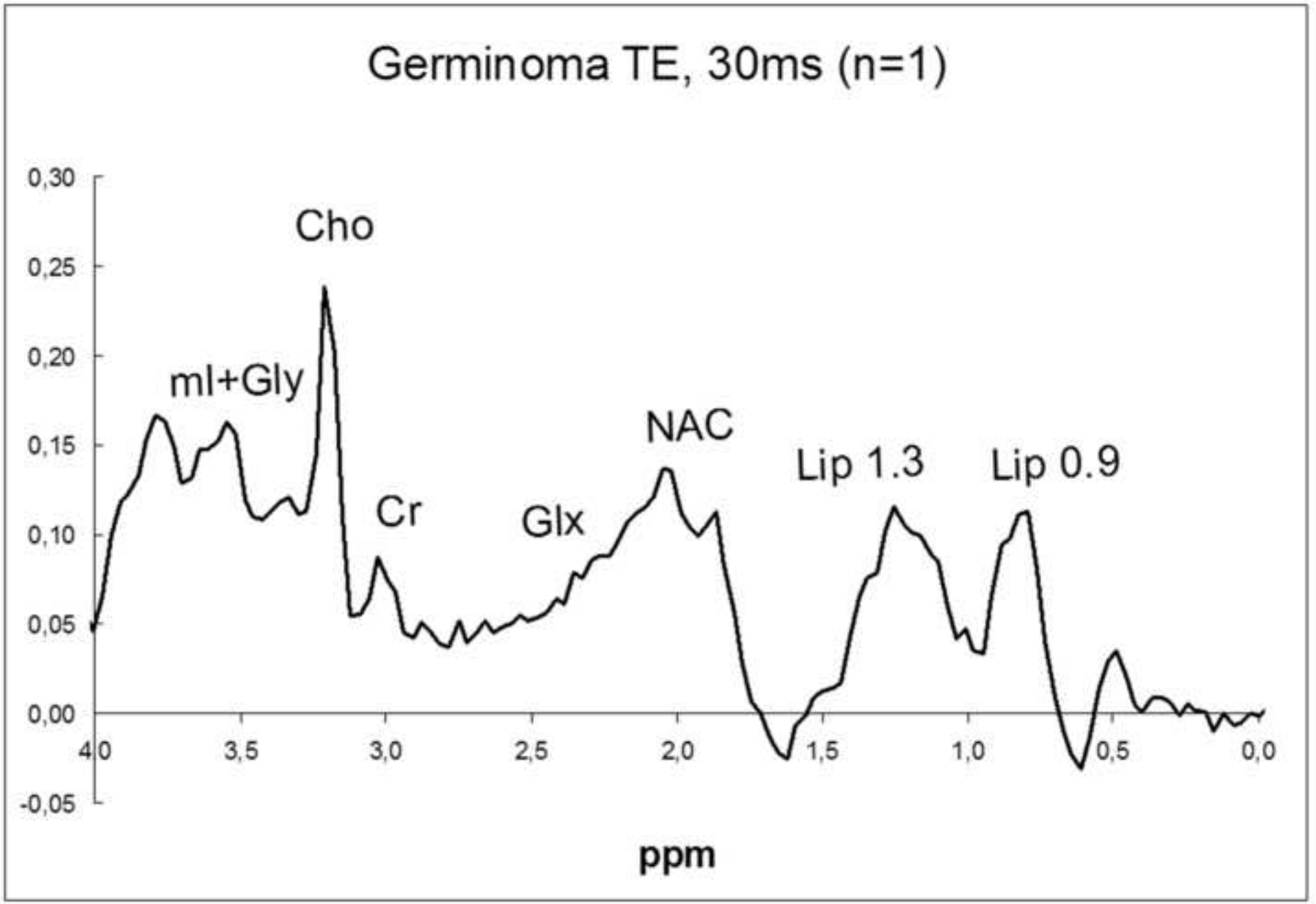

Figure 1AD

Click here to download high resolution image

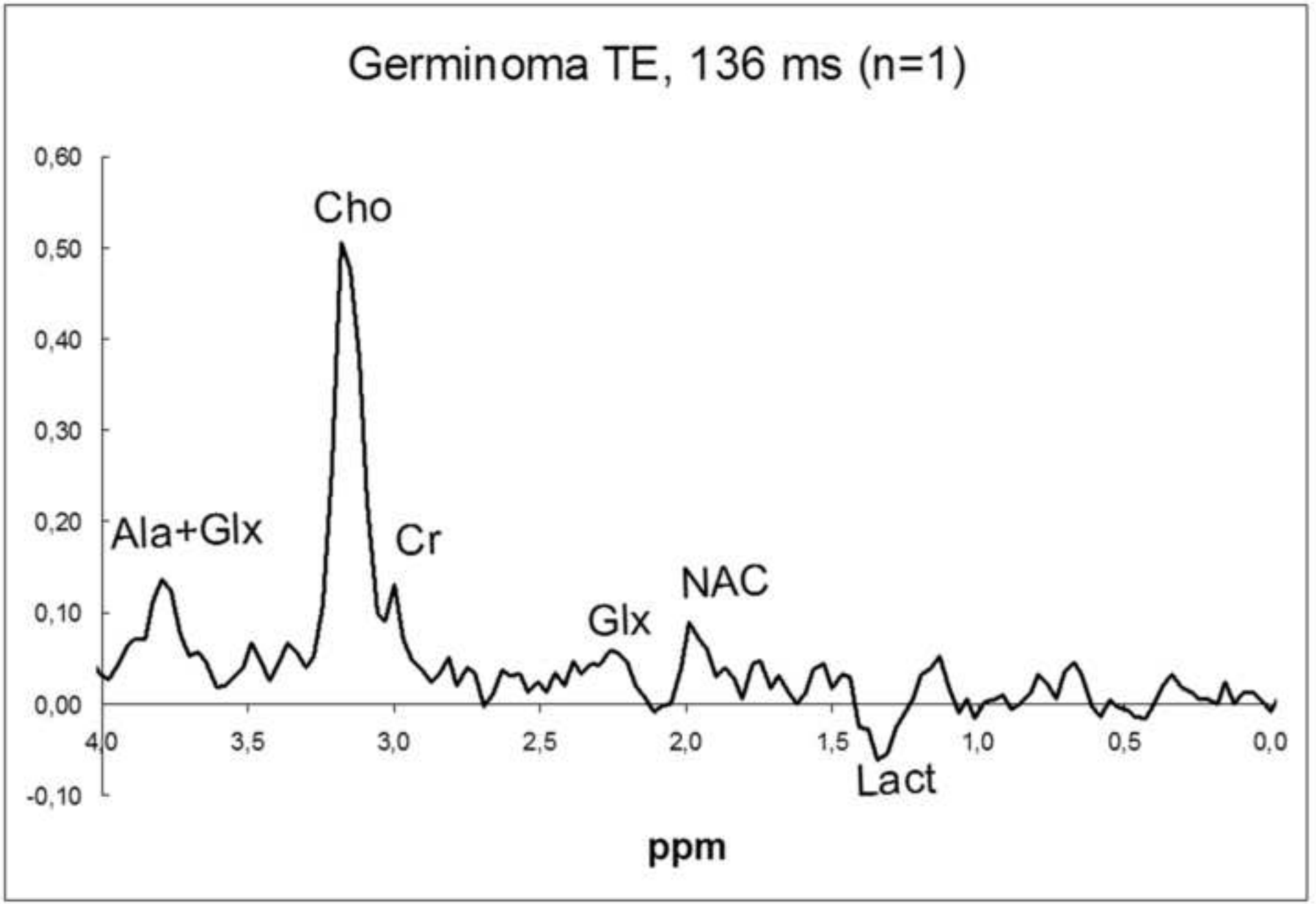

Figure 2A

Click here to download high resolution image

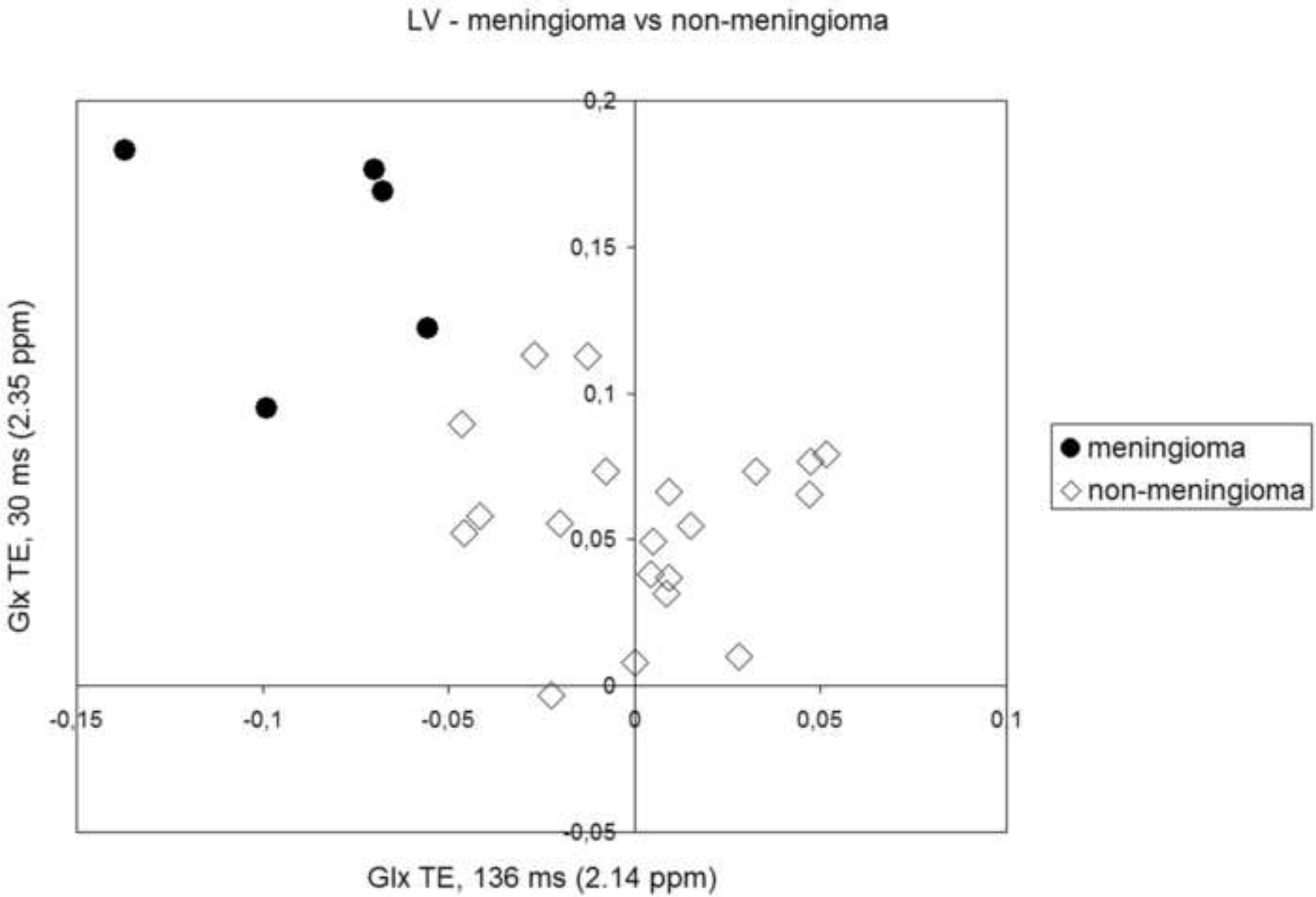

Figure 2B

Click here to download high resolution image

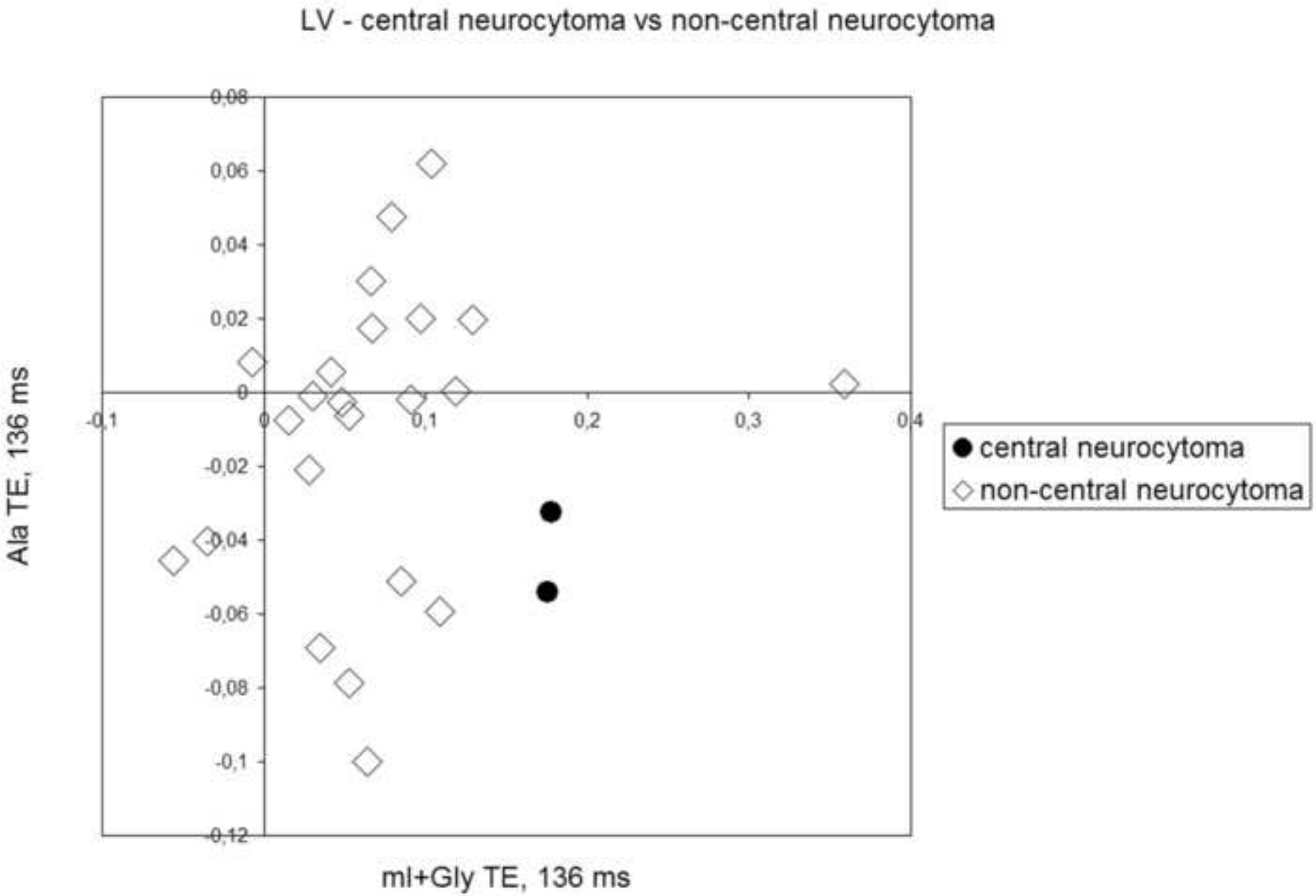

Figure 2C

Click here to download high resolution image

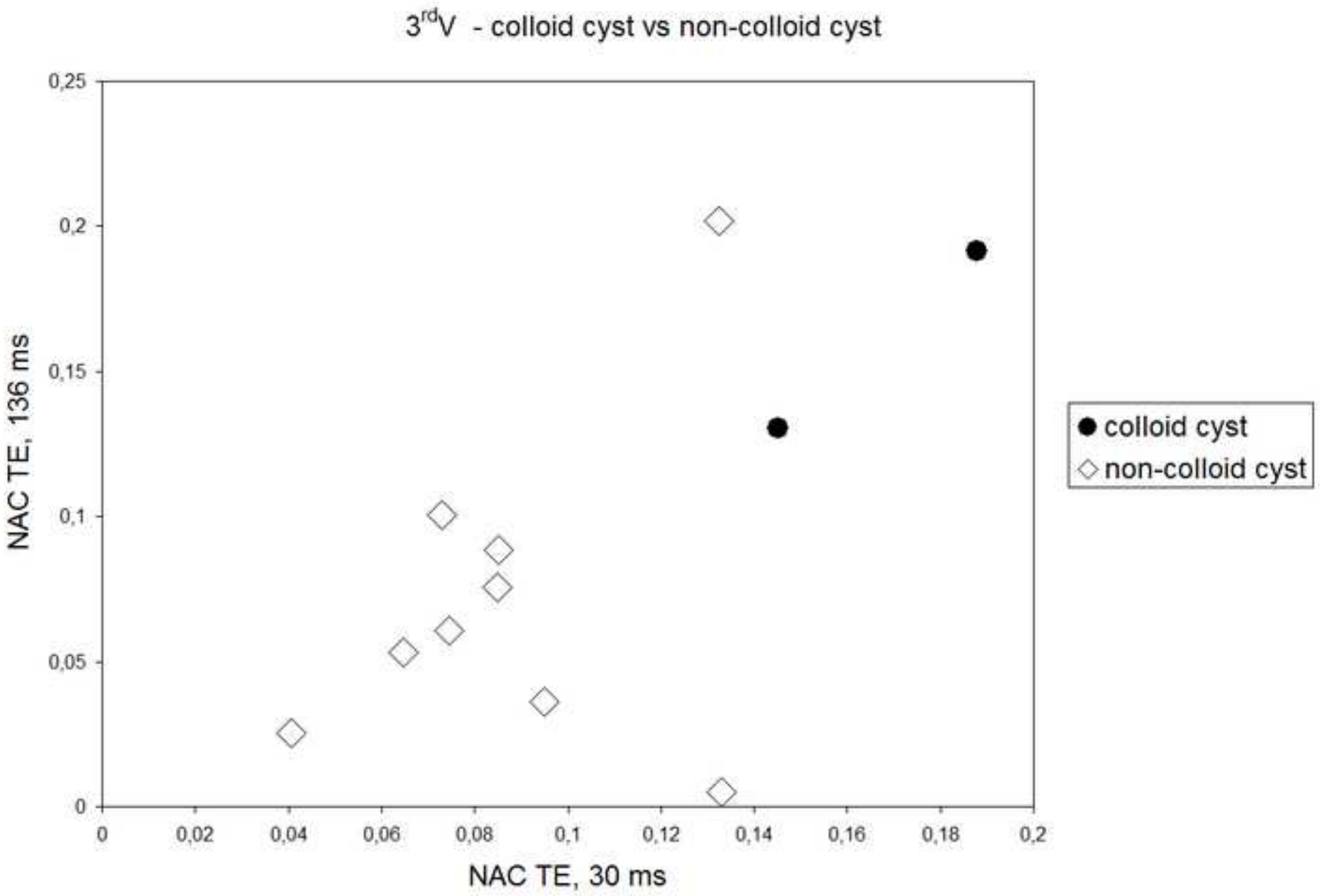

Figure 2D

Click here to download high resolution image

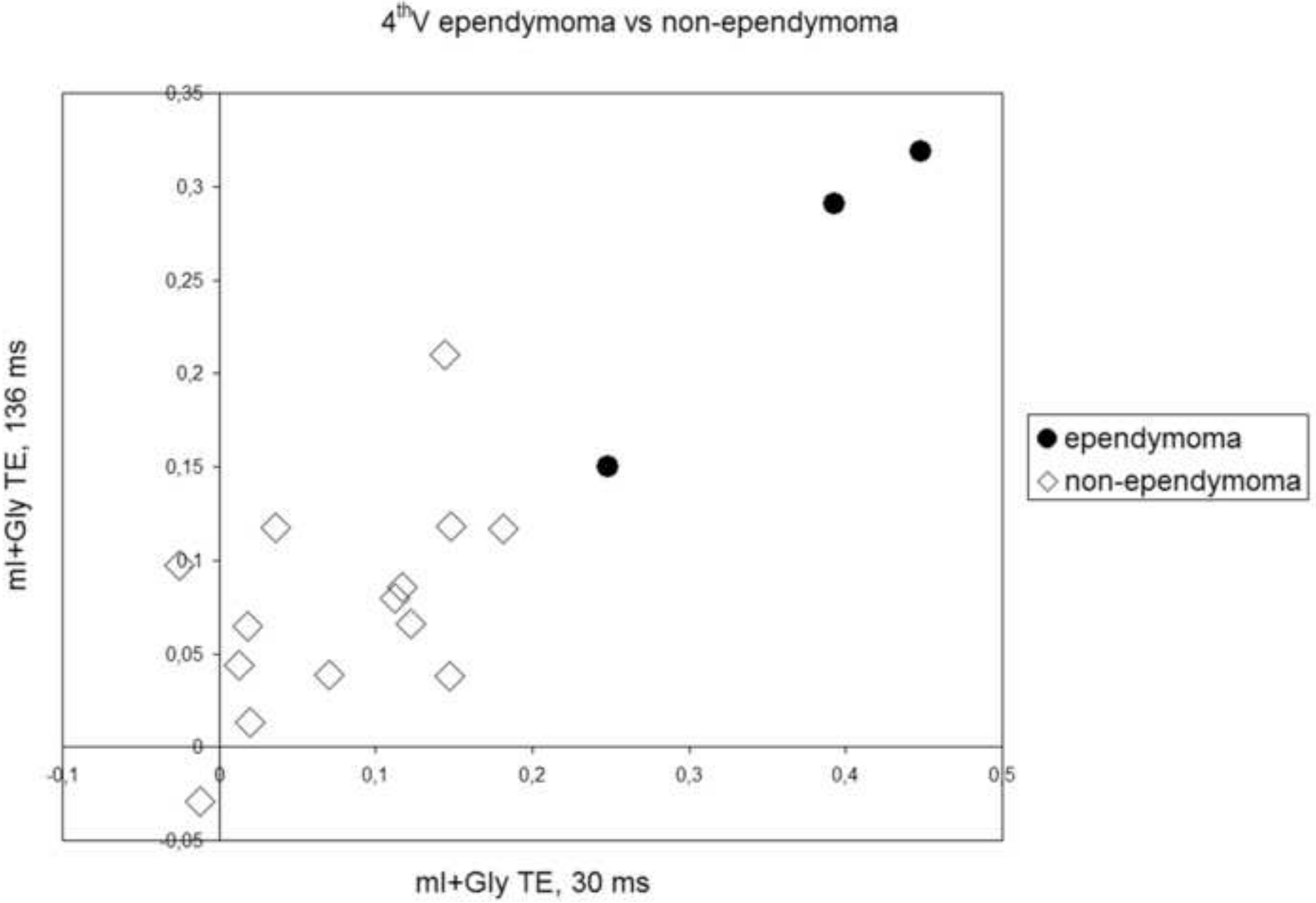

Figure 2E

Click here to download high resolution image

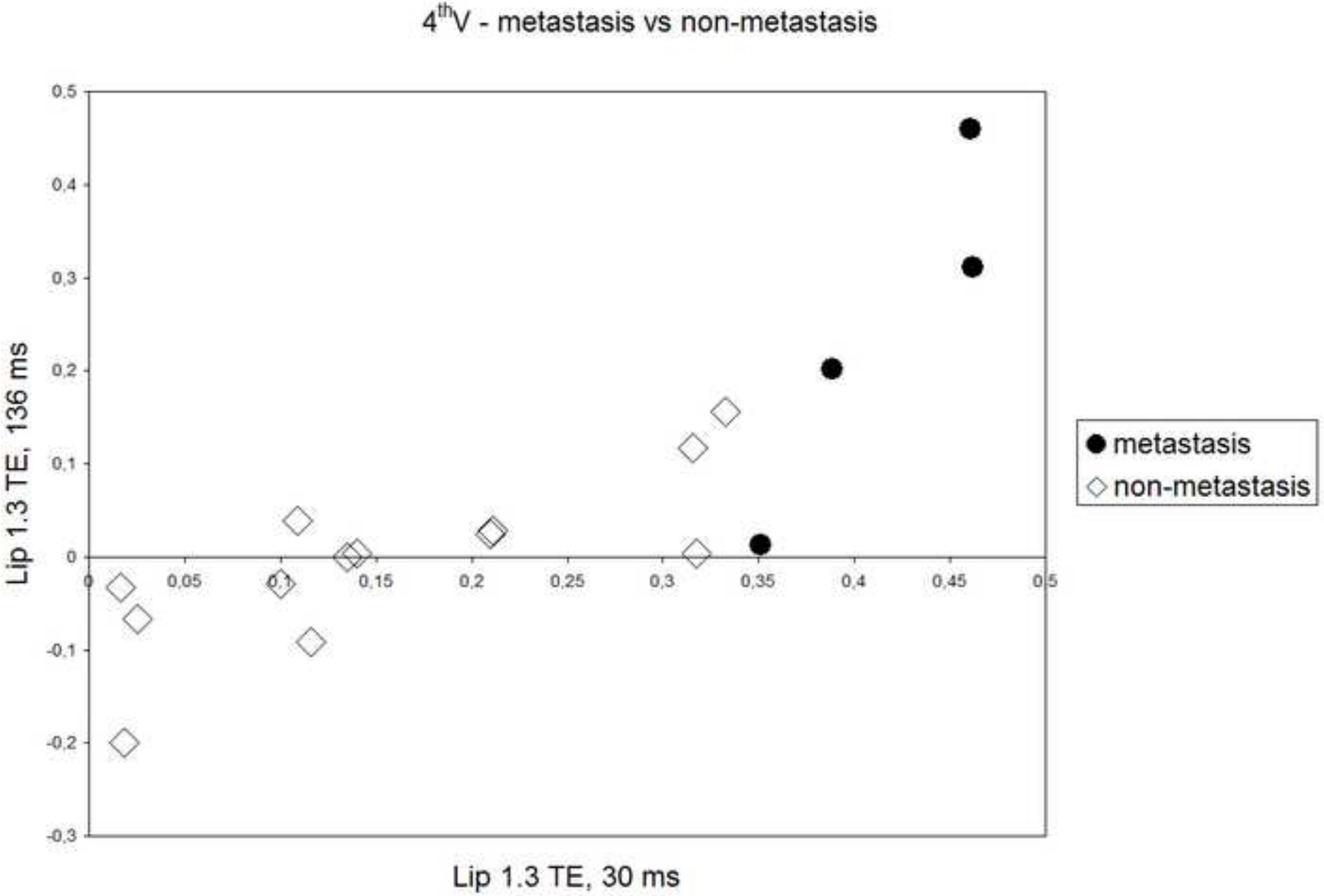

Figure 3A

Click here to download high resolution image

Figure 3B

Click here to download high resolution image

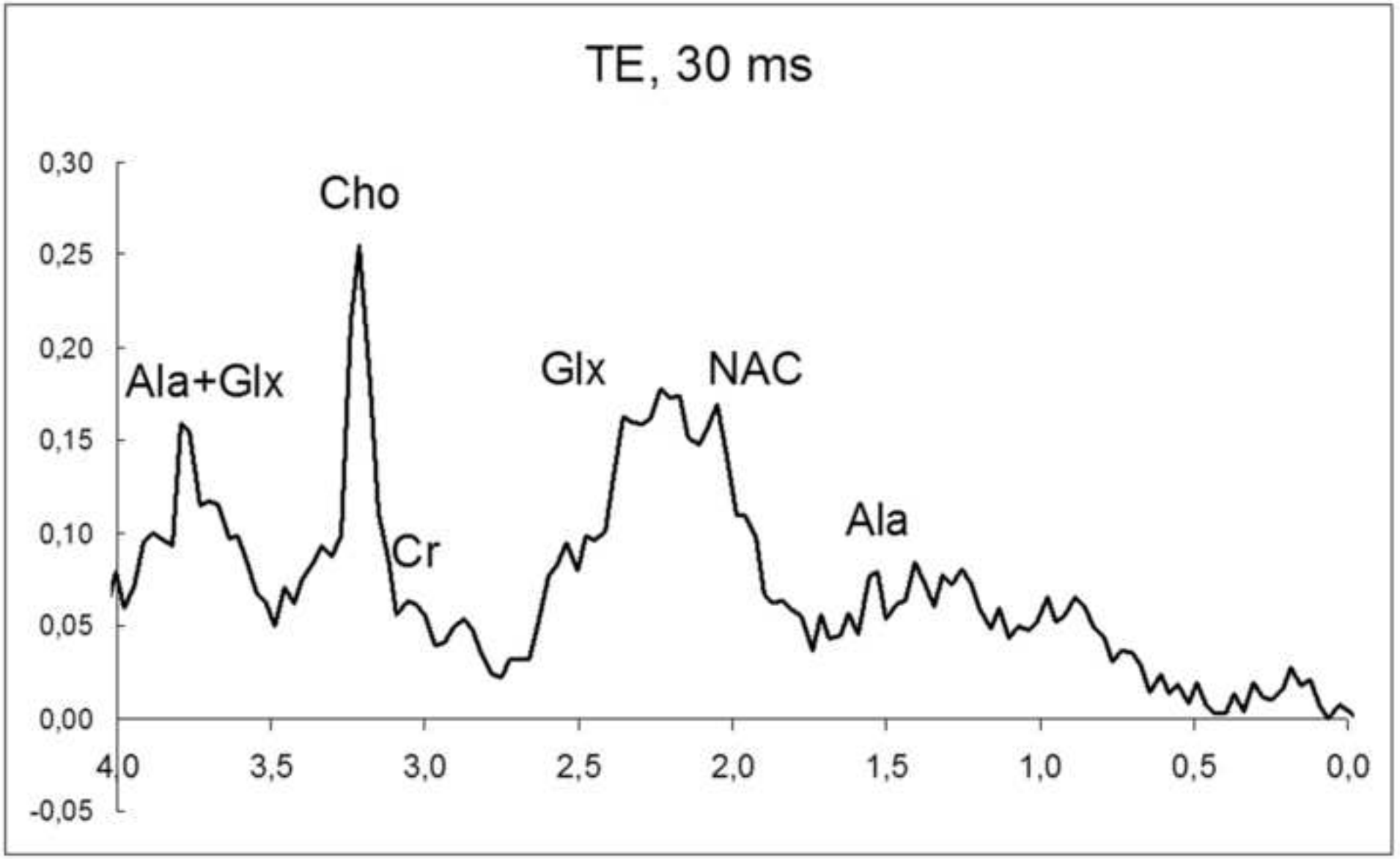

Figure 3C
Click here to download high resolution image

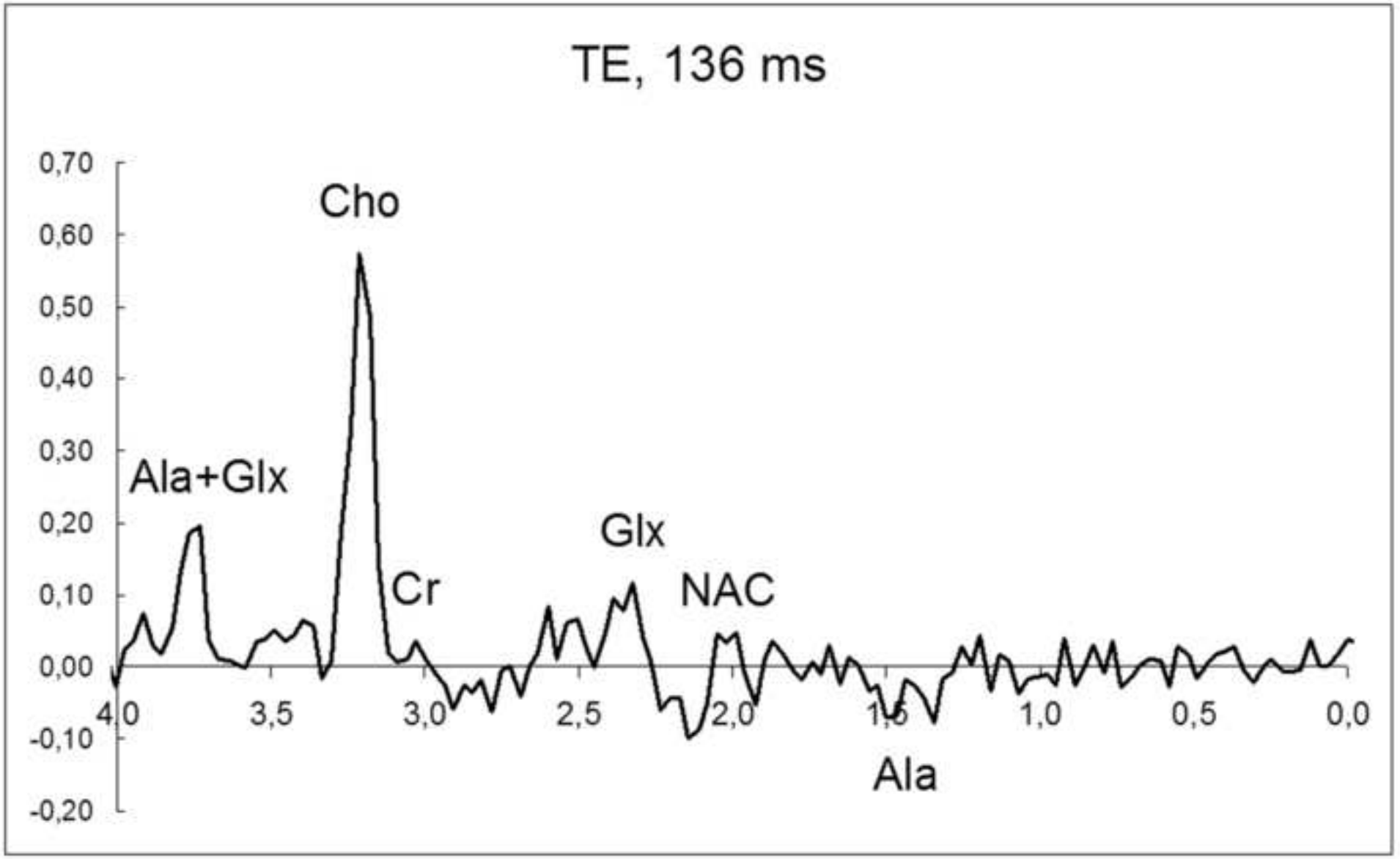

Figure 3D

Click here to download high resolution image

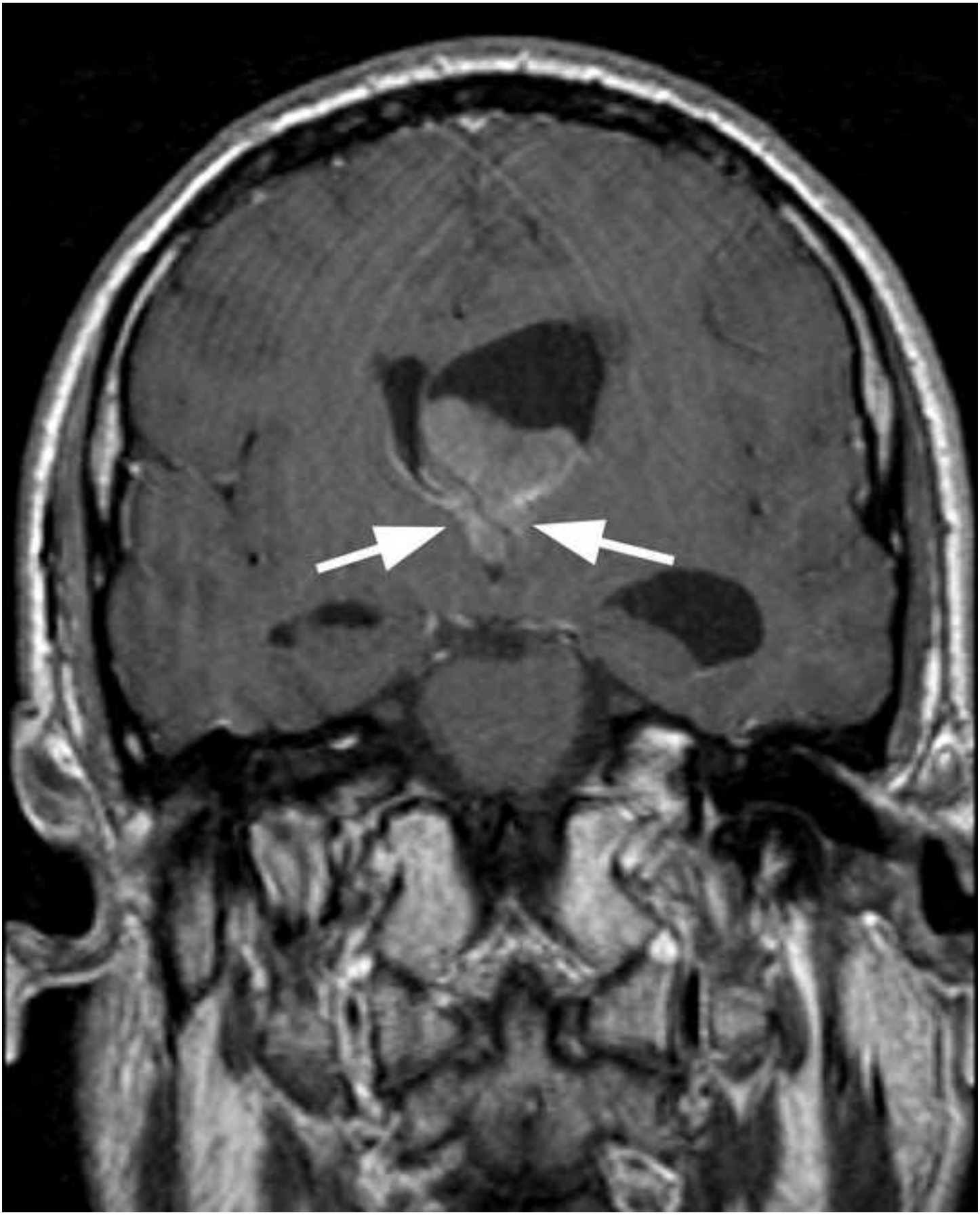

Figure 3E

Click here to download high resolution image

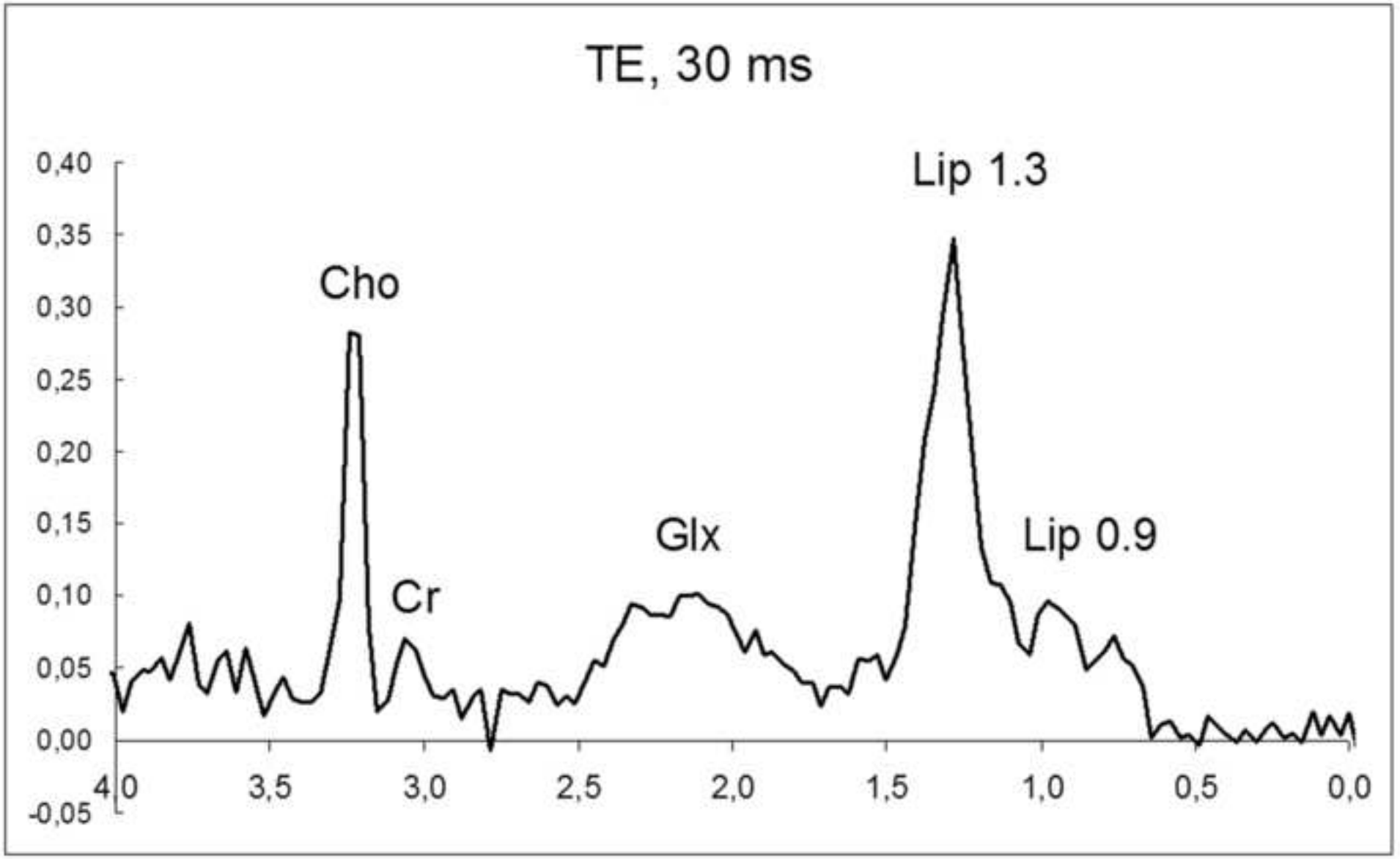

Figure 3F

Click here to download high resolution image

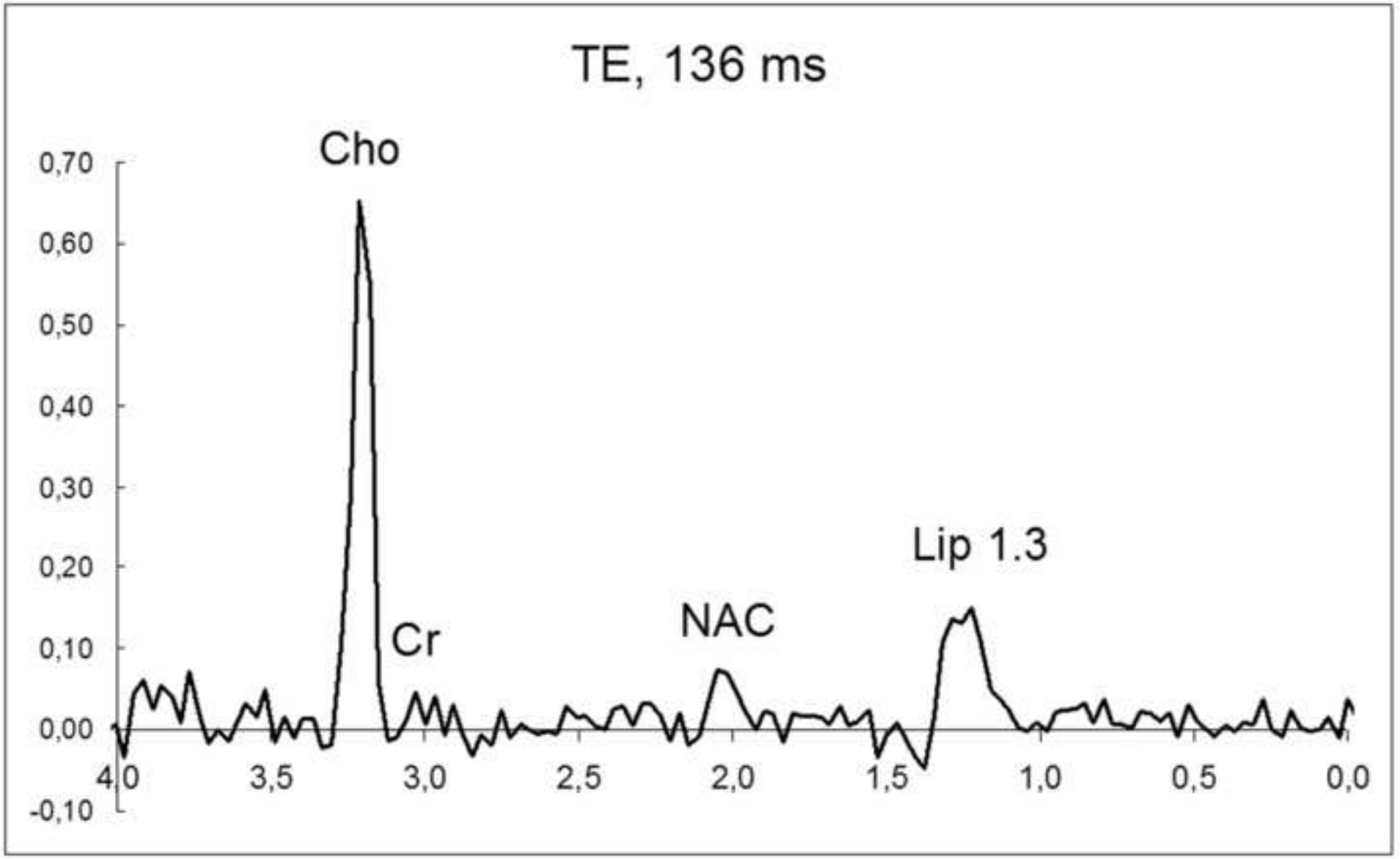

Figure 3G

Click here to download high resolution image

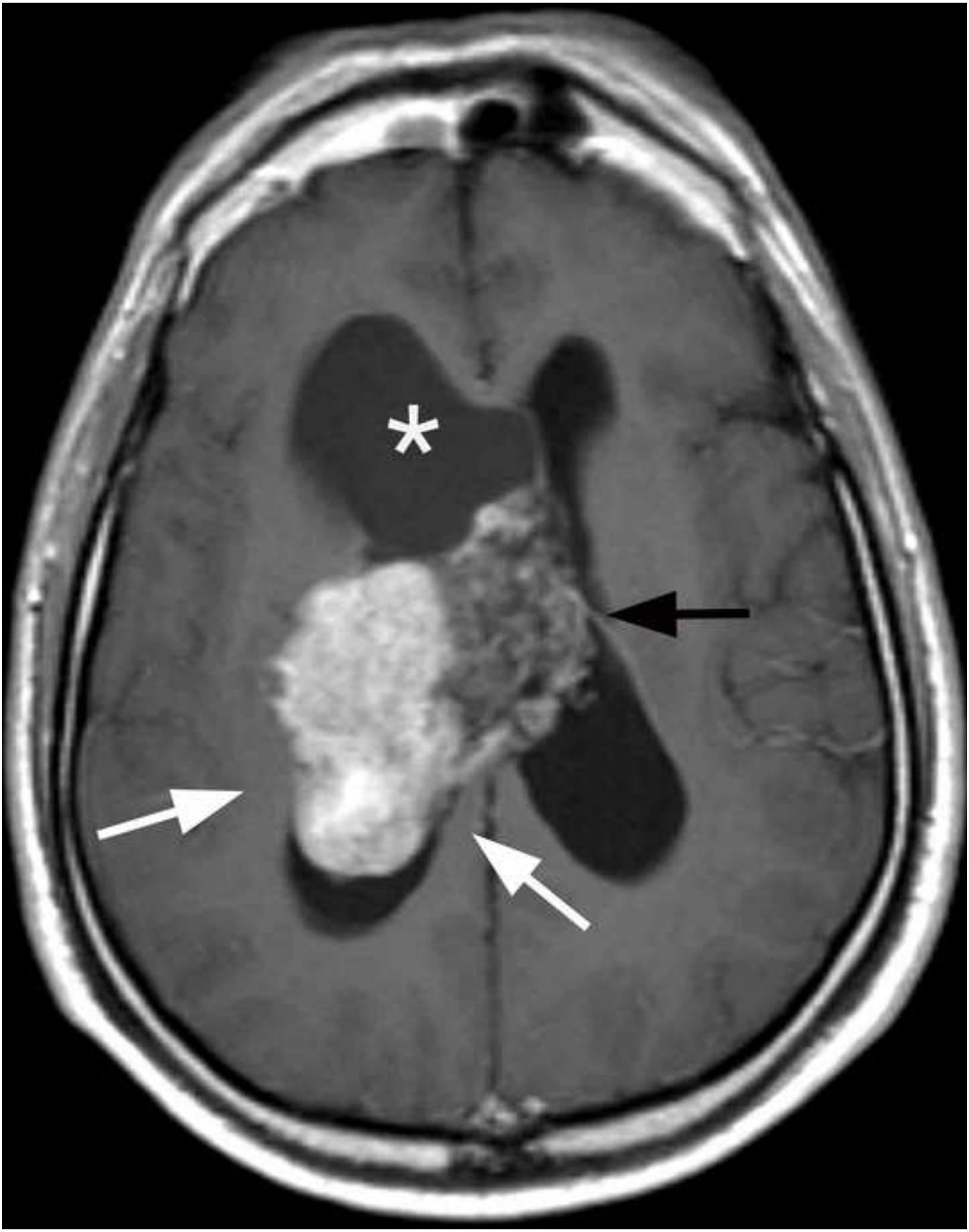

Figure 3H

Click here to download high resolution image

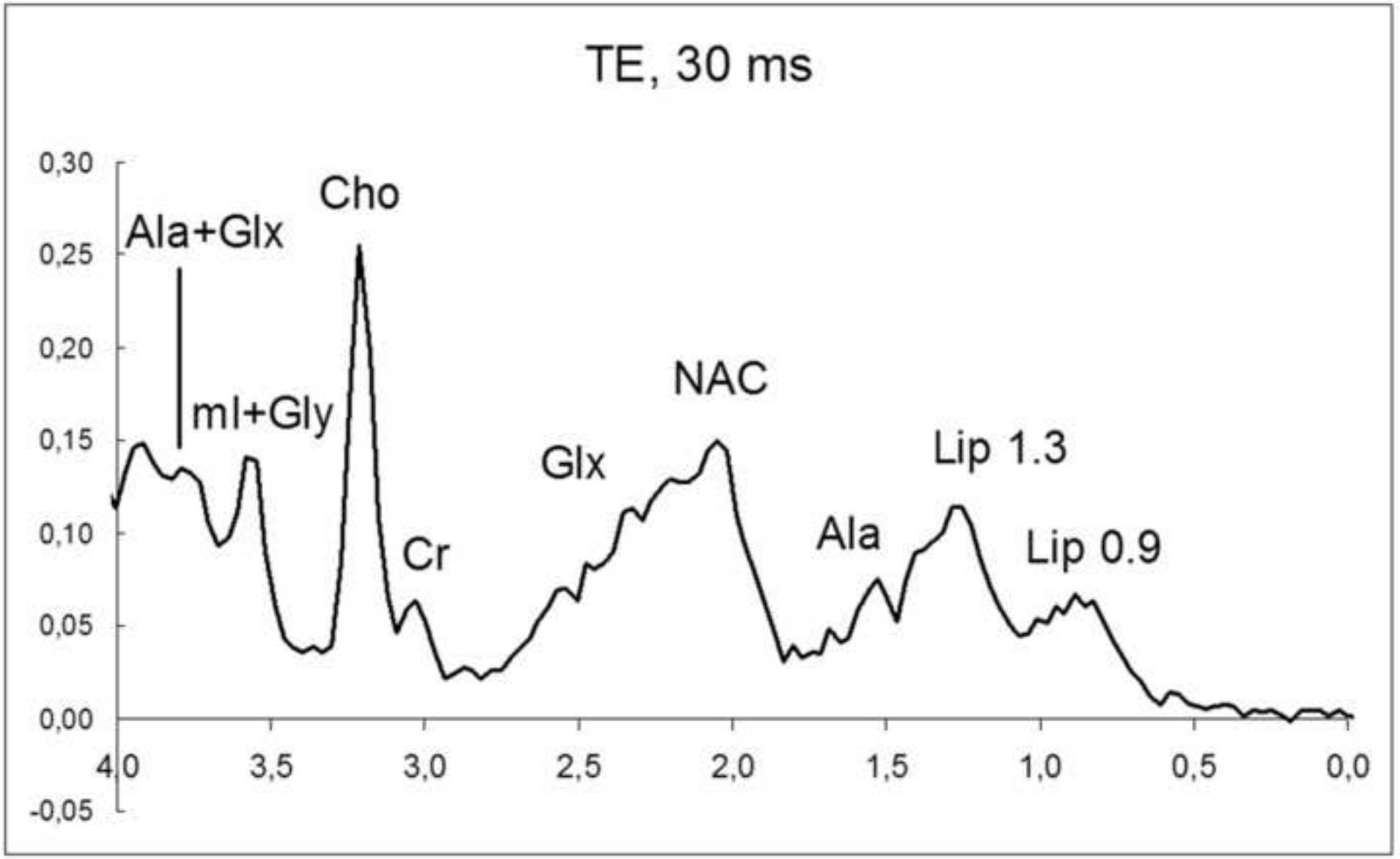

Figure 3I

Click here to download high resolution image

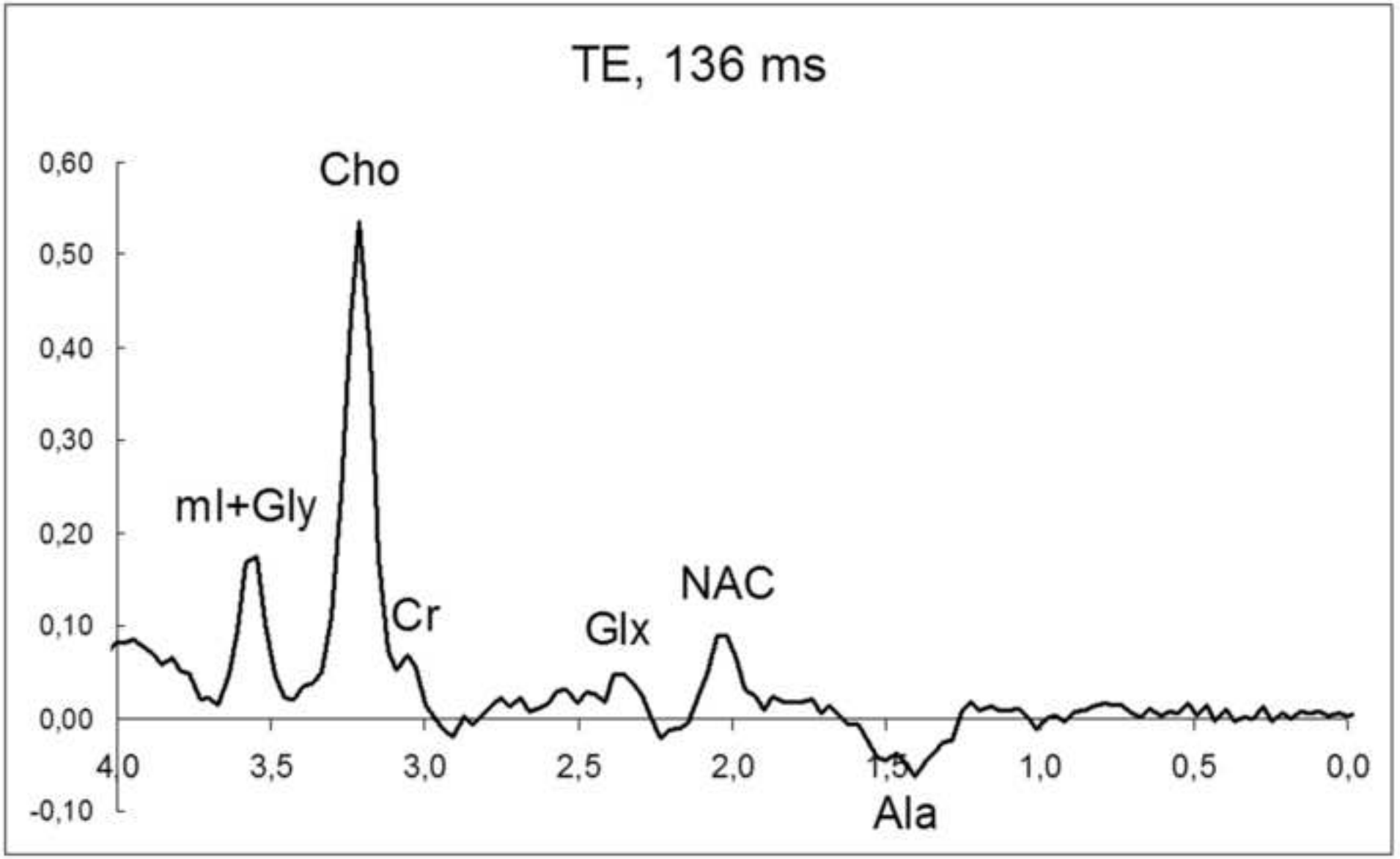

Figure 3J

Click here to download high resolution image

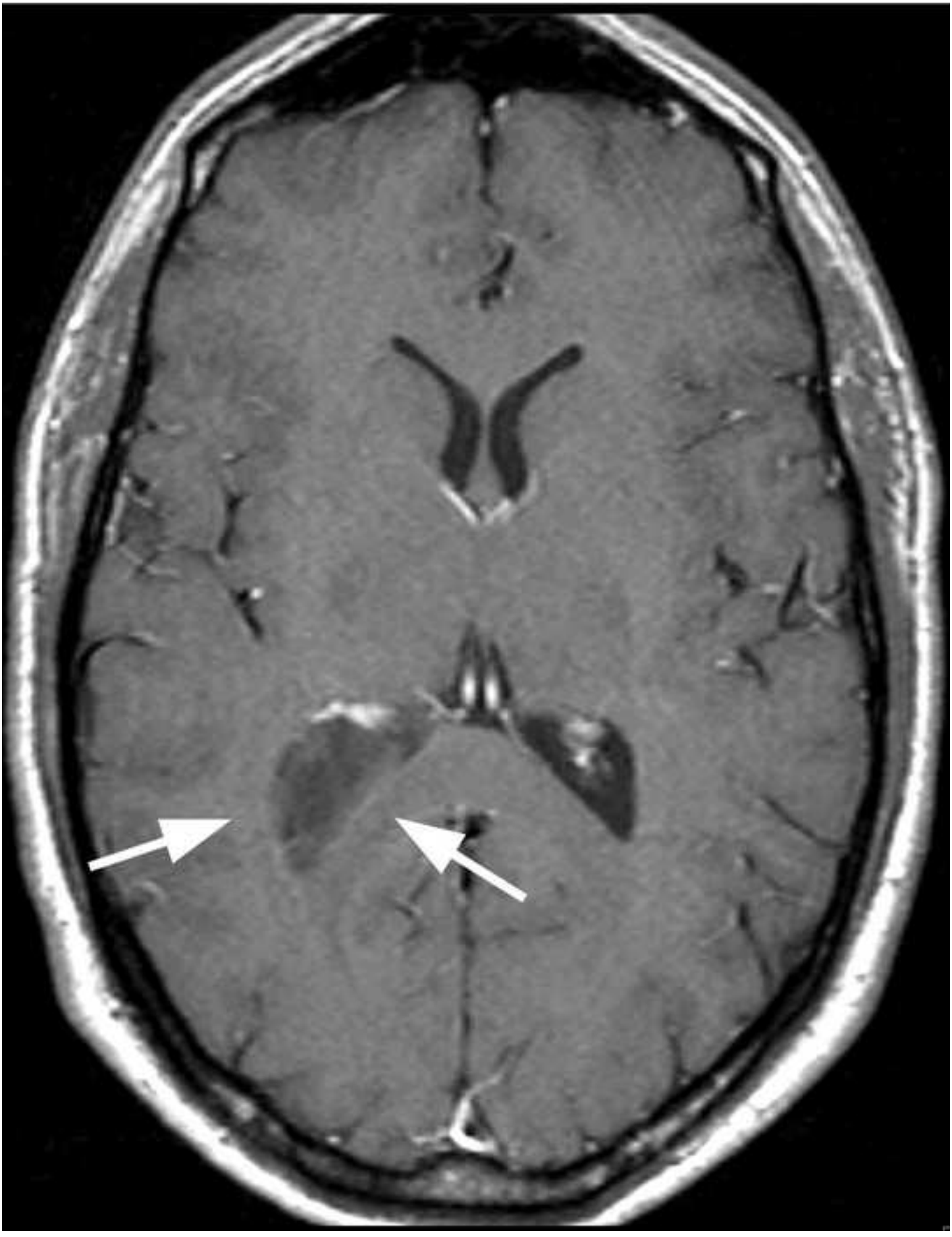

Figure 3K

Click here to download high resolution image

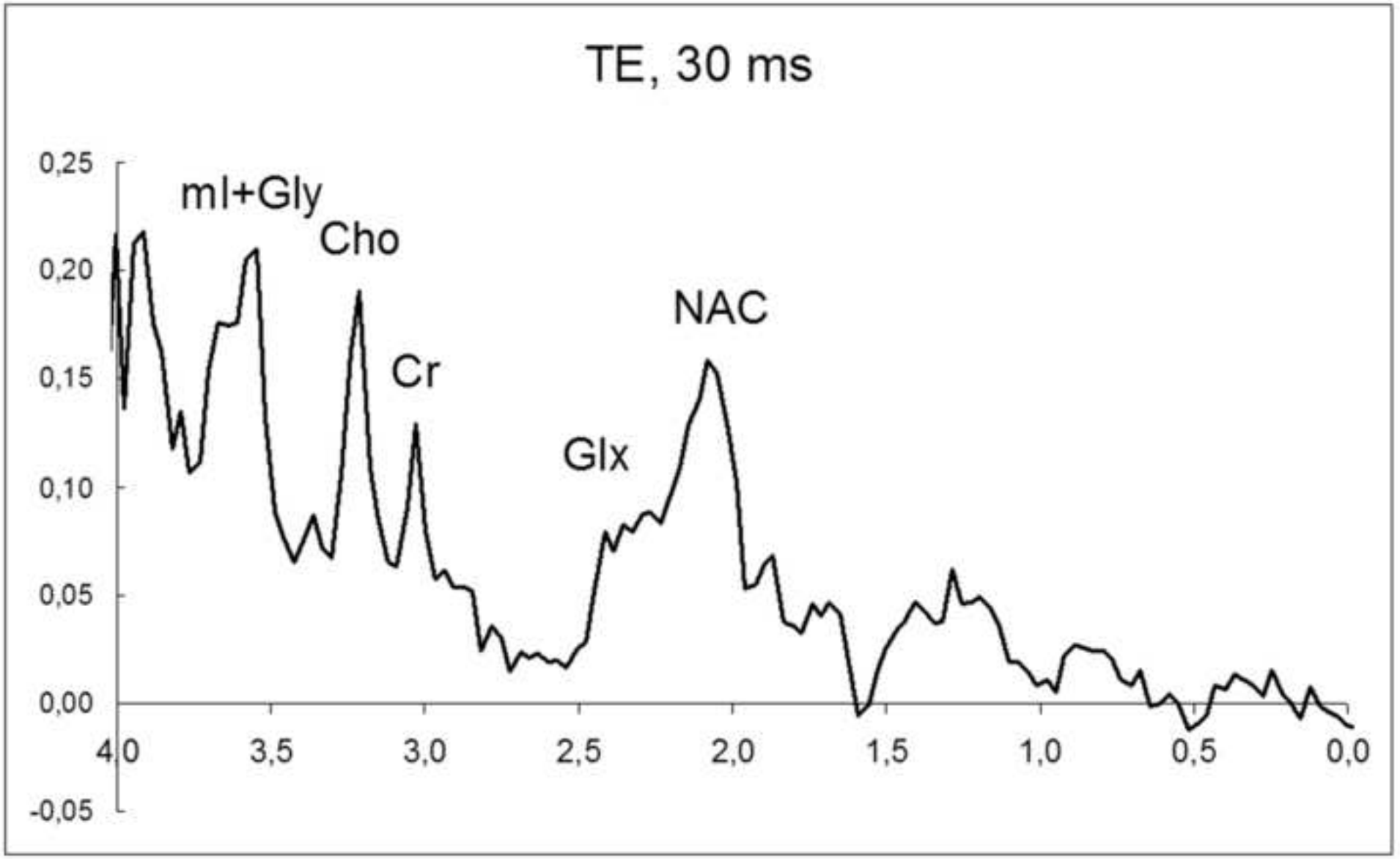

Figure 3L

Click here to download high resolution image

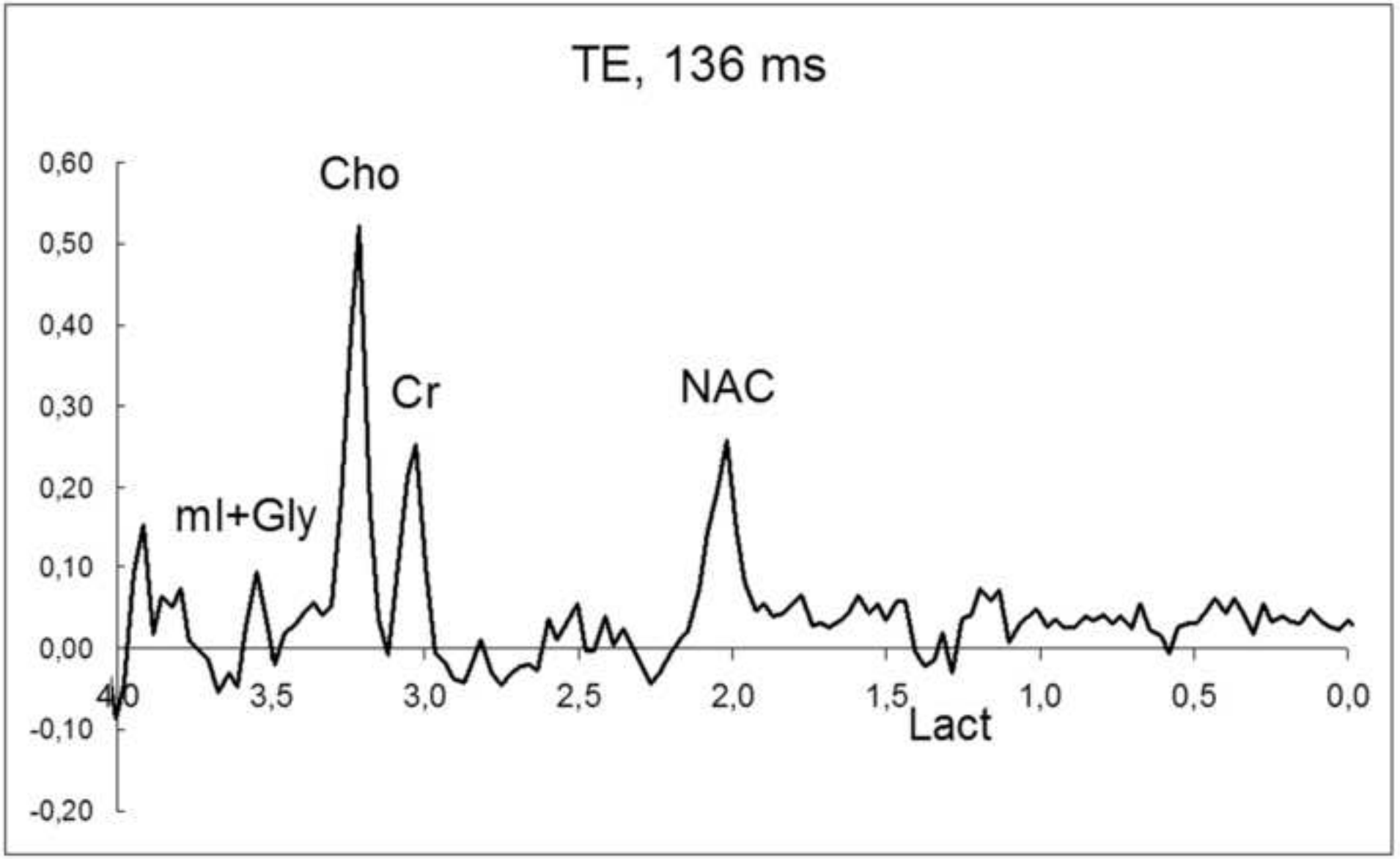

Figure 4A

Click here to download high resolution image

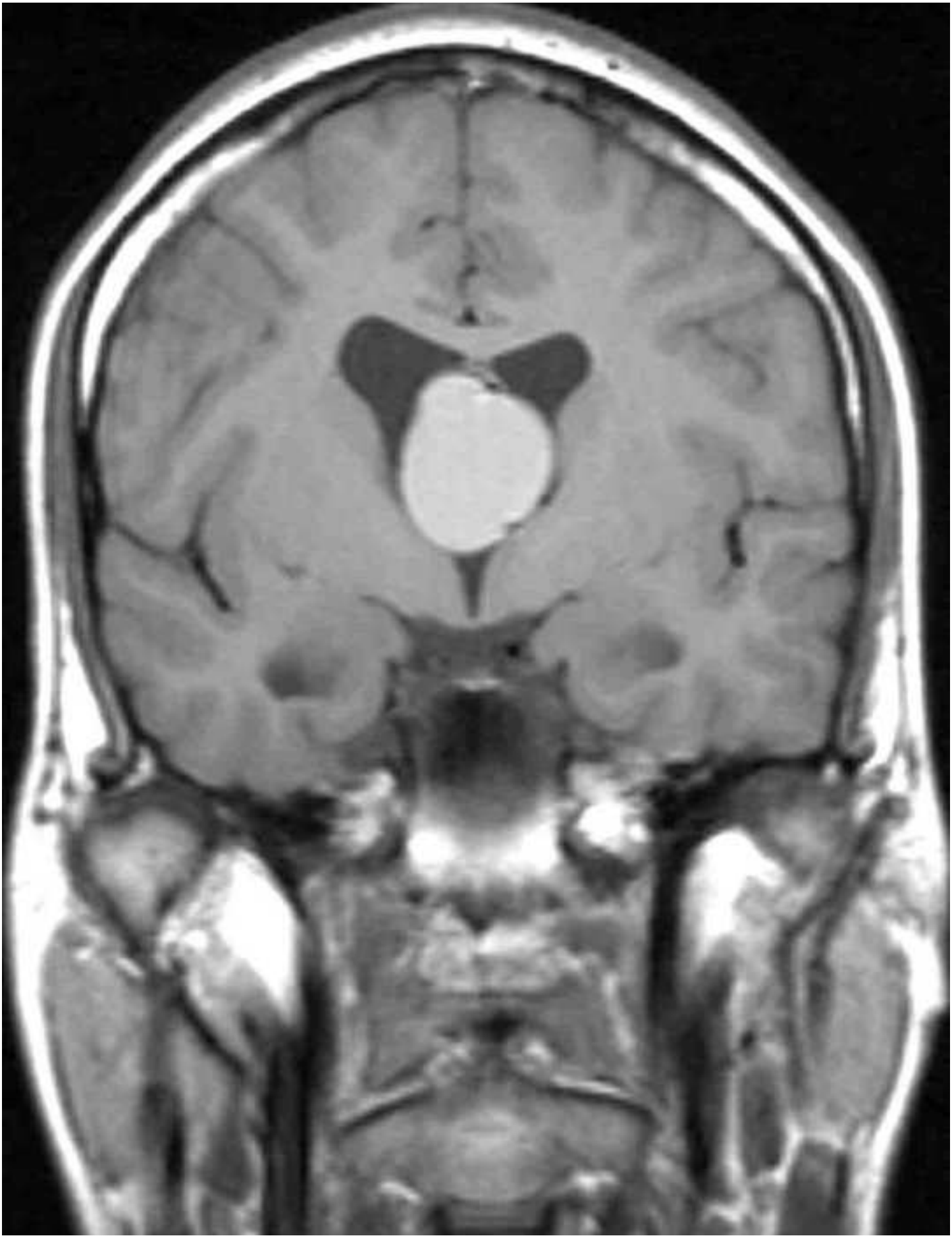

Figure 4B

Click here to download high resolution image

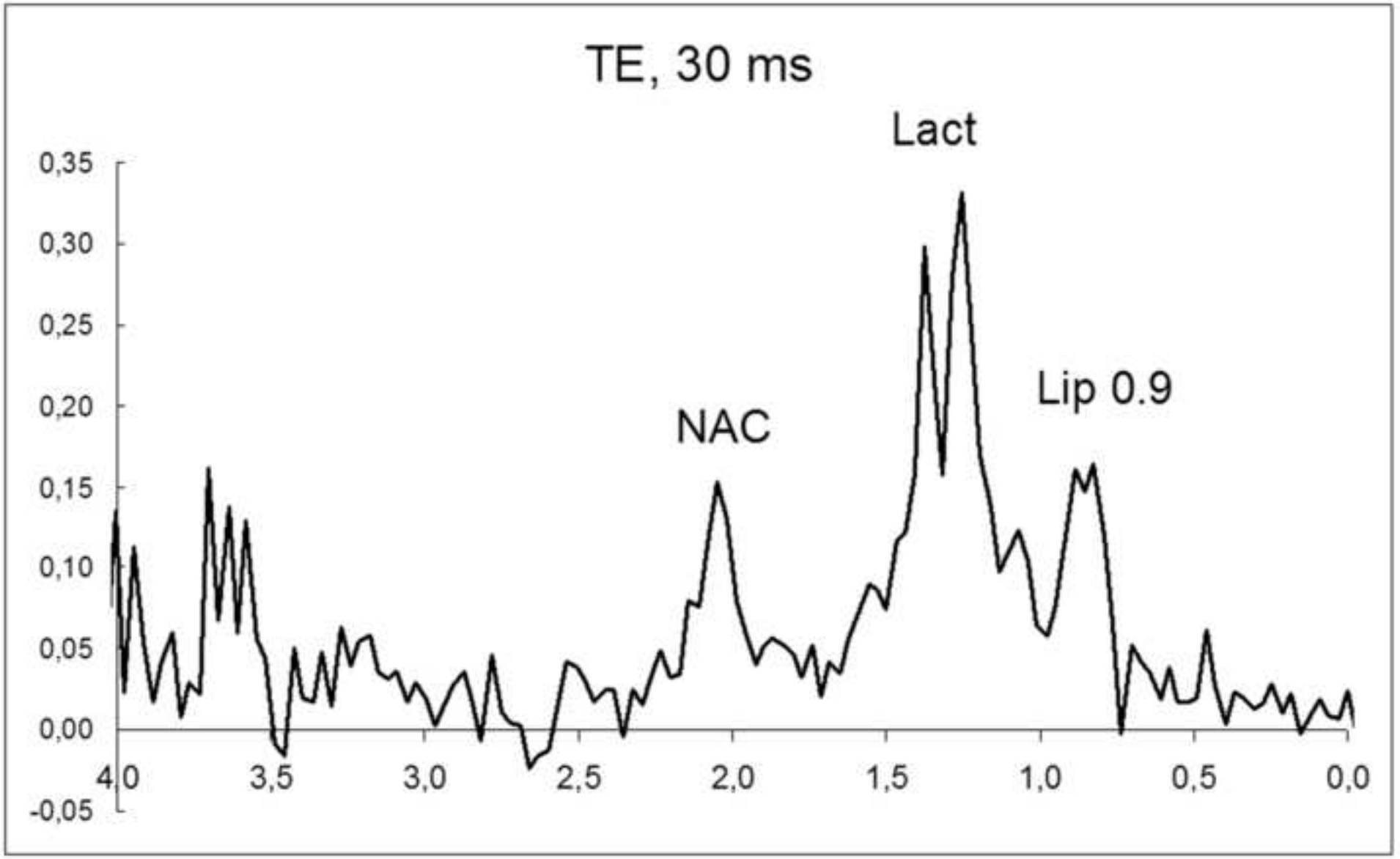

Figure 4C

Click here to download high resolution image

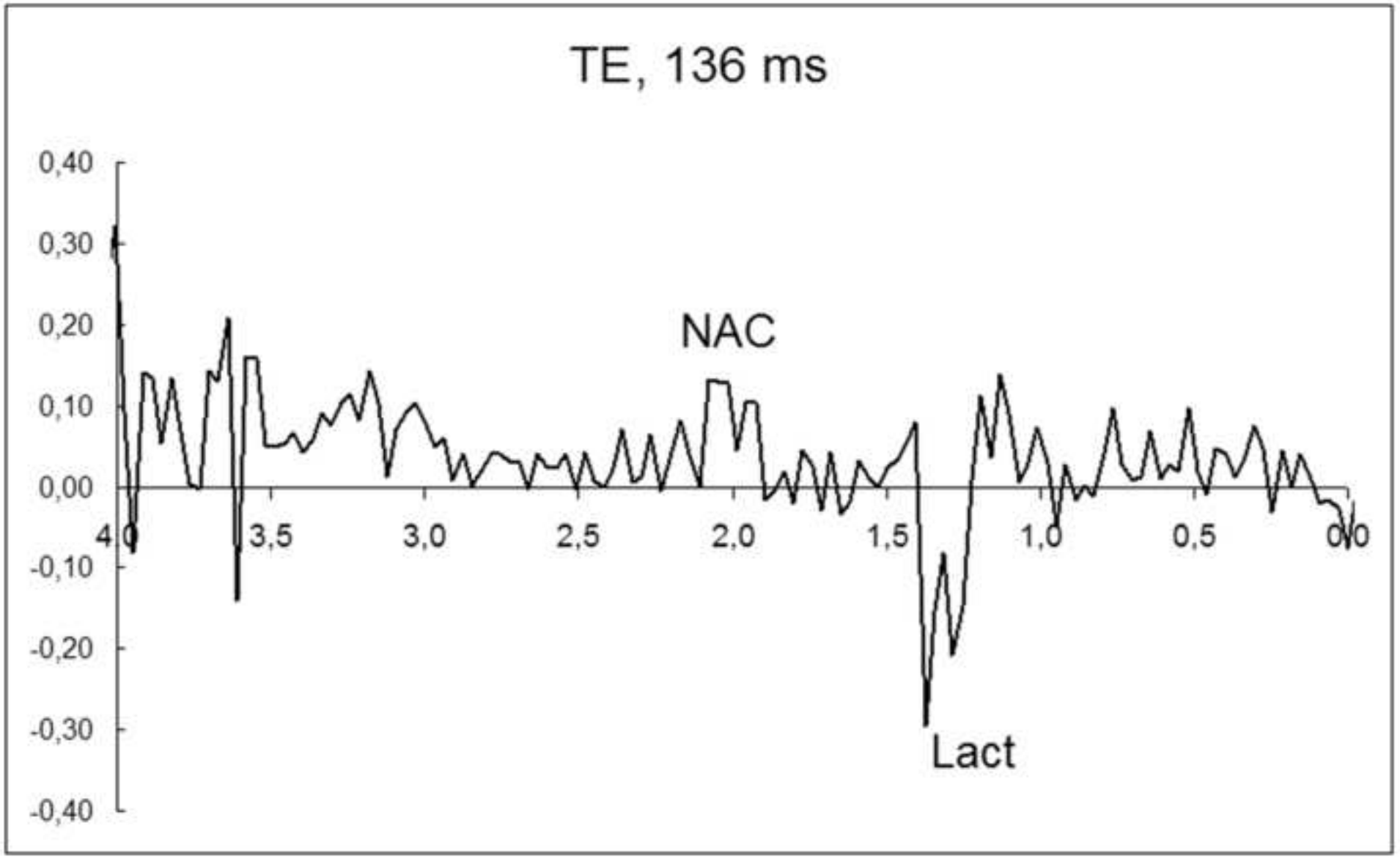

Figure 4D

Click here to download high resolution image

Figure 4E

Click here to download high resolution image

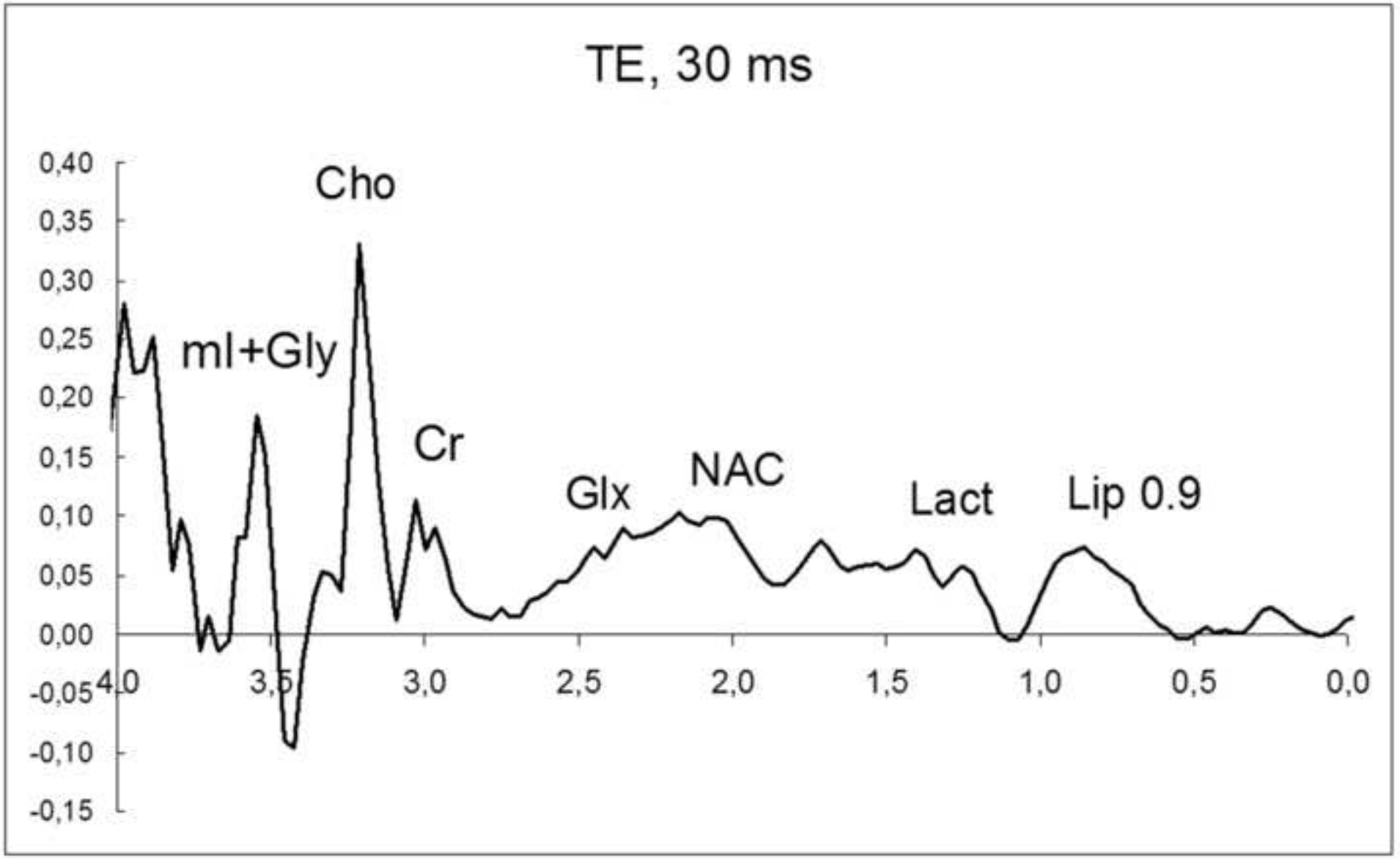

Figure 4F

Click here to download high resolution image

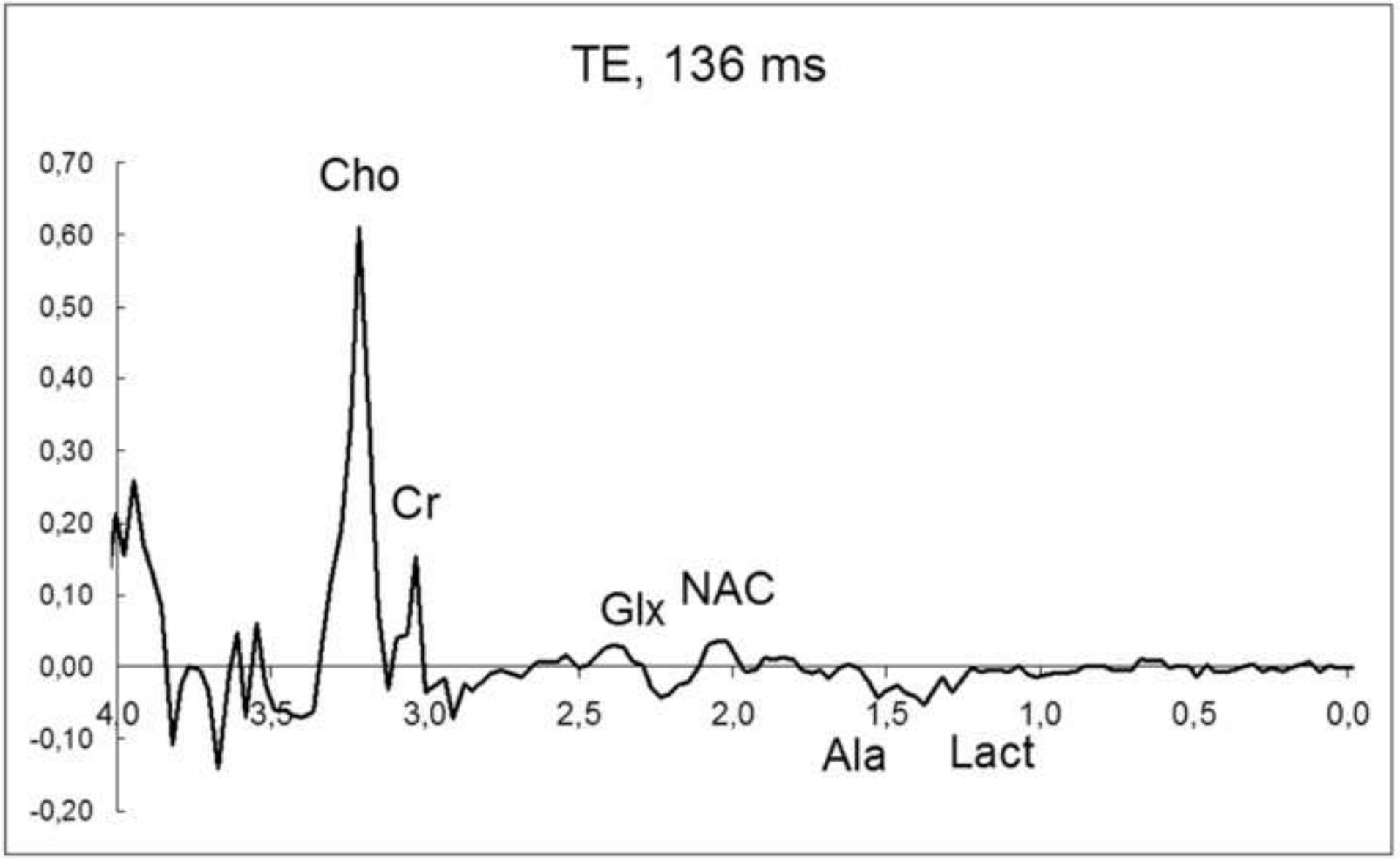

Figure 4G

Click here to download high resolution image

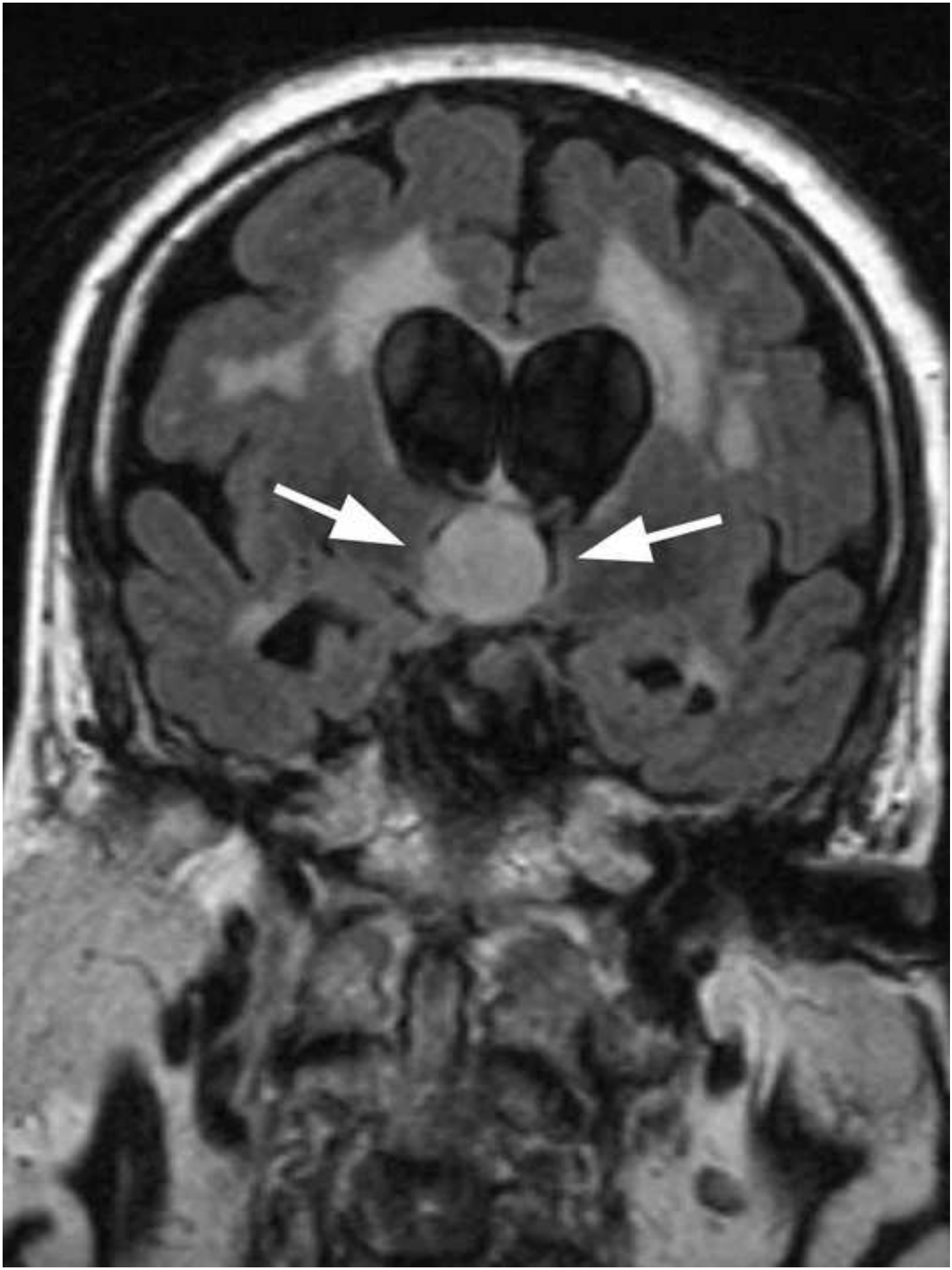

Figure 4H

Click here to download high resolution image

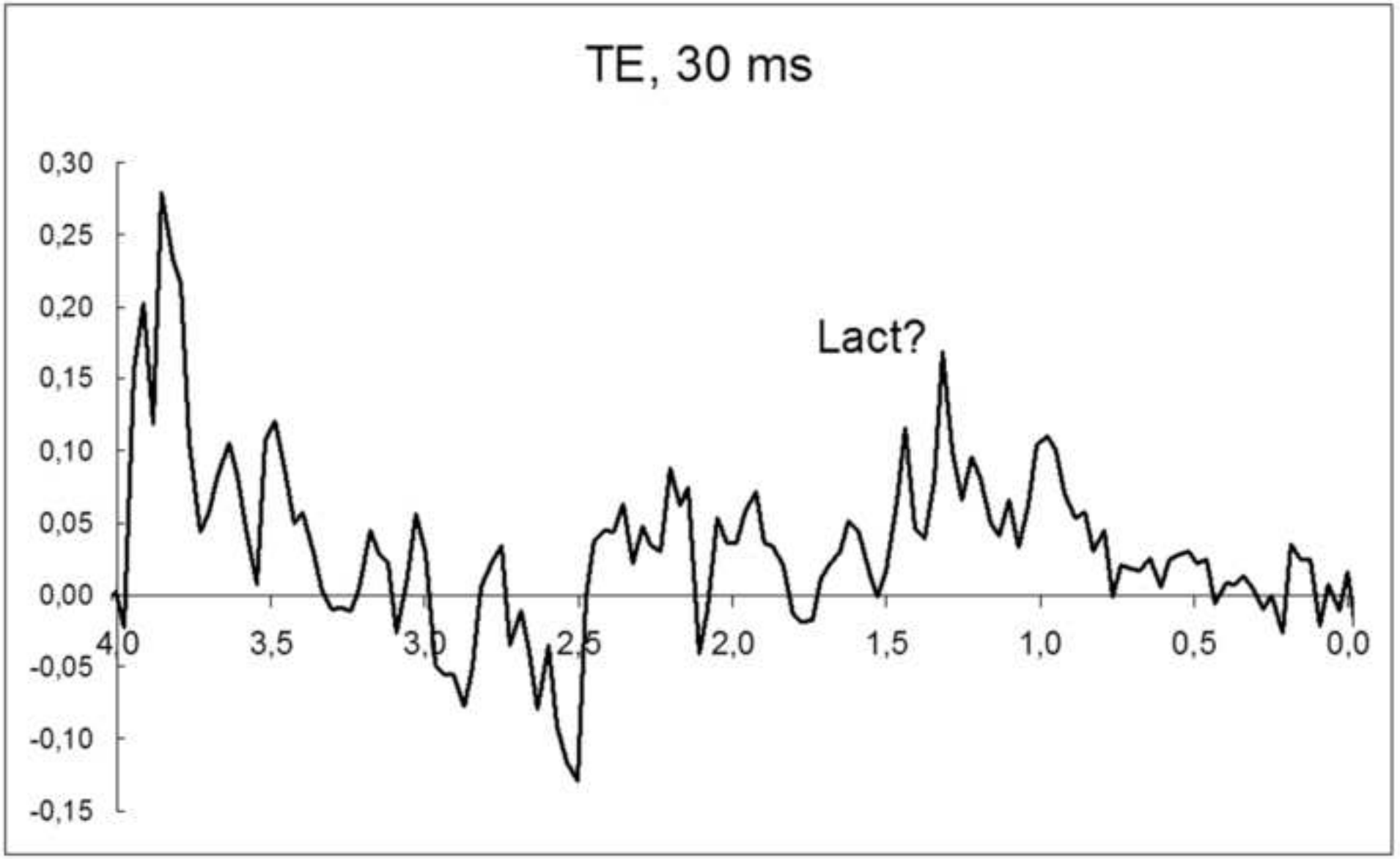

Figure 4l

Click here to download high resolution image

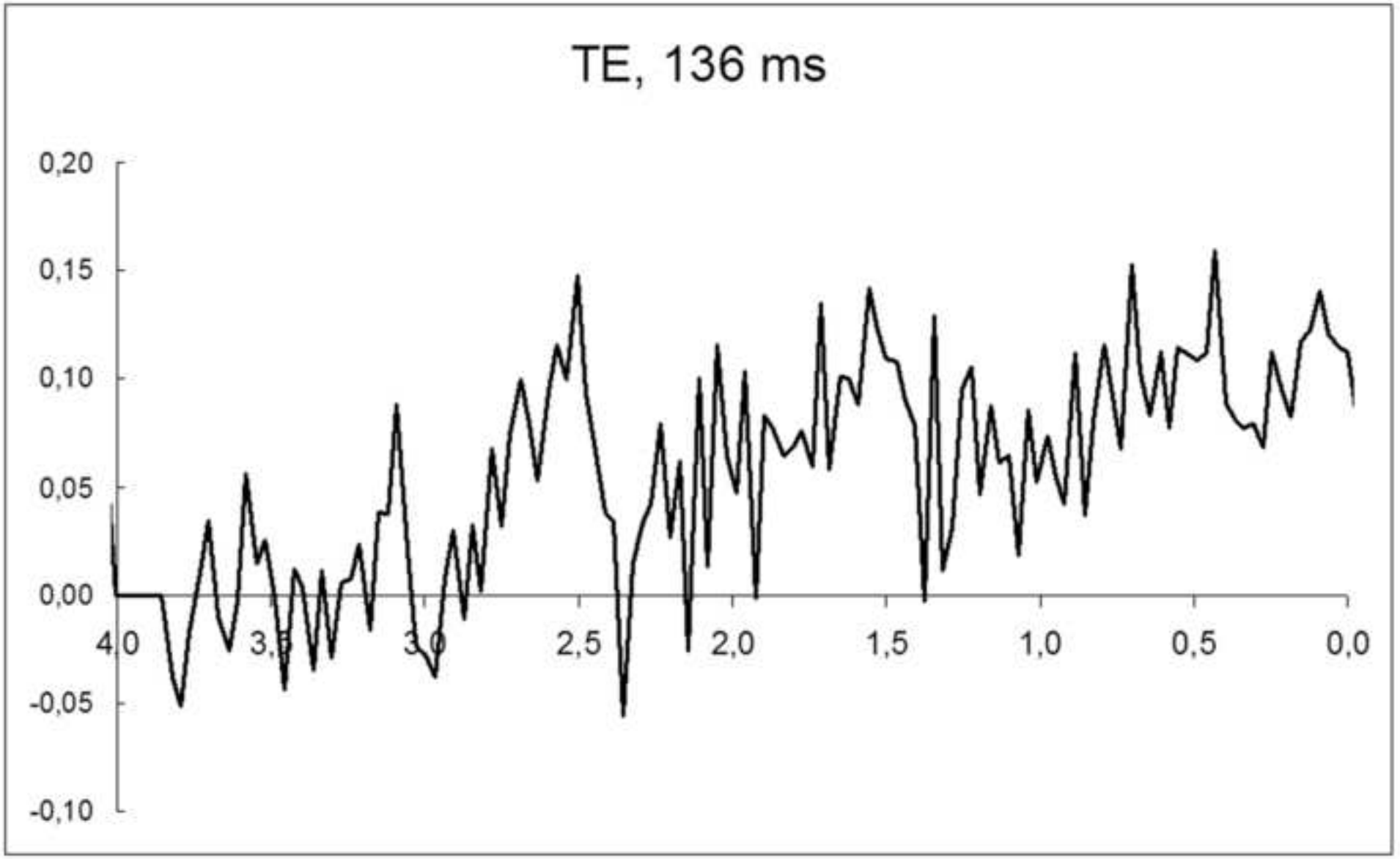

Figure 5A

Click here to download high resolution image

Figure 5B

Click here to download high resolution image

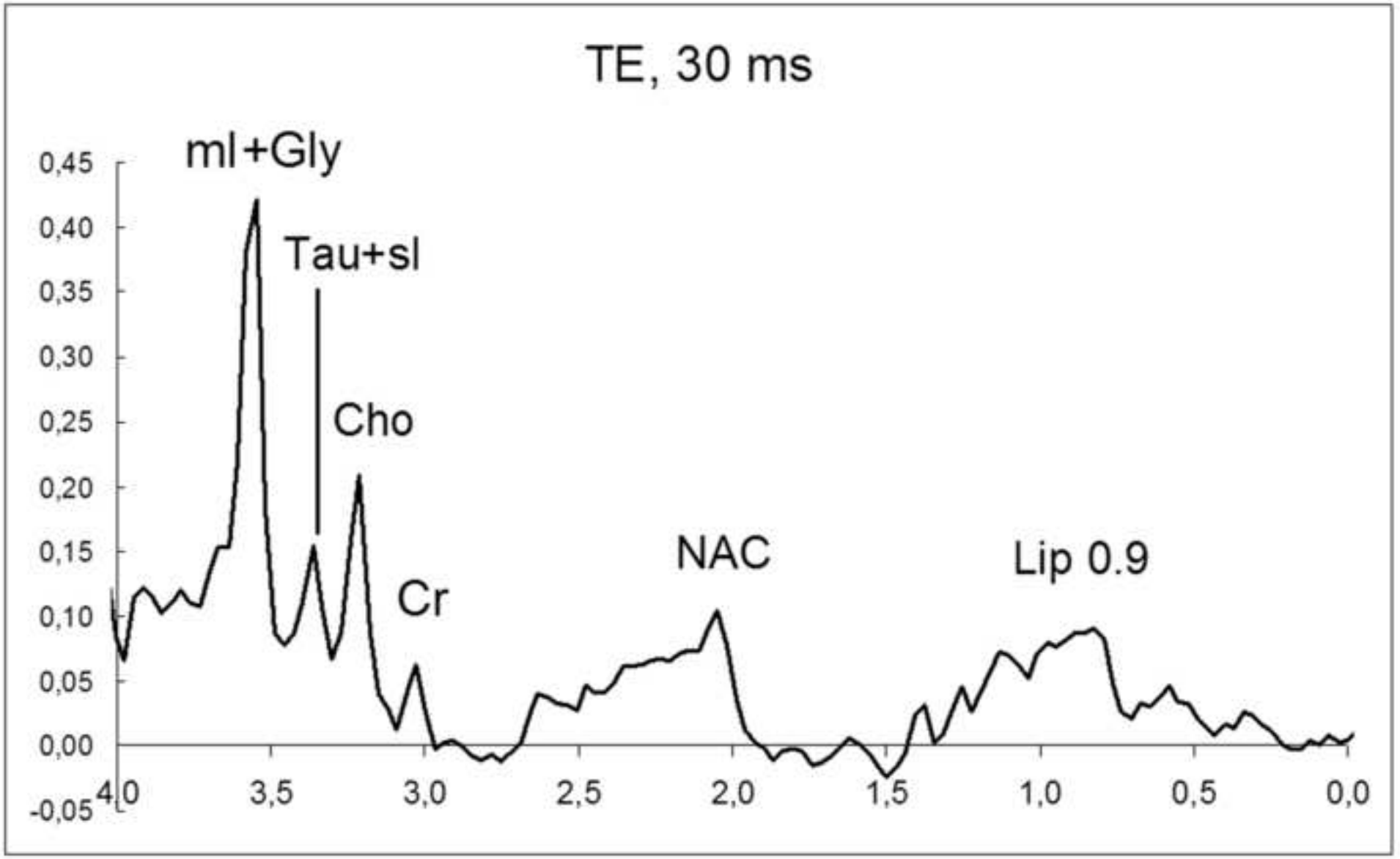

Figure 5C

Click here to download high resolution image

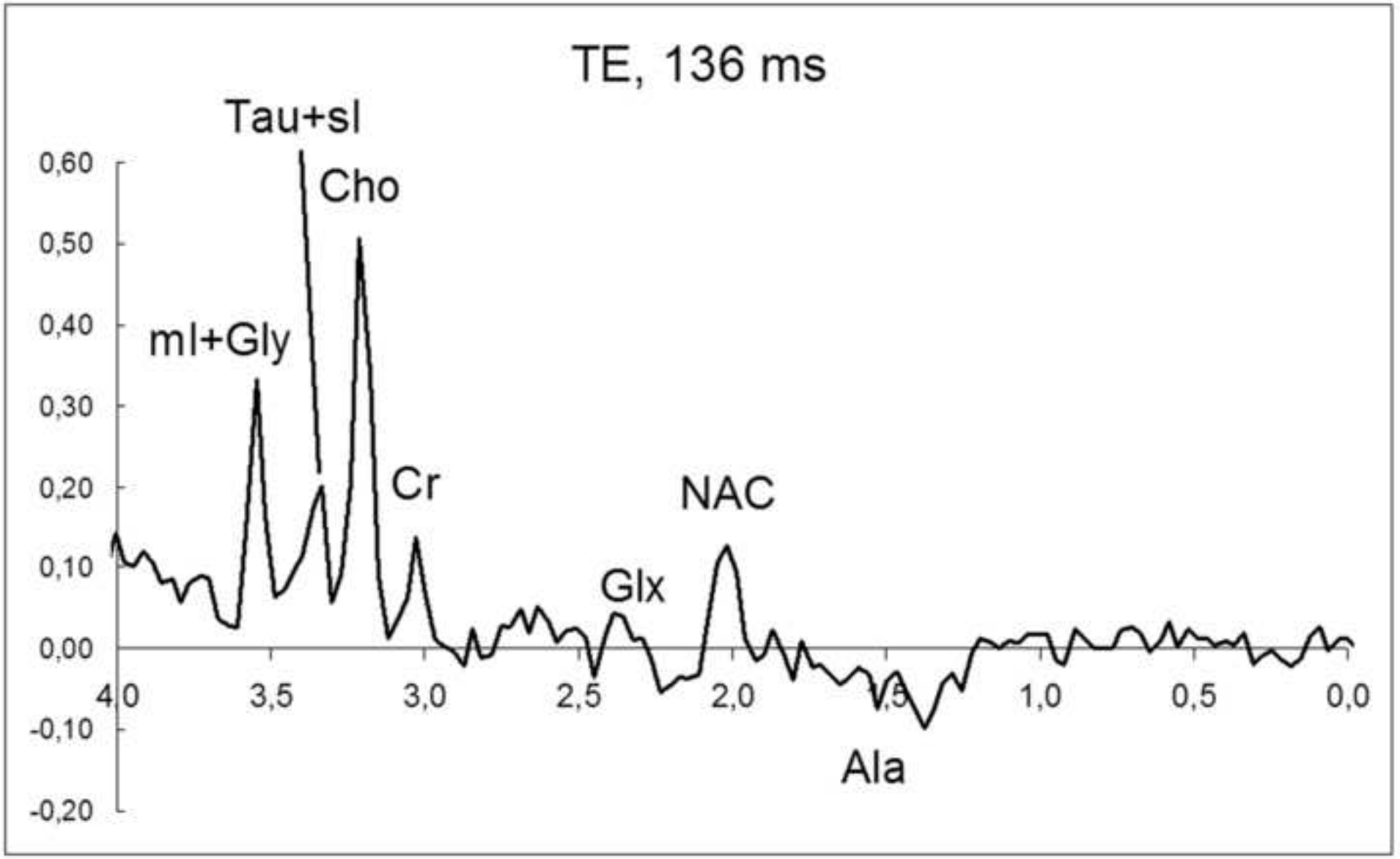

Figure 5D

Click here to download high resolution image

Figure 5E

Click here to download high resolution image

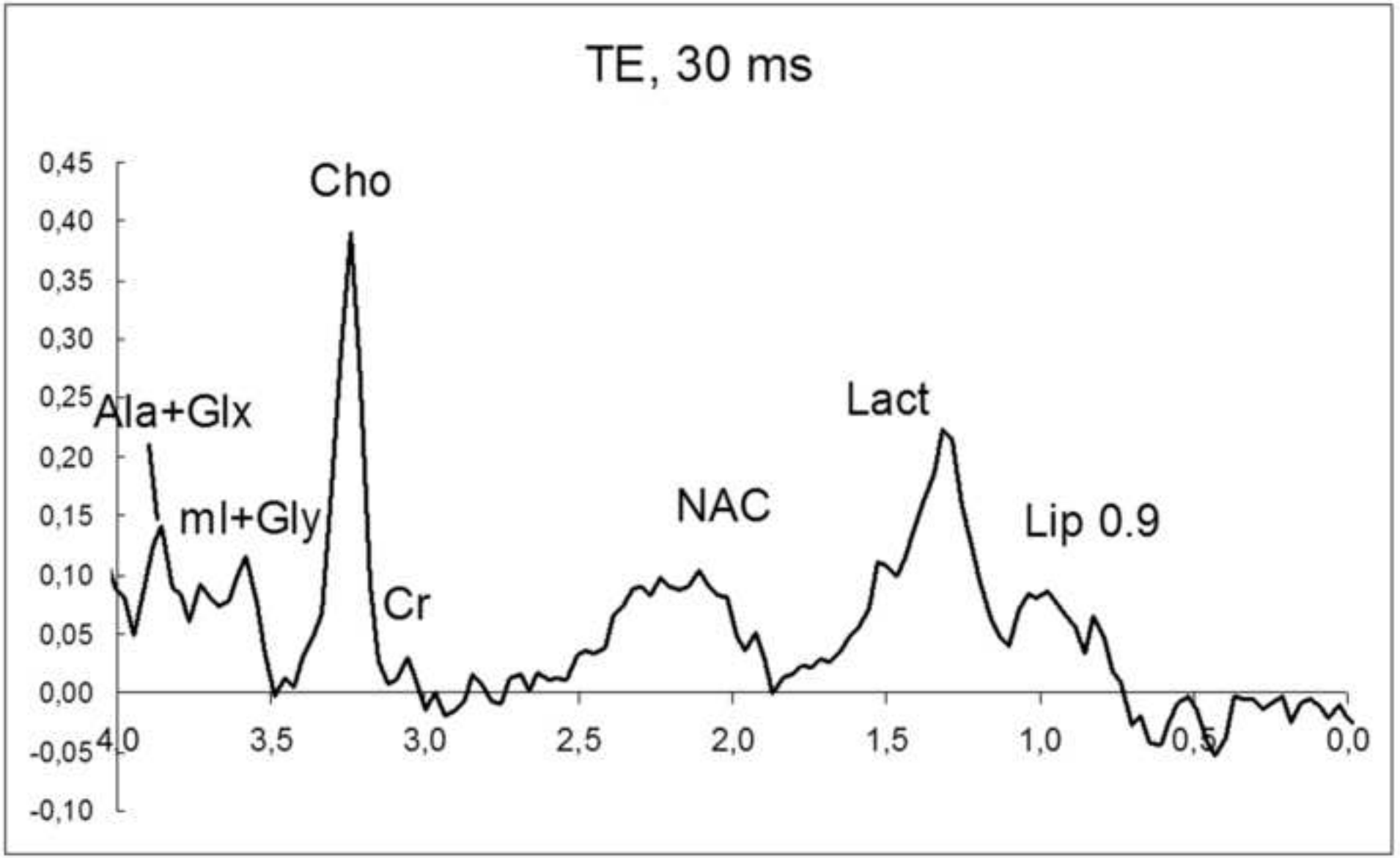

Figure 5F

Click here to download high resolution image

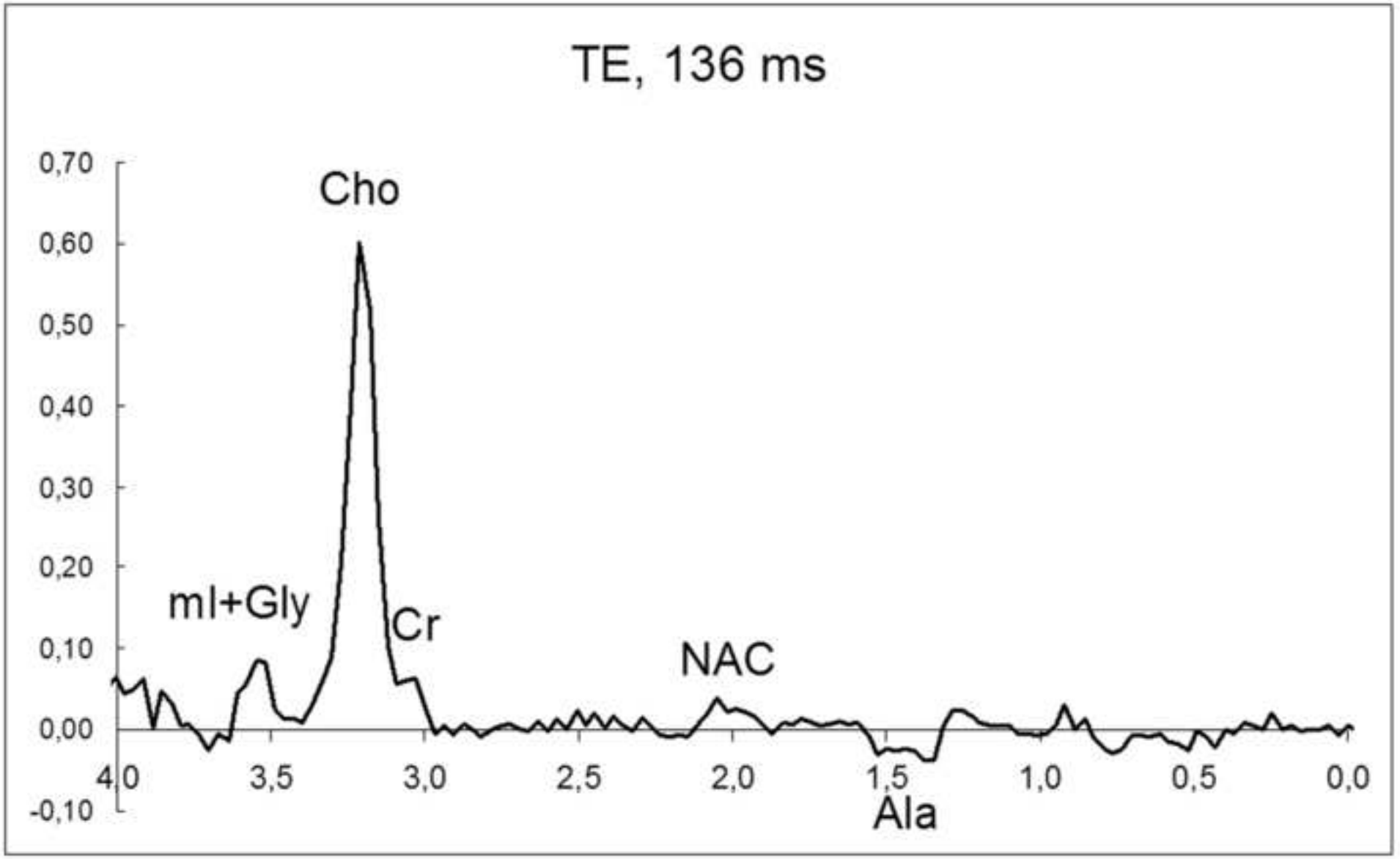

Figure 5G

Click here to download high resolution image

Figure 5H

Click here to download high resolution image

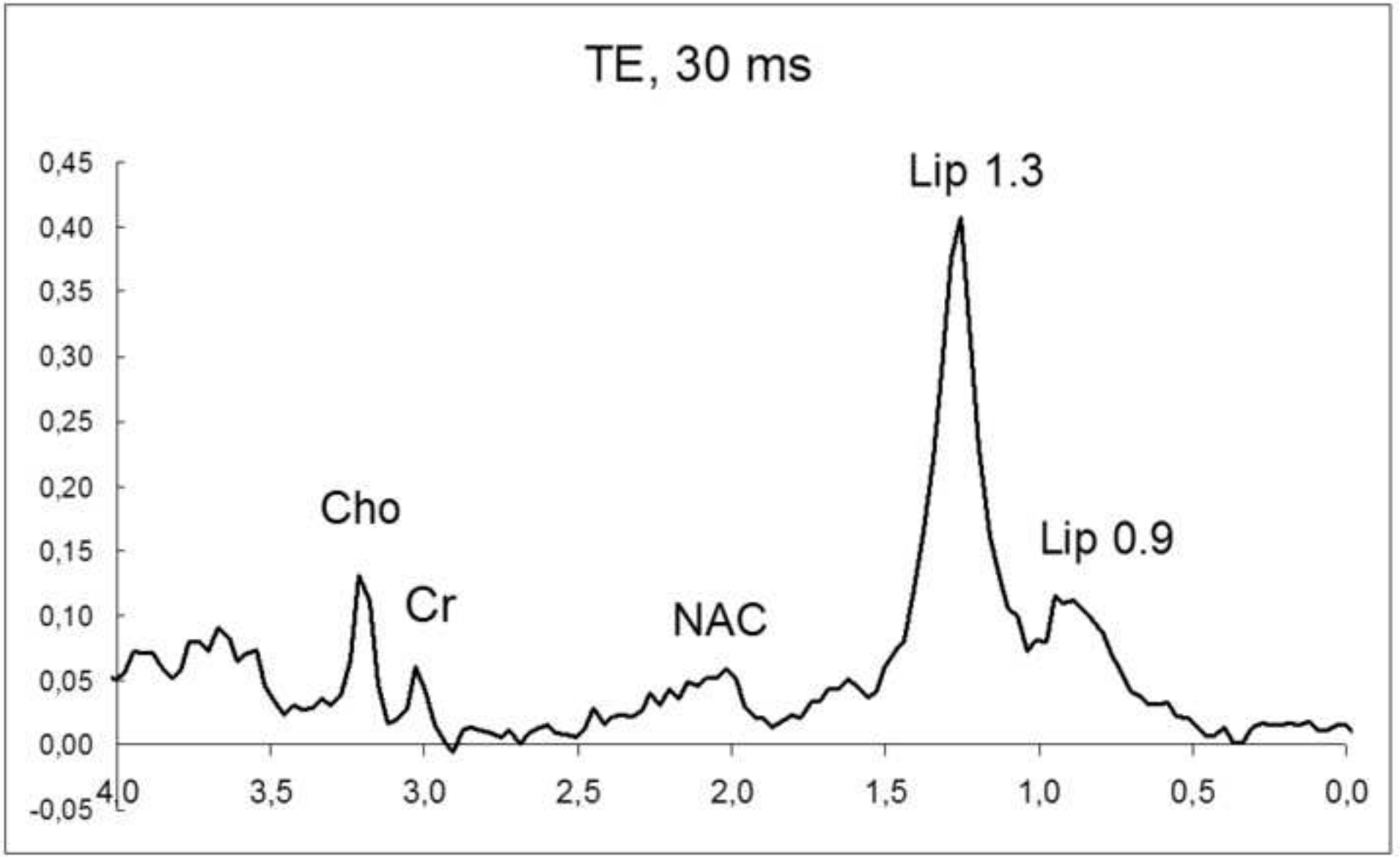

Figure 5l

Click here to download high resolution image

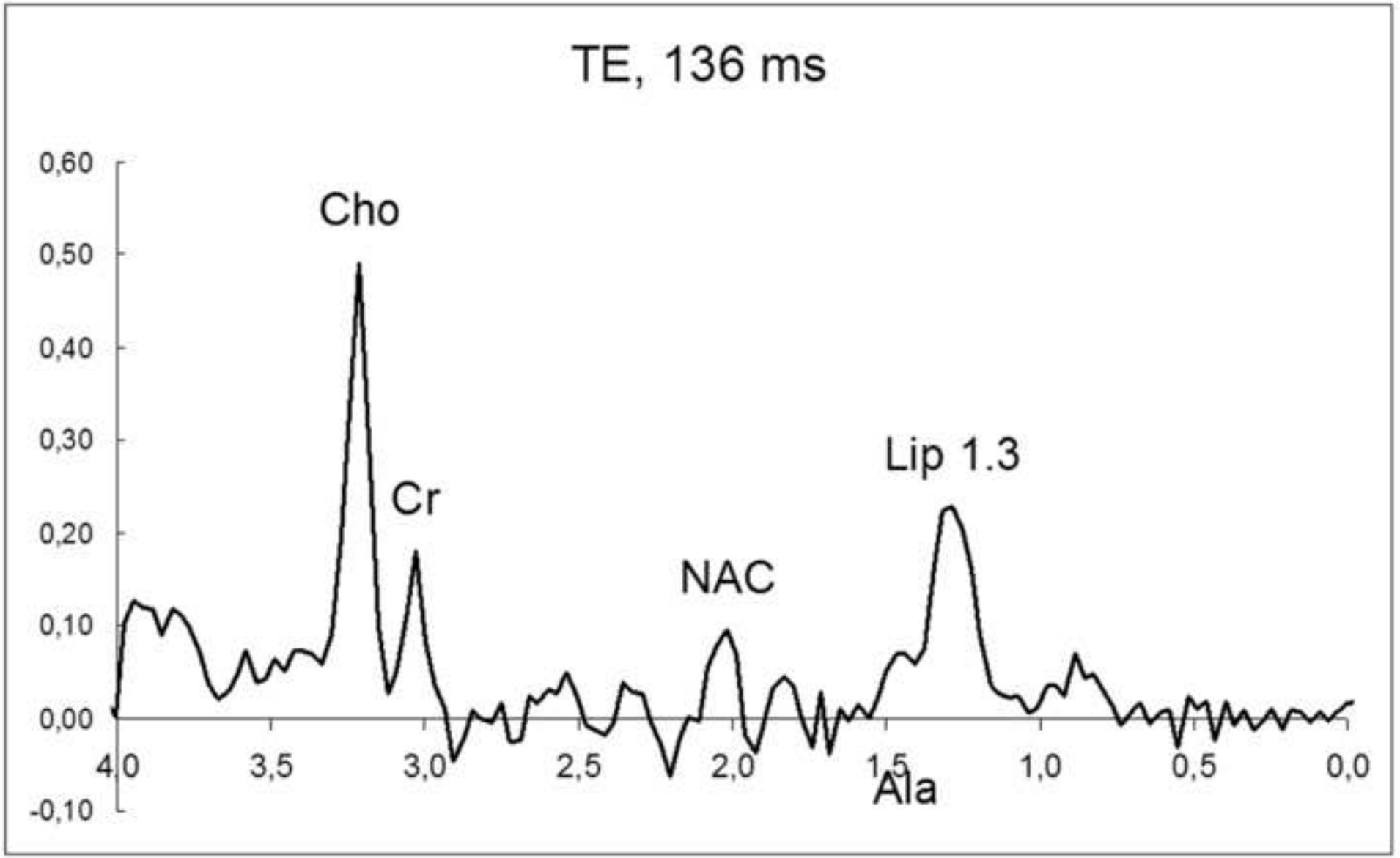

Figure 5J

Click here to download high resolution image

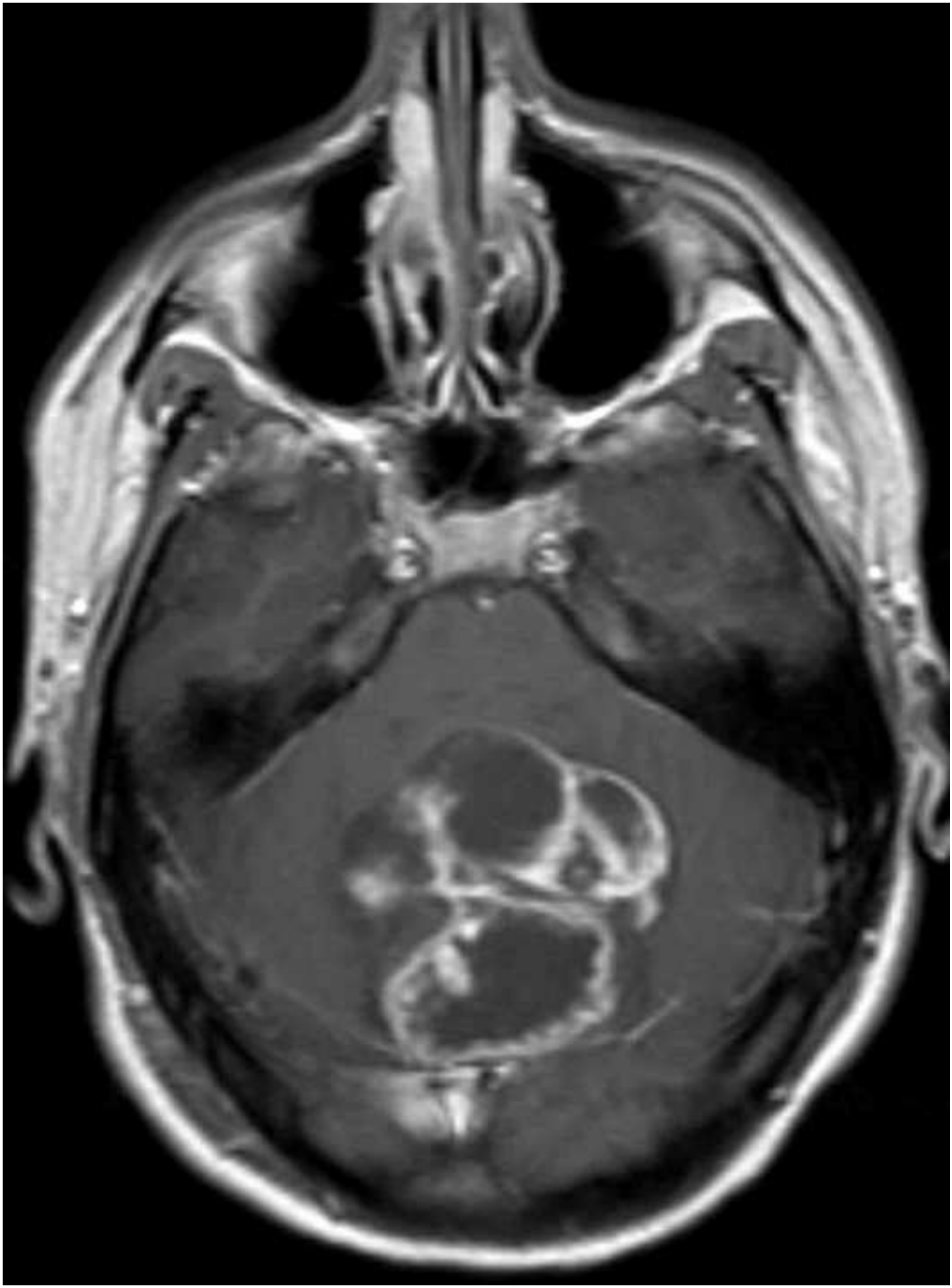

Figure 5K

Click here to download high resolution image

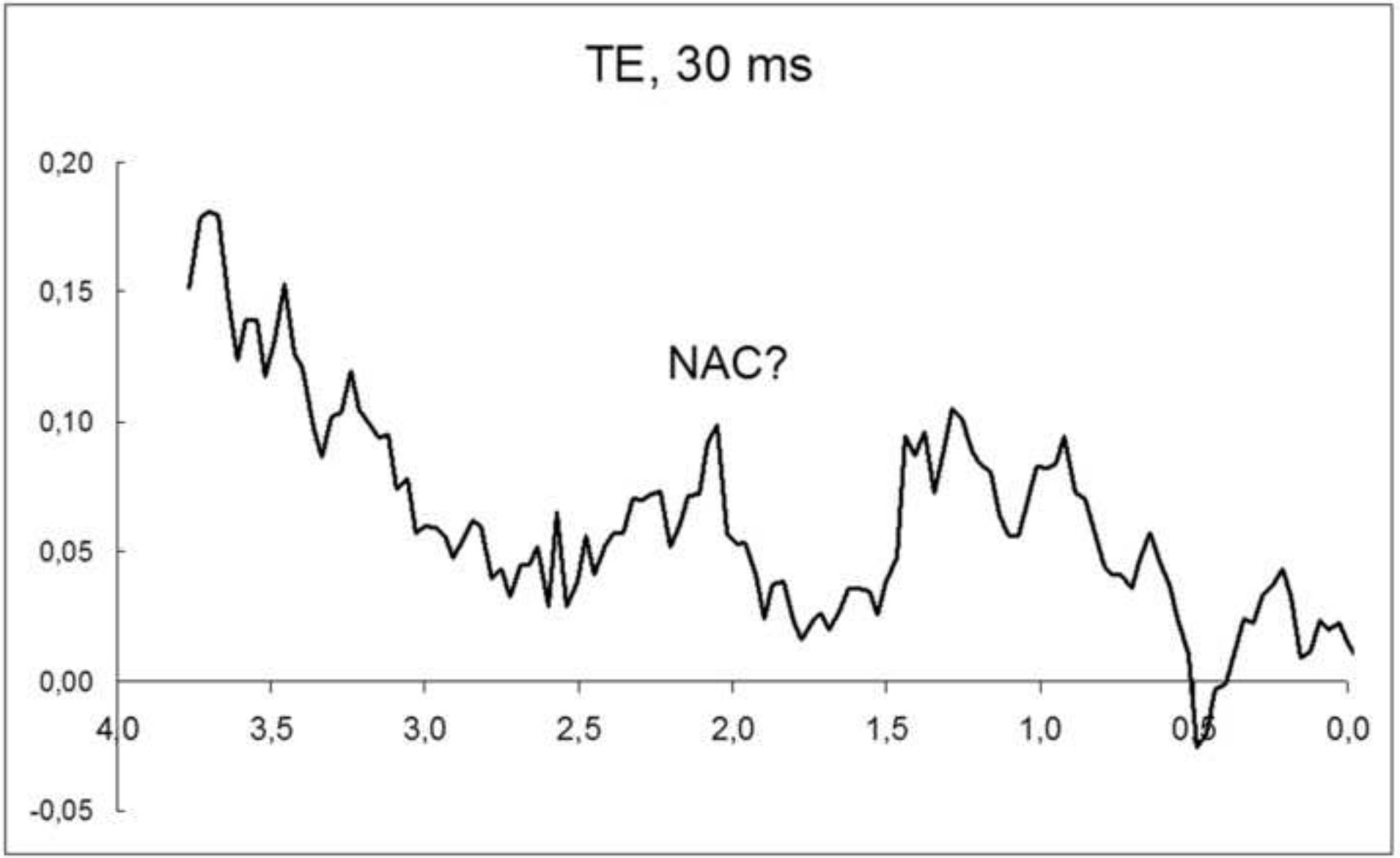

Figure 5L

Click here to download high resolution image

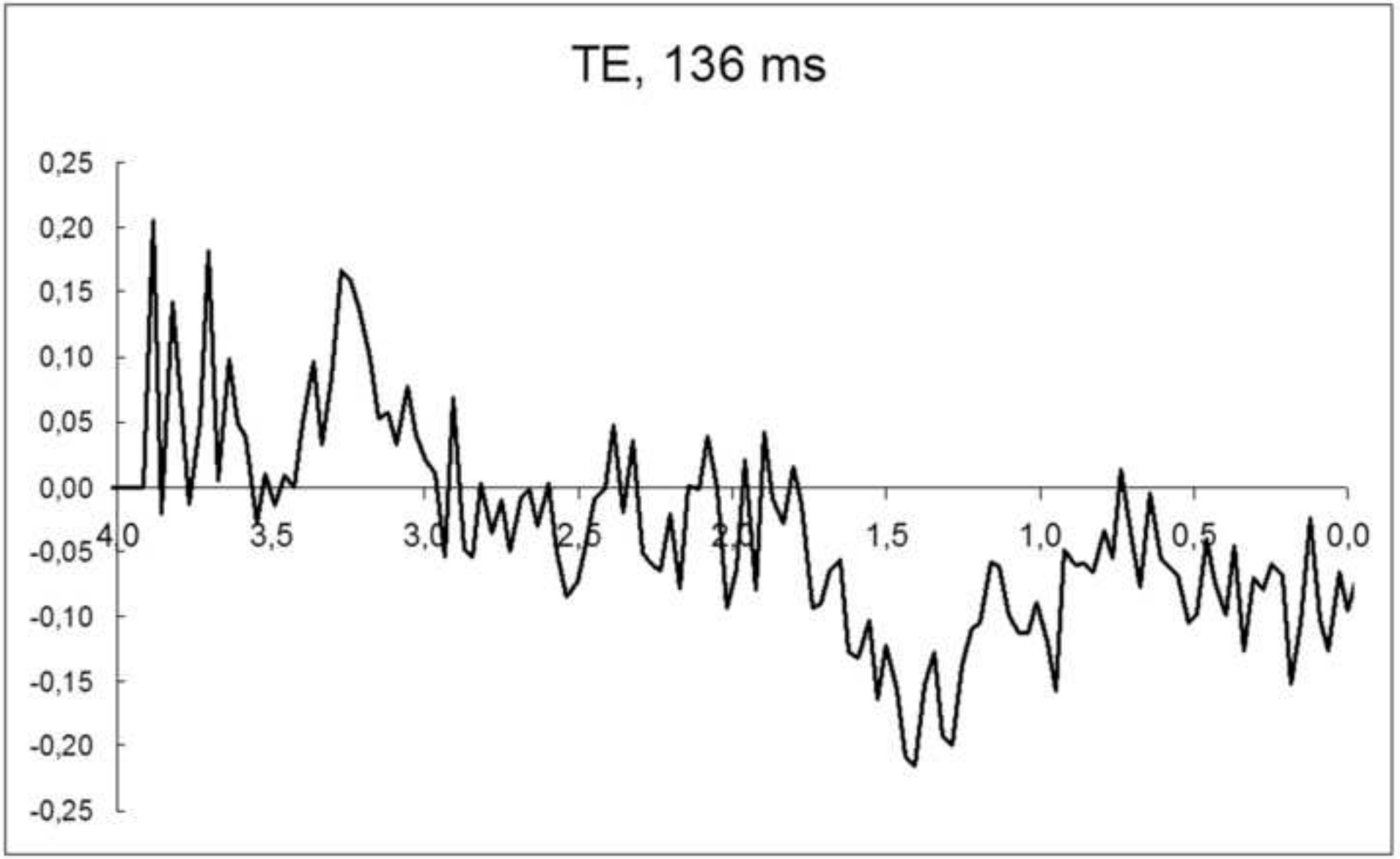

*** Conflict of Interest Disclosure Form**

Click here to download Conflict of Interest Disclosure Form: Conflict of Interest Disclosure Form.doc

Conflict of Interest Disclosure Form

It is the policy of the Journal *Neuroradiology* to ensure balance, independence, objectivity, and scientific rigor in the Journal. All authors are expected to disclose to the readers any real or apparent conflict(s) of interest that may have a direct bearing on the subject matter of the article.

This pertains to relationships with pharmaceutical companies, biomedical device manufacturers or other corporation whose products or services may be related to the subject matter of the article or who have sponsored the study.

The intent of the policy is not to prevent authors with a potential conflict of interest from publication. It is merely intended that any potential conflict should be identified openly so that the readers may form their own judgements about the article with the full disclosure of the facts. It is for the readers to determine whether the authors' outside interest may reflect a possible bias in either the exposition of the conclusions presented.

The corresponding author will complete and submit this form to the Editor-in-Chief on behalf of all authors listed below.

Article Title **IN VIVO PROTON MAGNETIC RESONANCE SPECTROSCOPY OF INTRAVENTRICULAR TUMOURS OF THE BRAIN**

Authors **Carles Majós, Carles Aguilera, Mònica Cos, Sara Castañer, Ana P Candiota, Teresa Delgado-Goñi, Juan J Sánchez, Àngels Camins, David Mato, Juan J Acebes, Carles Arús**

Please state below whether any conflict of interest exists:

X certify that no actual or potential conflict of interest in relation to this article exists.

☐ I certify that a conflict of interest in relation to this article exists and I define this conflict below:

(please describe financial interest/arrangement with one or more organizations that could be perceived as a real or apparent conflict of interest in the context of the subject of this article):

……..
……..
……..

Name **Carles Majós**

Signature …… Date **June 26, 2008**

Please upload this form together with your online manuscript submission since your manuscript cannot be assigned for review without it.

Please also insert a Conflict of Interest Statement at the end of your manuscript, preceding any Acknowledgements and References using the phrase, "We declare that we have no conflict of interest" or alternatively state your conflict of interest.

http://www.springer.com/journal/234